

Newcastle
University

The Interaction of Nanoparticles with Mucosal Barriers

Muneef Aldhafeeri

BSc, MSc

Thesis submitted for the Degree of Doctor of Philosophy

Medical School

Institute for Cell and Molecular Biosciences

March 2019

Acknowledgment

Firstly, I would like to express my gratitude to my supervisors, Professor Jeff Pearson and Dr. Chris Ward, for the continuous support of my PhD study and related research. Their guidance helped me throughout the research and writing of this thesis.

I thank Dr. Bernard Verdon for training me and his helpful advice during my laboratory work. I am also grateful for Dr Matthew Wilcox for his training of the rheology of mucus and permeation studies. I want to thank Mrs Maxine Geggie for her assistance with freezing samples and everything she has done for this project. My sincerest thanks also goes to the patients who contributed in this transplant study. I would like to express my gratefulness to all those who gave me the possibility to complete this project.

Last but not the least, I would like to thank my family: my parents, my wife Fatimah, and my sister Dr. Faten for supporting me throughout writing this thesis and my life in general.

Declarations

This thesis is based on research performed in the Institute for Cell and Molecular Biosciences, Newcastle University. I performed the laboratory work and analysis of the results. With the exception of the aspects of the work that are outlined below:

- Transplant department in Freeman Hospital: Initial dissection and preparations of primary human bronchial epithelial cells.
- Poly (DL-lactide-co-glycolide in a 50:50 molar ratio) (PDLG) was made and received in suspension from Nanomi (Nanomi B.V Oldenzaal, Netherlands).
- Poly (lactic-co-glycolic acid) (PLGA) was made and received in dry powder form from Aristotle University of Thessaloniki (AUTH, Greece).
- Polystyrene Nanoparticles were made and received in dispersion of DI water from Corpuscular Company (New York, NY).
- Self nanoemulsion drug delivery systems (SNEDDS) prepared by Aristotle University of Thessaloniki, Greece.

Abstract

Introduction:

The aim of this thesis was to assess the safety profile of different novel nanoparticles when interacting with lung bronchial epithelial cells in vitro, especially their role in inflammation and cytotoxicity. In addition, the permeation behaviour of self-nanoemulsifying drug delivery systems (SNEDDS) was measured by a novel mucus diffusion model utilizing standardized transwell diffusion plates.

Methods:

Primary bronchial epithelial and Calu-3 cells were cultured in 24 and 96 well plates. Different formulations of nanoparticles (NPs) were used to measure IL-8 production by cells as a marker of inflammation (measured by sandwich ELISA). The Celltitre blue (CTB) and MTT assays were used to test cell viability. The effect of cell density on the CTB assay was studied (500k, 400k, 300k, 200k, 100k, 50k, 42k, 33k, 25k, 17k, and 8.3k) in 24 well plates. Permeation studies were examined by using a mucus diffusion model. The rheology of the mucus was investigated to evaluate the gel structure of the mucus.

Results:

The viability of cell exposed to 52nm polystyrene NPs showed no statistical difference between cells with NPs and cells without NPs after 24 hour of exposure. The nanoparticles were shown to interfere with both the CTB and MTT assays. The standard curves in the CTB assay vary as the cell density decreased. Although IL-8 was shown to be slightly increased in human primary cells after exposure to different concentrations of NPs, IL-8 increased significantly after exposures to the same proportion of sterile water as these nanoparticles were delivered in (a control for osmolarity). The composition of SNEDDS might play a major role in their capacity to permeate the mucus such as lauroglycol. The small intestine mucus gels have some degree of frequency dependency; between 0.1 and 1 Hz, there was a decline in both

G' and G'' followed by a rise over 1-10Hz. G'' increased relative to G' suggesting a tendency to flow. This change at high frequency is verified by an increase in the phase angle, demonstrating a weaker gel. This biphasic behaviour may be explained by the gel forming interactions having time to break and make at a low frequency but at a high frequency, they do not have time to reform.

Conclusion:

I have found that both CTB and MTT assays may not be sensitive enough to test viability of cells exposed to nanoparticles. Therefore, other assay systems are required to test these NPs with respect to cytotoxicity. The composition of the SNEDDS played an important role in determining the permeation of the mucus gel layer.

Contents

Acknowledgements.....	ii
Declaration.....	iii
Abstract.....	iv
Introduction.....	iv
Methods.....	iv
Results.....	iv
Conclusion.....	v
Contents.....	vi
List of Figures.....	xii
List of Tables.....	xiv
List of Abbreviations.....	xvi
Chapter one: Introduction.....	1
1.1.Nanotechnology.....	1
1.1.1. Definitions.....	1
1.1.2. History of Nanoparticles and Drug Targeting.....	3
1.1.3. History of Nanotoxicology.....	3
1.2.The Lungs.....	5
1.2.1. Anatomy and Physiology of the Lungs.....	5
1.2.2. The Mucus Layer.....	9
1.2.3. Cell Culture.....	10
1.2.4. Cell Models.....	10
1.2.5. Primary Bronchial Epithelial Cell Cultures.....	13
1.2.6. Calu-3.....	13

1.2.7. Laboratory Considerations for Studying Cellular Nanotoxicology in Lungs Vitro.....	13
1.3.The Oxidative Stress Model.....	15
1.4.Nanoparticles and Drug Delivery.....	18
1.4.1. The Route of Delivery.....	18
1.4.2. Factors Affecting Drug Delivery with Nanoparticles: the Role of Particles Size and Shape.....	23
1.4.3. The Concept of a Magic Bullet in Nanoparticles Drug Delivery.....	26
1.4.4. Nanoparticles in the Market and in Clinical Trials.....	29
1.4.5. Challenges Facing Mucosal Nanoparticles Drug Delivery.....	40
1.4.6. The Release of Drug from Nanoparticles.....	43
1.5.Cytotoxicity.....	45
1.5.1. Cytotoxicity of Nanoparticles.....	45
1.5.2. The Use of Nanoparticles to Improve the Effectiveness of Cytotoxic Drugs.....	53
1.6.Nanoparticles as Promoters of Inflammation.....	62
1.6.1. The Use of Nanoparticles to Modulate Immunological Responses.....	62
1.7.Permeation of Mucus.....	63
1.8.Rheology of Mucus.....	64
1.9.The Aims of the Thesis.....	66
Chapter Two: Methodology and Materials.....	67
2.1.Cell Cultures.....	67
2.1.1. Primary Bronchial Epithelial Cells.....	67
2.1.2. Calu-3.....	70
2.2.Nanoparticles.....	71
2.2.1. Nanoparticles Characterizations.....	71

2.2.2. Dispersion Protocol for Nanoparticles.....	75
2.3.Sandwich ELISA.....	76
2.4.Cell Viability.....	77
2.4.1. CellTiter Blue.....	77
2.4.2. MTT.....	80
2.5.Light Microscopy.....	81
2.6.Cleaned Porcine Intestinal Mucus.....	82
2.7.Rheology.....	83
2.8.Permeation Studies.....	84
2.9.Statistics.....	87
Chapter Three: Nanomedicine and Lung Epithelial Cells.....	89
3.1.Abstract.....	89
3.1.1. Introduction.....	89
3.1.2. Methods.....	89
3.1.3.Resultls.....	89
3.1.4. Conclusion.....	90
3.2. Introduction.....	91
3.3.Methods.....	94
3.3.1. Cell Culture.....	94
3.3.2. Nanoparticles.....	94
3.3.3. Dispersion Protocol.....	94
3.3.4. IL-8 Measurement.....	94
3.3.5. Cell Viability.....	94
3.3.6.. Light Microscopy.....	94

3.3.7. Statistics.....	95
3.4.Results and Discussion.....	96
3.4.1. The Physiochemical Characterizations of the NPs.....	96
3.4.2. Light Microscopy.....	98
3.4.3. Cell Viability.....	100
3.4.4. The Effect of Cell Density on the CTB Assay.....	107
3.4.5. Measuring CTB Assay by Using 96 Well Plates.....	114
3.4.6. The Effect of Nanoparticles on the ELISA Standard Curve of IL-8.....	119
3.4.7. The Effect of NPs on IL-8 Levels Using Primary Human Epithelial Cells.....	122
Chapter Four: Mucosal Drug Delivery via Self-Nanoemulsifying Drug Delivery Systems..	124
4.1. Abstract.....	124
4.1.1. Introduction.....	124
4.1.2. Methods.....	124
4.1.3. Results.....	124
4.1.4. Conclusion.....	125
4.2.Introduction.....	126
4.3.Methods.....	128
4.3.1. Nanoparticles.....	128
4.3.2. Nanoparticles Dispersion.....	128
4.3.3. Calu-3.....	128
4.3.4. MTT Assays.....	128
4.3.5. Cleaned Porcine Intestinal Mucus.....	128
4.3.6. Rheology of Mucus.....	128
4.3.7. Permeation Studies.....	128

4.3.8. Statistics.....	128
4.4. Results and Discussions.....	129
4.4.1. Nanoparticles Characterization.....	129
4.4.2. Cytotoxicity.....	129
4.4.3. Mucus Permeation by Nanoparticles (Permeation Study).....	134
4.4.4. Rheology of Porcine Intestinal Mucus.....	143
Chapter Five: General Discussion, Conclusion, and Future Works.....	152
5.1. Introduction.....	152
5.2. The Oxidative Stress Model Approach.....	156
5.3. Interference with Viability Assays.....	162
5.3.1. The Mechanism of NPs Interference with CTB Assay.....	165
5.3.2. The Mechanism of NPs Interference with MTT Assay.....	165
5.3.3. Summary of Cytotoxicity Results.....	166
5.3.4. Approaches to Avoid Cytotoxicity Interferences.....	168
5.4. Nanoparticles and the Mucus.....	169
5.5. Future Works to Overcome the Mucus Barrier.....	171
References.....	175
Appendix 1.....	185

Lists of Figures

Figure 1: Basis of nanotoxicology.....	4
Figure 2: An oxidative stress model.....	17
Figure 3: Routes of nanoparticles drug administration.....	22
Figure 4: The effect of particle size on the nature (Brownian vs non-Brownian) of diffusive motion in mucus barriers.....	42
Figure 5: Images taken illustrating different confluency of Calu-3 cells.....	69
Figure 6: Transwell inserts covered with mucus and particles suspension.....	85
Figure 7: Time course of permeation.....	86
Figure 8: Primary epithelial cells.....	99
Figure 9: OD absorbance of polystyrene NPs with CTB assay (without cell culture).....	104
Figure 10: The effect of cell density in CTB assay in Calu-3.....	111
Figure 11: The effect of cell density in CTB assay in Calu-3.....	112
Figure 12: Images taken illustrating different confluency of Calu-3 cells.....	113
Figure 13: 100% confluent calu-3 grown in well of 96-well plate.....	115
Figure 14: The standard curves of IL-8.....	121
Figure 15: Permeation results for SNEDDS-a.....	137
Figure 16: Permeation results for SNEDDS-b.....	139
Figure 17: Permeation results for SNEDDS-c.....	141

Figure 18: Permeation results for all SNEDDS together.....	142
Figure 19: Amplitude sweep of cleaned porcine intestinal mucus.....	148
Figure 20: Gradient slopes of G' and G''	150
Figure 21: The use of oxidative stress model as method for predictions of nanoparticles hazard.....	159
Figure 22: Nanoparticles Characterization and Interference with Assays.....	164
Figure 23: Characteristics of permeation through the pores in the mucus gel.....	170

Lists of Tables

Table 1: Different definition of nanotechnology and nanomedicine.....	2
Table 2: Anatomy and structure of human respiratory system.....	7
Table 3: The size dependent regional deposition of micro- and nanoparticles in the lungs.....	8
Table 4: The Advantages and disadvantages of cell cultures.....	12
Table 5: Examples of marketed nanomedicines.....	31
Table 6: Examples of nanomedicines in clinical development.....	34
Table 7: Cytotoxicity studies of nanoparticles involving lung epithelial cells (in vitro).....	55
Table 8: Physiochemical characterizations of NPs used in this study.....	72
Table 9: Characterizations of nanoparticles.....	74
Table 10: The advantage of using CellTiter-Blue assay.....	79
Table 11: Physiochemical characterizations of NPs 7 and 8 used in this study.....	97
Table 12: The percentage of live cells in primary human bronchial epithelial cells after 24 hours exposure of 50µg/ml of 52nm PNP.....	101
Table 13: The OD absorbance of polystyrene NPs with CTB assay (without cells).....	103
Table 14: Results of the CTB assay of three different PDLG NPs in human primary epithelial cells.....	106
Table 15. Summarized results of cell density effect on the CTB assay.....	108
Table 16: Correlation analysis between cell densities of Calu-3.....	109
Table 17: Correlation analysis between cell densities of Calu-3.....	110

Table 18: The effect of 20K cell seeding density on the CTB assay.....	116
Table 19: The average and standard division of 20K cell seeding density on CTB.....	117
Table 20: Concentration of IL-8 with control (cells without NPs) and with 50µg/ml of 52nm PNP.....	120
Table 21: IL-8 concentration with three different NPs.....	123
Table 22: Cytotoxicity results of SNEDDS-a.....	131
Table 23: Cytotoxicity results of SNEDDS-b.....	132
Table 24: Cytotoxicity results of SNEDDS-c.....	133
Table 25: SNEDDS-a percentage of permeation over 6 hour.....	136
Table 26: SNEDDS-b percentage of permeation over 6 hour.....	138
Table 27: SNEDDS-c percentage of permeation over 6 hour.....	140
Table 28: Rheological characteristics of the porcine intestinal mucus from the small intestine.....	149
Table 29: Gradient Slopes of G' and G''	151
Table 30: Examples of toxicity paradigms.....	160

List of Abbreviations

α 1AT	Alpha 1- antitrypsin
δ	Phase angle
Ag	Silver
AMB	Amphotericin B
ARE	Antioxidant response element
Au	Gold
A549	Adenocarcinomic human alveolar basal epithelial cells
BEAS-2b cells	Transformed human bronchial epithelial cells
bEGF	Biotinylated-EGF
BEGM	Bronchial epithelial cell growth medium
Calu-3	A lung adenocarcinoma cell line derived from a 25-year old Caucasian male
CB	Carbon black
CFTR	Cystic fibrosis transmembrane conductance regulator
Chitin-PCL CNGs	Chitin-poly (caprolactone) composite nanogels
CorL105 cells	A human lung epithelial cancer cell line
CP	Carbopol
CS	Calcium silicate
CTB	CellTiter blue
C ₆₀	Fullerenes
DCF	Dichlorofluorescein
DDAB	Didodecyltrimethylammonium bromide
DOC	Deoxycholate
DOCA-GC	deoxycholic acid-modified glycol chitosan
DOTAP	Dioleoyltrimethylammonium propane
Dox-Chitin-PCL	Doxorubicin chitin-poly (caprolactone) composite nanogels
DMEM	Dulbecco's modified Eagle's medium
ESF	The European Science Foundation
Ex4-C16	Palmityl acylated exendin-4
FAP-B	Fibronectin attachment protein of mycobacterium bovis
FCS	Foetal calf serum
Flt1	Vascular endothelial growth factor receptor 1
GI	Gastrointestinal
GP-PT	The anticancer activities of CDDP-incorporated in GPs
GP-Pt-bEGF	The anticancer activities of GP-Pt with bEGF modification
GPs	Gelatin nanoparticles
G'	Elastic modulus
G''	Viscous modulus
HA	Peptide-hyaluronate acid
H ₂ O ₂	Non-radical hydrogen peroxide
IL	interleukin
INS/DMPG	Insulin/dimyristoyl phosphatidylglycerol
IMR-90	Normal human lung fibroblast cells
ELISA	Enzyme linked immunosorbent assay

LDH	Lactate dehydrogenase
LFC131	A peptide inhibitor of CXCR4-ligand binding
LPS	Lipopolysaccharide
LVER	Linear viscoelastic region
MAPK	Mitogen-activated protein kinase
MNPs	Magnetic nanoparticles
MNP-PEI	Magnetic nanoparticles (100nm) in diameter coated with poly(ethylenimine)
MNP-PEI-PEG	Magnetic nanoparticles (100nm) in diameter coated with poly(ethylenimine) and poly(ethylene glycol)
MTS	The 3-(4, 5-dimethylthiazol-2-yl)-5-(3-carboxymethoxyphenyl) - 2-(4-sulfophenyl)- 2H-tetrazolium.
MTT	3-[4,5-dimethylthiazol-2-yl]-2,5- diphenyl tetrazolium bromide
NAC	N-acetylcysteine
ND	NanoDisk
ND-AMB	NanoDisk which added amphotericin B as a payload.
NEM	Nano-embedded microparticles
NF-kB	nuclear factor kB
NMR	Nuclear magnetic resonance
NPs	Nanoparticles
Nrf2	Transcription factor
NO	Nitric oxide
O ₂ ^{•-}	Superoxide anion
·OH	Hydroxyl radicals
Pal-Ex4	Palmitic acid-modified exendin-4
PAMAM-NH ₂	Cationic poly (amidoamine) dendrimers
PBEC	Primary bronchial epithelial cell cultures
PCR	Polymerase chain reaction
pDNA	Plasmid DNA
PDLG	Poly (DL-lactide-co-glycolide in a 50:50 molar ratio)
Pd-NPs	Palladium nanoparticles
PEG	Polyethylene Glycol
PEG-CH ₁₂ K ₁₈	PEG maleimide 12 histidines – 18 lysines forming a tripolymer
PEI	Polyethylenimine
PCL	Poly (ε-caprolactone)
PL	Phospholipid
PLA-PCL-TPGS	d-α- tocopheryl polyethylene glycol 1000 succinate
PLG	Poly (D, L-lactide-co-glycolide)
PLGA	Poly (lactide-co-glycolide)
pMDI	Pressurised metered dose inhalers
PNP	Polystyrene nanoparticles
PVA	Polyvinyl alcohol
QD	Quantum dots
RAW 264.7	Mouse macrophage cells
ROS	Reactive oxygen species
RPMI	Roswell Park Memorial Institute Media

SH-SY5Y	Human neuroblastoma cells
siRNA	Small interfering RNA
SNEDDS	Self-nanoemulsifying drug delivery systems
STP	Serine, threonine and proline
SWCNTs	Single walled carbon nanotubes
TAS-103	The anticancer drug 6-/[2-(dimethylamino)ethyl]amino]-3-hydroxyl-7H-indeno[2,1-c]quinolin-7-one dihydrochloride.
Tb	Tobramycin
THB-1	Human alveolar macrophage cells
TNF α	Tumour necrosis factor alpha
TNP	Thiolated chitosan-modified PLA-PCL-TPGS nanoparticles
TPGS	Vitamin E d- α -tocopheryl polyethylene glycol 1000 succinate
TT1	Transformed human alveolar epithelial type 1-like cells
UNP	Unmodified PLA-PCL-TPGS nanoparticles
U251	Human glioblastoma cells
WGA	Wheat germ agglutinin
WST-1	Cell proliferation reagent.

Chapter 1: Introduction

1.1. Nanotechnology:

1.1.1. *Definitions:*

One of the most promising strategic technologies in the 21st century is nanotechnology [1]. Although there are uncertainties as to the definition of nanotechnology (**Table 1**), it can be defined as the manipulation and study of materials in the range between 1 and 100 nm (a billionth of a meter) [2]. The use of nanotechnology in medicine is known as nanomedicine, which is the medical application of nanotechnology and related research [3].

Table 1. Different definition of nanotechnology and nanomedicine

Organization	Definitions
The Europische Akademie	Nanotechnology is dealing with functional systems based on the use of sub-units with specific size dependent properties of the individual sub-units or of a system of those.
Royal Society and Royal Academy of Engineering	Nanoscience is the study of phenomena and manipulation of materials at atomic, molecular and macromolecular scales, where the properties differ significantly from those at a larger scale. Nanotechnologies are the design, characterisation, production and application of structures, devices and systems by controlling shape and size at a nanometer scale.
Nanoforum	Nanotechnology is made up of areas of technology where dimensions and tolerances in the range of 0.1 nm to 100 nm play a critical role.
National Institutes of Health	Nanomedicine is an offshoot of nanotechnology which refers to highly specific medical interventions at the molecular scale for curing disease or repairing damaged tissues, such as bone, muscle or nerve.
The European Science Foundation (ESF)	Nanomedicine is the science and technology of diagnosing, treating and preventing disease and traumatic injury, of relieving pain, and of preserving human health using molecular tools and molecular knowledge of the human body.

Adapted from [4, 5].

1.1.2. History of Nanoparticles and Drug Targeting:

The idea of nanoparticles and drug targeting was born when Paul Ehrlich's visited Karl Maria von Weber's German romantic opera "Der Freischütz" (The Marksman). During this opera, "Frikugeln", or "magic bullets" were made by calling the spirit of the devil. Although the rifleman didn't aim well or the goal was out of reach, these Freikugeln always hit their goal. After this opera, Paul Ehrlich thought that this concept of targeted delivery could greatly improve drug therapy. The first efforts to apply this concept were by Ursula Scheffel and colleagues, and the group of Professor Peter Speiser at the ETH (Swiss Federal Institute of Technology), Zürich in the late 1960s and early 1970s. In the early 1980s, Oppenheim and Kreuter presented a definition which was later adopted by the Encyclopaedia of Pharmaceutical Technology and the Encyclopaedia of Nanotechnology: 'Nanoparticles for pharmaceutical purposes are solid colloidal particles ranging in size from 1 to 1000 nm (1µm). The first commercial nanoparticle product containing a drug (Abraxane™, human serum albumin nanoparticles containing paclitaxel) appeared on the market at the beginning of 2005. It was put on the market by a US company, Abraxis Oncology [6].

1.1.3. History of Nanotoxicology:

While the production of nanoparticles has been increasing, research into the toxicology of these particles and their potential hazard to human health is still in its infancy [7]. Nanotoxicology is the study of the potential adverse effect of the nanoparticles (NPs) on living organisms and ecosystems. The roots of the existing science of nanotoxicology can be found from a diversity of origins (**Figure.1**) [3, 8]. The fate of nanoparticles needs to be understood with the consideration of the toxicology of metal fumes, radionuclides, nuisance dusts, the toxicology of silica, asbestos and synthetic vitreous fibres and, more recently, from the toxicology of air pollution particles (PM₁₀=particles below 10 µm). In addition to this, virology and other sciences have contributed to our understanding [9].

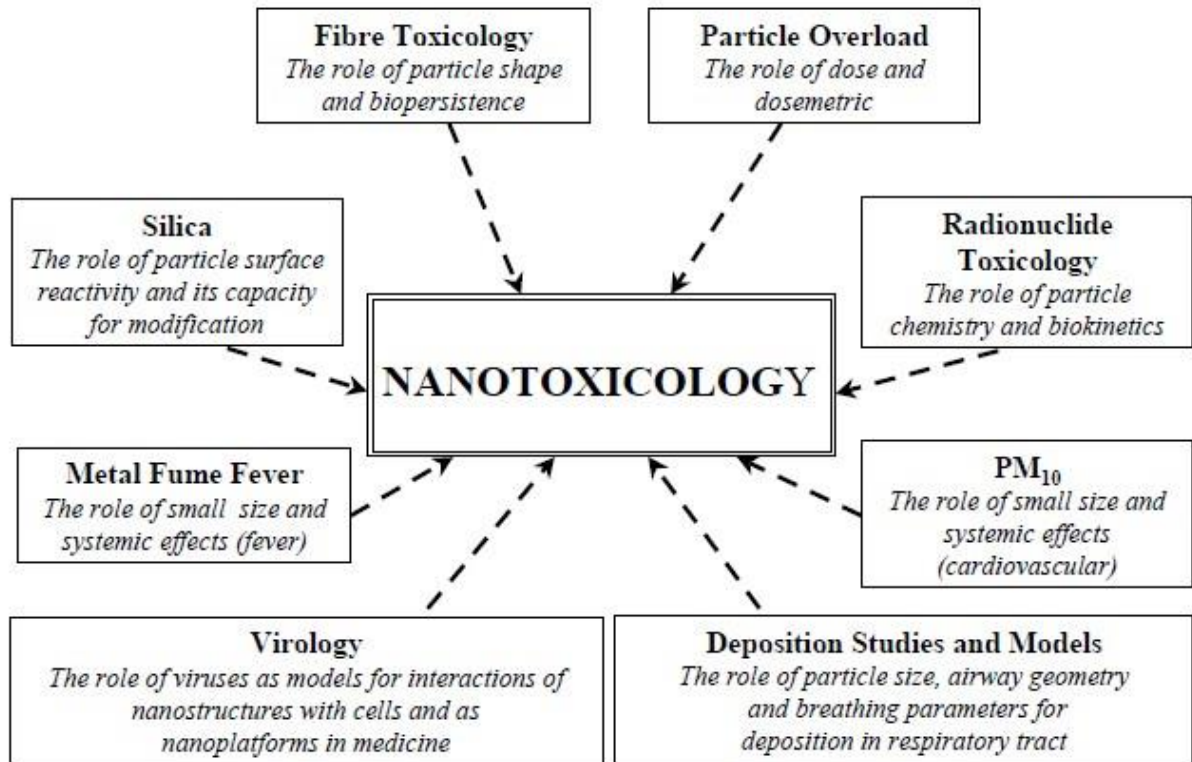


Figure 1. Basis of nanotoxicology. Adapted from [9].

There are many variables to consider when working with nanomedicine, including, but not limited to: material, size, shape, surface, charge, coating, dispersion, agglomeration, aggregation and concentration [7]. A detailed assessment is outside the scope of this thesis, however, excellent articles have been published regarding the physiochemical characterization of nanotechnology [10-12].

1.2.The Lungs:

1.2.1. Anatomy and Physiology of the Lungs:

The respiratory and circulatory systems work together to deliver oxygen and return carbon dioxide to the lungs. The conducting airways contain regions that do not undergo gaseous exchange and starts with the trachea (**Table 2**). The trachea divides into two main bronchi which separates into a sequence of intra-pulmonary bronchial and bronchiolar airways. Peripheral airways are followed by the respiratory bronchioles and the terminal parts of bronchi are the thin walled alveoli, where gas exchange occurs. The entire respiratory tree is lined by a continuous layer of epithelial cells which are essential to sustain the normal functions of the respiratory system. These include creating a barrier to various insults, driving mucociliary clearance and secreting protective substances (e.g. surfactant proteins, mucus and antimicrobial peptides). The pulmonary epithelial cells have the ability to repair, regenerate and modulate the response of other airway components. The conducting zone is a pseudo-stratified, columnar epithelium composed of secretory goblet cells, basal cells and ciliated cells that afford the mechanisms for mucociliary clearance. The respiratory zone contains alveolar type I and II cells which make up the alveolar epithelium. Only 5% of the internal lung surface is built by alveolar type I cells, which perform the role of gas exchange. The first line of physicochemical defence in the lung is the airway epithelial cells; this defence includes mucociliary clearance, secretion of ions, regulation of the airway surface liquid water content (dysregulation decreases defence against infections), and the production of anti-inflammatory, antibacterial and antioxidant molecules in the mucus. The second line of physicochemical

defence is by inter-cellular tight junctions that create a competent physical barrier against inhaled pathogens or noxious agent intrusions. Tight junctions are important to regulate the flow of molecules between the apical and basolateral compartments, regulating ion and solute homeostasis, controlling airway surface liquid height and ionic composition necessary for lung defence [13]. The size-dependent regional deposition of micro- and nanoparticles in the lungs are summarized in **table 3**.

Table 2. Anatomy and structure of the human respiratory system. Adapted from [13].











	Anatomy	Structure	Generation (Z)	Cell Types
Conducting zone		Larynx	N/A	<ul style="list-style-type: none"> • Ciliated cells • Goblet cells • Basal cells
		Trachea	0	<ul style="list-style-type: none"> • Ciliated cells • Goblet cells • Basal cells • Serous cells
		Primary bronchi	1	<ul style="list-style-type: none"> • Serous gland cells • Mucous gland cell
		Secondary bronchi	2	<ul style="list-style-type: none"> • Ciliated cells • Goblet cells • Basal cells • Serous cells
		Tertiary bronchi	3	
		Small bronchi	4	
		Bronchioles	5	
		Terminal bronchioles	6-16	<ul style="list-style-type: none"> • Ciliated cells • Clara cells • Basal cells
Respiratory zone		Respiratory bronchioles	17-19	<ul style="list-style-type: none"> • Ciliated cells • Clara cells • Basal cells • Alveolar type I cells • Alveolar type II cells
		Alveolar sacs	23	<ul style="list-style-type: none"> • Alveolar type I cells • Alveolar type II cells

Table 3: the size dependent regional deposition of micro- and nanoparticles in the lungs.

Airway Region	Diameter of Airway	Deposited Particle Size
Trachea	1.7 cm	2-16 μm
Bronchi 8-13 generations	2-8 mm	2-16 μm
Bronchioles 3-10 generations	0.5-2 mm	2-16 μm
Terminal Bronchioles 1 generation	0.6 mm	2-16 μm
Respiratory Bronchioles 3-5 generations	0.5 mm	< 2 μm
Alveolar Ducts 2-3 generations	0.3- 0.5 μm	< 2 μm
Alveolar Sacs 300-600 million	250- 300 μm	< 2 μm

Consequently nanoparticles of 100- 200 nm would be deposited as far as the alveoli. Data taken from [14].

1.2.2. The Mucus Layer:

Mucus cannot be considered as simple because it is a heterogeneous hydrogel with properties of both a gel and a viscous liquid. The mucus layer is the thinnest in the eye (0.2-1.0 μm) and thickest in the colon (800 μm). Mucus consists of 95% of water and the major gel forming components, mucins (~5%). Mucus also contains other components such as IgA, actin, DNA, protein, and lipid. There are three subgroups of mucins: membrane bound, secreted soluble and secreted gel forming. They are commonly large molecular weight glycoproteins ranging from 200,000 to 3 million Daltons. They are synthesized as a protein core backbone with a region rich in serine, threonine and proline (STP). 50-90% of the accounted molecular weight of mucins are carbohydrates. They are joined to the protein core by N- acetyl galactosamine which is joined to the hydroxyl amino acids serine or threonine. The extent of the carbohydrate chains may vary from 1 to 20 residues and the other sugars are fucose, galactose, N-acetyl glucosamine and sialic acid. Furthermore, mucins also have N-glycosylation by links to asparagine. Therefore, mucins will be negatively charged at physiological pH due to the sialic acid content and ester sulphation. Mucins also consists of areas of the protein core which are globular and have little or no glycosylation. Membrane bound mucins contain sea urchin sperm protein enterokinase and agrin module (SEA domains) which are potential cleavage sites. Consequently, membrane bound mucins may be released from the cell membrane by proteolytic action. In addition, membrane bound mucins consist of a transmembrane domain and a small cytoplasmic tail containing tyrosine, serine and threonine residues that can be phosphorylated, indicating a signaling function. The N and C-terminals of the gel forming mucins are comprised of globular domains homologous with the B, C and cysteine rich D domains of von Willebrand factor [15]. Mucus gels can be reformed in vitro with gradual concentrations of the component mucins. Irreversible gel formation occurs at around 20mg/ml (in vivo mucin content of mucus gels is 30-50mg/ml). Gel forming mucins have a polymeric structure based on disulphide bridges. This polymeric structure is essential

for gel formation as depolymerised mucins will not form a gel. The gel properties of mucus gels can be characterised using a rheometer measuring G' (Pa) elastic modulus, G'' (Pa) loss modulus and the phase angle (δ). Mucus gels contain pores which vary in reported sizes of 40nm-1 μ m based on methods such as particle tracking, atomic force microscopy, transwell diffusion and fluorescent recovery after photobleaching [16-19].

1.2.3. Cell Culture:

Although exposure to and the delivery of nanoparticles is growing, there is no clear regulatory guidelines on testing and evaluating nanoparticles [1]. If all nanoparticles were investigated in animals – taking into account manipulations in composition, size, routes of exposure and so on – then massive numbers of animals would be required to comprehensively assess the effects of these materials [20]. Furthermore, scientists usually work within the three R's principles of 'Reduction, Refinement and Replacement' in animal experimentation [13]. Therefore, a major aim of the researcher is to establish and develop in vitro/in vivo systems to represent and show any toxic effects of nanoparticles in humans [20].

1.2.4. Cell Models:

There are many advantages and disadvantages of using cell culture (**Table 4**). It should be noted that the correct choice of a cell system in vitro should be based on a working hypothesis [21]. For instance, Soto et al. (2007) demonstrated that the human alveolar macrophage (THB-1) cell line generally had very similar responses to a murine macrophage cell line, but inorganic nanoparticles were shown to be more toxic to the human lung epithelial cell line derived from a cancer cell (A549) [22]. It has been suggested that the usage of cancer cells should be minimized because this model may produce abnormal results [23]. Another consideration in lung deposition for nanoparticles is size, as smaller nanoparticles means they will penetrate deep into the lung [21]. In addition to that, it has been suggested that certain historical cell lines may be not the cell originally reported [13]. For example, an investigation by Drexler et al. (2003) demonstrated that over 500 reported human leukemia-lymphoma cell

lines had been misidentified by as much as 15% [24]. Another consideration is that the response of immortalised and primary cells to the same drug may be clearly different [13]. For instance, Wilkinson et al. (2011) demonstrated that human primary bronchial epithelial cells (PBEC) are more likely to internalize Palladium nanoparticles (Pd-NPs) and are also more vulnerable to cell death induction at higher doses of Pd-NPs compared to A549 cells. Therefore, using primary cells may be considered as the gold standard [25]. In vitro cell cultures of human bronchial epithelium may be sourced from primary cells obtained as (i) medical waste from lung resections and patient donations (includes post-mortem samples) or (ii) cell lines generated from cancerous tissues and (iii) primary cells transformed by viruses [13].

Table 4. The advantage and disadvantage of cell cultures

Advantages	Disadvantages
Efficiency, rapidity and cost-effectiveness.	Limited to acute toxicity
Identification of primary effects on target cells in the absence of secondary effects caused by cytokines.	The time between exposure and the measurement of the subsequent biological effects.
Identification of primary mechanisms of toxicity in the absence of the physiological and compensatory factors.	The induction of genotoxicity can only be measured by post-exposure incubation of the challenged cells for different durations. Commercial cell cultures can be contaminated or no longer reliably represent the cell phenotype claimed.

Adapted from [1, 20, 21, 26].

1.2.5. Primary Bronchial Epithelial Cell Cultures:

Forest et al. 2005 established primary bronchial epithelial cell cultures (PBEC) from lung allografts. In their study, PBECs were grown to confluence from 12 out of 33 (39%) brushings [27]. In another study, Brodlie et al. 2010 established PBECs from people's lungs with cystic fibrosis – a chronic condition caused by abnormalities in the cystic fibrosis transmembrane conductance regulator (CFTR) gene. PBECs were grown to confluence from 15 of 22 patients. In addition to that, they reported that the PBECs remained viable after storage in liquid nitrogen [28]. The unsuccessful cultures failed due to early infection with bacteria/fungi. Considering these two studies, we established a program to culture PBECs from lungs at the largest lung transplantation centre in the United Kingdom (UK) [27, 28]. The experience indicates that PBEC culture, though demanding, is possible even in patient groups where there is a high background rate of lung infection.

1.2.6. Calu-3:

Calu-3 is a lung adenocarcinoma cell line derived from a 25-year old Caucasian male. Calu-3 cells have been the subject of a large number of investigations, including tight barrier properties in electrophysiological studies and metabolic processes [29]. This cell line is immortalised, forms confluent mono-layers, develops cilia, and expresses mucin genes, particularly MUC5AC [13, 30]. Calu-3 cells have been used widely to study toxicology of nanoparticles for drug delivery [31-37].

1.2.7. Laboratory Considerations for Studying Cellular Nanotoxicology in lungs Vitro:

There is a critical requirement for standardization of the protocols used with nanotoxicology to improve the comparison of generated data and to develop our understanding in nanotoxicology. For each type of nanoparticle, the concentration range and incubation times should be defined and should be the same for all studies. Cell viability is a general term and can be assessed using several assays that determine one or more cellular parameters such as: (1) 3-

[4,5-dimethylthiazol-2-yl]-2,5- diphenyl tetrazolium bromide (MTT) assays (mitochondrial activity), (2) lactate dehydrogenase (LDH, cytosolic enzyme activity), trypan blue or propidium iodine assays (cell membrane permeability), (3) calcein AM (intracellular esterase activity), and (4) fluorescent Annexin V or caspase substrates (apoptosis indicators) [23]. These review articles [26, 38-41] deal with the subject in more detail. As they measure different parameters, the results from one assay cannot be compared directly with those of another [23]. In choosing an assay, all potential interfering factors must be considered to avoid obtaining false-positive or false-negative results. To avoid misinterpreting the results, cytotoxicity data should be verified with at least two or more independent tests [41]. It has been suggested to first test nanoparticles at a minimum of three different concentrations (low, middle, and high) based on doses required in vivo. Another consideration is interference with the assay used. Therefore, proper controls should also be carried out to confirm the results [42]. One method to reduce interference is to wash the cells with PBS after incubation with the NPs but prior to applying the cytotoxicity assay [43, 44]. Another method to avoid interference from nanoparticles is to centrifuge the plates [20, 45]. A further problem with nanotoxicology is agglomeration of nanoparticles in the culture media. It has been suggested that 5 minutes sonication with short times of vortexing is able to overcome this issue [20]. Moreover, multiple cell types should be included in models to generate data which is more representative for in vivo studies [23]. Another problem is the current deficiency of understanding between cell assays of nanoparticles in serum containing media versus those in serum free media. Serum free media is frequently employed to avoid the complication of protein particle interactions in the media [26], but this may not be the most physiologically accurate. As well as acute cytotoxicity, nanoparticles can interact with biological components in many ways; therefore, critical parameters must be selected, e.g. inflammation [23]. In addition to that, Geys et al. (2010) proposed the following consideration when publishing nanotoxicity studies: (1) a detailed explanation of the study design should include initial cell seeding density and

incubation time, and the dispersion medium (e.g. dispersion of the NPs, dilution steps, handling, vortexing, sonication time and so on), (2) metrics used for particle exposure should include volume and growing area (surface area) of the wells or cells, (3) state the cell type in the study as actively dividing or fully differentiated cells, and (4) nanoparticles should be suspended in physiologically relevant solutions [46].

1.3.The Oxidative Stress Model:

Nanoparticles can cause the formation of pro-oxidants which disrupt the balance between the biological system's ability to produce and detoxify reactive oxygen species (ROS). ROS include free radicals such as the superoxide anion ($O_2^{\bullet-}$), hydroxyl radicals ($\bullet OH$), nitric oxide (NO), and the non-radical hydrogen peroxide (H_2O_2). They are always produced in cells under normal conditions as a result of aerobic respiration. When cells are exposed to any foreign body, this may result in the production of ROS and this is a useful and physiological response to infection and is part of "innate immunity". Due to the highly chemical reactive nature of ROS, they can react with DNA, proteins, carbohydrates and lipids in a destructive manner causing cell death either by apoptosis or necrosis [1]; this shows potential detrimental effect of ROS. The ability to characterize the effects of ROS, therefore, has a wide range of applications which include the potential for nanoparticles to cause ROS related damage. Nel et al. (2006) have categorized oxidative stress models as methods for evaluating a wide range of cellular injury responses when screening systems for nanoparticles toxicity (**Figure 2**). Firstly, tier 1 (lowest level of oxidative stress) represents the induction of antioxidant and protective responses which are mediated by the transcription factor, Nrf2. Nrf-2 activates the promoters of phase II genes via an antioxidant response element (ARE). This factor regulates the activation of the antioxidant response element in the promoters of phase II genes. Secondly, tier 2 (a higher level of oxidative stress) involves the protective response that might cause pro-inflammatory responses. Inflammation is initiated through the activation of

pro-inflammatory signalling cascades [e.g., mitogen-activated protein kinase (MAPK) and nuclear factor kB (NF- kB) cascades], whereas programmed cell death could result from mitochondrial perturbation and the release of proapoptotic factors. Finally, tier 3 (the highest level of oxidative stress) is indicated as damage of the mitochondrial inner membrane electron transfer chain and the open/closed status of the permeability transition pore which can trigger cellular apoptosis and cytotoxicity [47, 48].

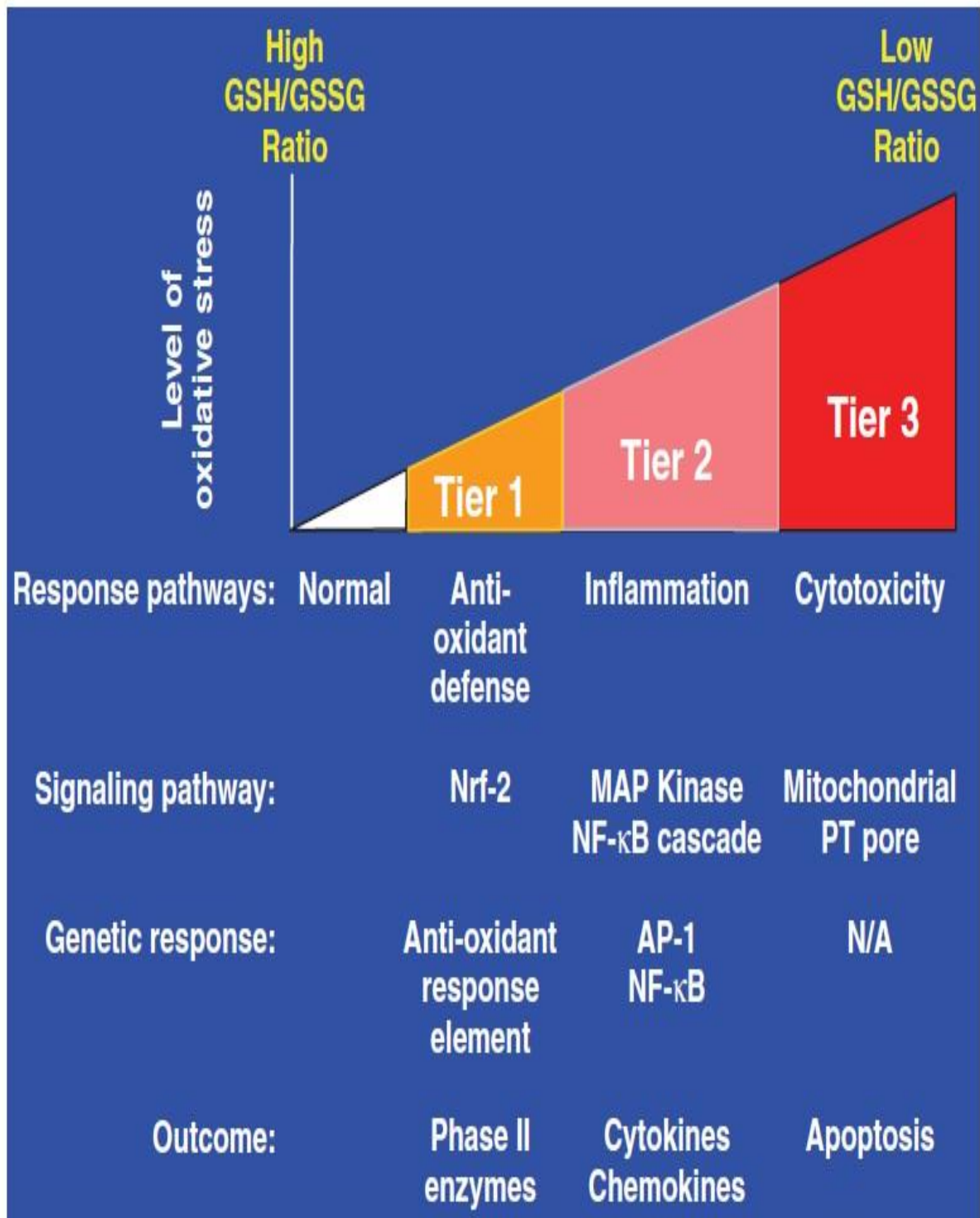


Figure 2. : An oxidative stress model. At a lower level of oxidative stress (tier 1), transcriptional activation of the antioxidant response element induces phase II antioxidant enzymes. At an intermediate level of oxidative stress (tier 2), pro-inflammatory responses are induced by activation of the MAPK and NF-κB cascades. At a high level of oxidative stress (tier 3), perturbation of the mitochondrial PT pore and disruption of electron transfer causes cellular apoptosis or necrosis. N/A means not applicable. Adapted from [47].

1.4.Nanoparticles and Drug Delivery:

1.4.1.The Route of Delivery:

The major goal of designing NPs for drug delivery is to improve drug accumulation at the targeted disease site. Drugs can be given through different administration routes, including oral, parenteral, topical, ocular, pulmonary and nasal inhalation (**Figure 3**). The principal challenge in designing NPs for drug delivery is the necessity to know which route of administration will lead to the best accumulation at the target site. NPs drug based therapy is used to deliver drugs by traditional oral and/or topical routes. An example is 5 fluorouracil (5 FU) loaded within poly DL lactide co glycolide (PLGA) NPs, which has been developed for topical delivery. The main barrier for NPs in the subcutaneous route are the keratinous layer of the skin and the chemically harsh environment in the intestinal lumen (digestive enzymes and diverse, fluctuating pH levels in the stomach, duodenum and small intestine). There are commonly three layers of topical/skin penetration: the epidermis (composed of stratum corneum (SC), lucidum, granulosum, spinosum, and basale from outermost to innermost), the dermis (a system of capillaries, nerves and epidermal appendages of hair follicles, sebaceous and sweat glands), and the hypodermis (including a layer of fat). Drugs mostly enter by transcytosis and adsorption mechanisms upon surface administration. The SC layer of the epidermis is regarded as being the main challenge for NPs because it contains a hydrophobic structure of several layers (10–20 μm) with non-living corneocytes (or bundles of keratin) surrounded by lipid bilayers. Chemical penetration enhancers (e.g., Monoolein) are used to stimulate drug diffusion and solubility within this skin layer. Therefore, disturbance of the lipid bilayers in the SC region is primarily utilised to improve permeation of the drug via the skin. On the other hand, hydrophobic encapsulation is ideal for lipophobic or hydrophilic drugs. Under the SC layer, the viable epidermis (50–100 μm) and the dermis (1–2 mm) form an immunological obstacle for foreign materials, since these layers are immunologically active regions as a result of the

existence of Langerhans and dendritic cells. Nevertheless, the coating of nanocarriers with polyethylene glycol (PEG) coating allows them to escape and avoid macrophage removal as well as improving their hydrophobicity, consequently helping NPs penetration through the SC layer. When drugs penetrate the dermis layer of the skin, they could be directed to the systemic circulation via the blood vessels of the dermis where they encounter the next obstacle – the blood components [49].

For orally administered NPs and drugs, the main challenge is the mucus layer in the intestine [49]. The mucus layer is an important component of the physical barrier and is made by a glycoprotein, mucin. Mucin comprises a glycosylated peptide backbone that generates an very viscous mucus layer effective at preventing pathogen penetration [50]. Furthermore, hydrated mucins act as a charge selective diffusion barrier. Components (cells, bacteria, lipid, salt, protein, macromolecules, and cellular debris) present in the mucus gel act to obstruct NP transportation. The morphological and physicochemical obstacles of the GI tract must be taken into account when designing orally administered NPs. The main problems include the proteolytic enzymes in the gut (pepsin, trypsin, and chymotrypsin), the brush border membrane enzymes (endopeptidases), bacterial gut flora, and the epithelial layer itself. Therefore, orally administered drugs need to be loaded in a colloidal carrier system, stimulating and extending the interaction between the drug delivery system and epithelial layer existing in the GI tract. For example, chitosan colloidal nanoparticles have been used to deliver drugs to the GI tract due to their exceptional solubility and muco-adhesive properties at acidic pH. These are insoluble at neutral pH while they become positively charged and soluble at acidic pH. This helps the muco-adhesiveness and dissolution of chitosan colloidal nanoparticles in the acidic portions of the GI tract [49].

Due to the complications associated with orally administered drugs, the parenteral route has been investigated to facilitate drug delivery directly to the systemic circulation, avoiding the intestinal or SC route. There are three categories in the parenteral route: intravenous (vein

lumen), intramuscular (large muscle such as deltoid and triceps), and subcutaneous (such as tissue under the skin). A range of NPs have been used in the parenteral routes, such as nanospheres, liposomes, niosomes and solid lipid NPs. For example, liposomes are an aqueous volume surrounded by lipid membranes, this facilitates drug delivery to the target site, in a nontoxic and rapid way. However, they have stability problems as they are susceptible to physical and chemical degradation. Thus, niosomes are used instead as they have vesicles consisting of non-ionic surfactant such as tweens, and have been studied to solve the problem of stability [49].

The injection of nanoparticles directly into the systemic circulation evades the problem of the skin and mucus barriers as well as helping in gaining access to some varieties of cancers; such as leukemia and breast cancer. The problem of this type of administration is that NPs interact with the plasma proteins and other blood components which reduces the chance of NPs reaching their target tissues. Opsonisation is a central controlling factor in the circulation, where the opsonins (e.g., complement proteins, albumin, fibrinogen, etc.) adsorb onto the surface of NPs. This renders the NPs noticeable to the mononuclear phagocyte system (MPS) (including blood monocytes and macrophages) of the immune system. The system generally works as a hunter to destroy any foreign particles in the human body. The immunological reactions produced by the MPS system, as well as the action of other plasma proteins (e.g., albumin and β -globulin) may weaken NPs and cause the premature release of the encapsulated drug [49].

The administration of NPs/drug by the pulmonary route (i.e., aerosol inhalation and intra-tracheal instillation) is being actively studied in respiratory illnesses (such as lung cancer, asthma and chronic obstructive pulmonary disorder). It is potentially the best method of drug delivery for respiratory illnesses because this route results in drug delivery straight into the lung alveoli, an environment that may not interfere with NP stability and which may have a less toxic effect. Nevertheless, the size of the NPs may affect their absorption efficiency in lung alveoli. The size range of ~50–200 nm is preferred for maximized drug localization upon

administration by inhalation. Besides the mucociliary (surface) and the macrophagic (on route) obstacles, there are further cellular obstacles in the lungs that challenge the internalization of particles (particularly hydrophilic NPs) through the cellular membrane via endocytosis. There are five mechanisms controlling the uptake of NPs in the lung alveoli: phagocytosis, macropinocytosis, clathrin-mediated, caveolin-mediated, and clathrin/caveolin-mediated endocytosis [49].

To enter the central nervous system (CNS), the key restrictions for drugs to reach the brain are the sensitivity of the brain and blood brain barrier (BBB). This barrier severely limits the drug or nanocarrier delivery, both physically (endothelial tight junctions) and metabolically (enzymes). To bypass the highly selective boundary of the BBB, NPs need to have the features of high lipophilicity and a molecular weight < 500Da. It has been discovered that surface-charged and targeted molecule-loaded polymeric nanoparticles allow quick transcytosis by the brain capillary walls as a result of improved absorption into endothelial cells [49].

Other, less used, methods of nano-drug administration are through the intranasal and the ocular route. The intranasal route is used to achieve rapid drug action avoiding the problem of degradation of labile drugs in the GI tract or inadequate transport through the epithelial cell layers. The hydrophilic coating of nanoparticles help in delivering the drugs through interaction with the nasal mucosa [49].

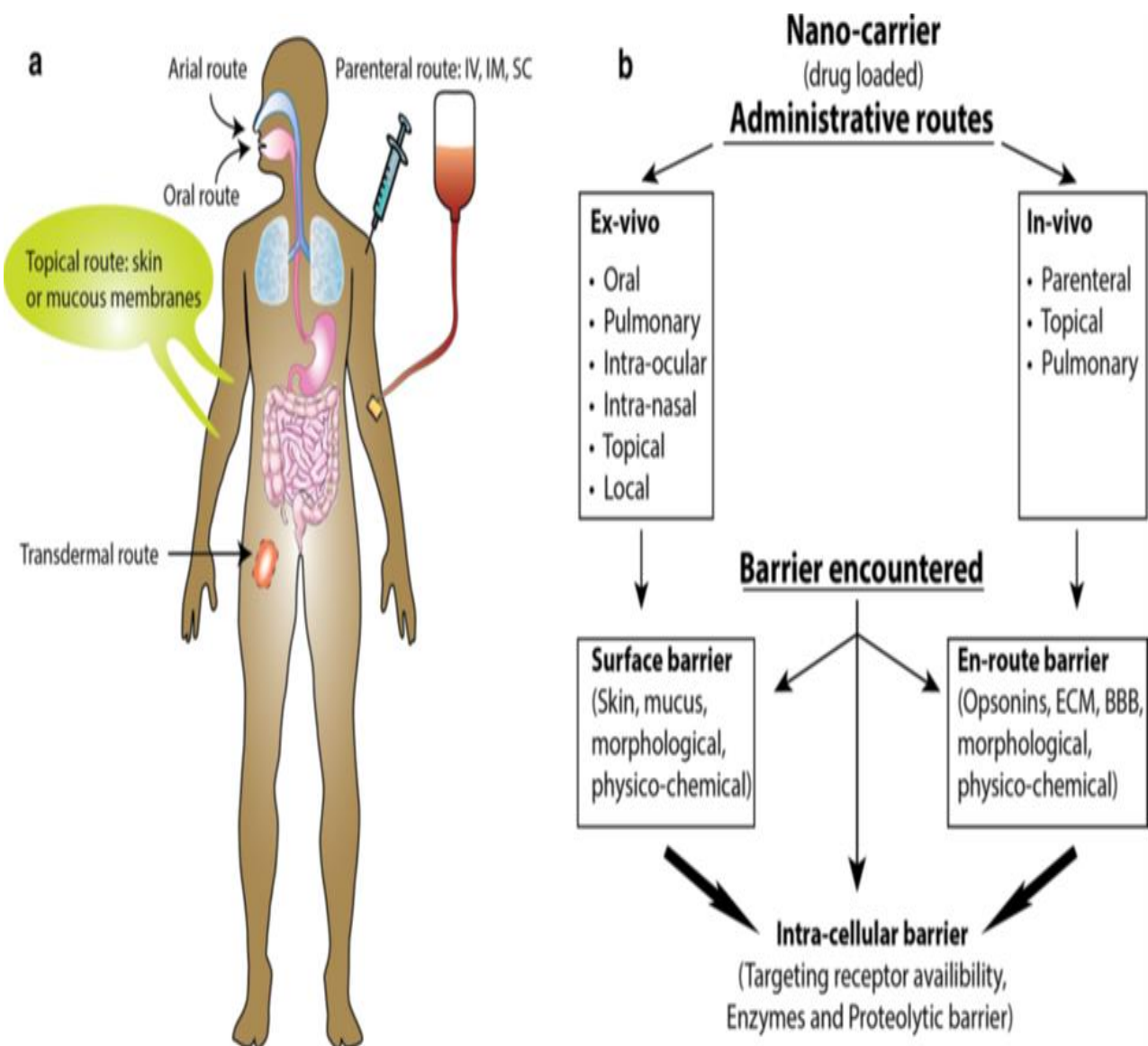


Figure 3: (a) Routes of nano-drug administration (b) and various barriers faced by nanoparticles before they reach their respective targeted tumour site. Adapted from [49].

1.4.2. Factors Affecting Drug Delivery with Nanoparticles: the Role of Particles Size and

Shape:

Particle size and size distribution are the most vital characteristics of nanoparticles which determines the *in vivo* distribution, biological fate, toxicity, and targeting ability of these delivery systems. Furthermore, size and size distribution can affect drug loading, drug release, and stability of nanoparticles. In general, NPs have shown greater cellular uptake compared to microparticles. Nanoparticles are suitable for a varied choice of cellular and intracellular targets because of their small size and mobility [51]. It has been shown that 100nm NPs had a 2.5-times greater uptake rate than 1 μ m microparticles, and a 6 times greater uptake than 10 μ m microparticles by Caco-2 cells [52]. In another study, NPs were revealed to penetrate into the submucosal layers of a rat intestinal loop model, whereas microparticles were mostly localized in the epithelial lining [53]. Dunn et al. (1997) prepared biodegradable poly (lactide-co-glycolide) (PLGA) nanosphere surface modified by the adsorption of poloxamers and poloxamines in the size range 80–150 nm. They found that PLGA nanospheres coated with poloxamer or poloxamine showed extended blood circulation times accompanied by a combined decrease in liver and spleen accumulation after intravenous injection in the rat. They also showed that 39% and 28% of the administered dose of poloxamer and poloxamine-coated PLGA nanospheres remained in blood circulation three hours post intravenous injection [54]. Gaur et al. (2000) prepared hydrogel nanoparticles of polyvinylpyrrolidone of a size less than 100 nm diameter with a precise size distribution. They demonstrated that biodistribution of these particles showed minor (<1%) uptake by the macrophages in the liver and spleen, and ~5–10% of these particles remained in circulation even 8 h after intravenous administration [55]. Liu et al. (2016) produced a novel gene carrier by binding low molecular weight chitosan with TAT (transactivator of transcription) peptide and LHRH (luteinizing hormone-releasing hormone). With the resultant TAT-LHRH-chitosan conjugate (TLC), they

studied the *in vivo* distribution of TLC/DNA NPs (TLCDNPs) in nude mice with subcutaneous hepatoma xenografts. They found that TLCDNPs delayed renal clearance of DNA and extended its time in the circulation compared to CS/DNA complexes (CDNPs) and naked DNA. However, it did not show improved build-up of DNA in the hepatoma xenografts [56]. Kumar et al. (2010) investigated multi modal organically modified silica (ORMOSIL) NPs (diameters of 20-25nm) and demonstrated that these NPs slowly clear out of the animal body by hepatobiliary excretion, without causing any clear toxicity and tissue damage [57]. Huang et al. (2011) studied the effect of shapes in fluorescent mesoporous silica NPs. They found that short rod NPs are easily trapped in the liver, while long rod NPs accumulate in the spleen. They also demonstrated that these NPs are mainly excreted in urine and faeces. The clearance rate of these NPs is mainly dependent on their shape as short rod NPs have a more rapid clearance rate than long rod NPs in urine and faeces [58]. It was shown that NPs can be also utilised in delivering therapeutic agents to try and treat diseases such as brain tumors since they can cross BBB by opening tight junctions through the action of hyper-osmotic mannitol. Tween-80 coated nanoparticles have also been reported to cross the blood-brain barrier. Drug release is also affected by particle size, in which smaller particles have an overall larger surface area, consequently, much of the related drug may be at or closer to the surface of the particle, resulting in quick drug release. On the other hand, large size particles have big cores, allowing a larger quantity of drug to be packed in allowing the contents to slowly diffuse out [59]. In addition to the size of NPs, their hydrophobicity controls the level of blood components that bind to their surface; therefore, hydrophobicity influences the *in vivo* fate of NPs. Certainly, NPs with an unmodified surface are rapidly opsonized and quickly cleared by the mononuclear phagocyte system (MPS) once they are in the blood stream. It is important to reduce the opsonisation and extend the circulation of NPs *in vivo* to maximise their ability to target and deliver the drug. This can be accomplished by coating NPs with hydrophilic polymers/surfactants or formulating NPs with biodegradable copolymers with hydrophilic

characteristics such as polyethylene glycol (PEG), polyethylene oxide, polyoxamer, poloxamine and polysorbate 80 (tween 80) [51].

Cellular internalization or uptake is the essential physicochemical criteria to be achieved before *in vivo* application. Endocytosis is the main mechanism by which cells take up small molecules. Endocytosis is a bulk active transport process where the lipid bilayer wraps to form essential vesicles, consuming energy in the form of ATP. Phagocytosis and pinocytosis are the two main endocytosis mechanisms. Phagocytic cells such as macrophages, neutrophils and dendritic cells, mediate cellular internalization by surrounding large particles ($>1\mu\text{m}$). Adsorption or receptor dependent internalization is the key mechanism of pinocytosis, which is primarily associated with particle uptake by the cells via different pathways, for example, macro-pinocytosis, clathrin mediated, caveolin dependent or independent pinocytosis. The size and surface charge of polymeric NPs are probably the primary physicochemical variables, which affect the endocytosis dependent, cellular uptake. Moreover, a positive charge on the surface of polymeric NPs might enhance further cellular attachment, initiating higher uptake either by endocytosis or by direct penetration. Cationic surfaces of polymeric NPs bind with anionic terminals of phospholipid, proteins and glycans on the cell surface [60]. Bhattacharjee et al. (2012) investigated the effects of size and surface charge of fluorescent, monodisperse tri-block co-polymeric NPs based on cellular uptake via different endocytotic pathways. They found that positive, smaller NPs (45nm) showed a higher cytotoxicity compared to the positive, bigger NPs (90nm). They also showed the involvement of size and charge in cellular uptake of NPs by clathrin (for positive NPs), caveolin (for negative NPs), and mannose receptors (for hydroxylated NPs) with smaller NPs. This is because smaller NPs have stronger interactions with the receptors than bigger NPs [61].

It has been suggested that NPs with a diameter of less than 100nm are considered best for tumor targeting via a leaky vasculature. NPs have to avoid the reticulo-endothelial system and escape early clearance by the spleen and liver to reach the targeted disease sites. The size of the particles might play a vital role in build up at diseased sites. The NPs used in nanomedicine typically range from 20 to 200 nm. NPs larger than 200 nm are automatically cleared by the spleen, whereas those smaller than 100 nm leave the blood vessels via openings in the endothelial lining [62].

1.4.3.The Concept of a Magic Bullet in Nanoparticles Drug Delivery:

In 1900, Paul Ehrlich theorized the “side-chain theory of immunity,” later replacing “side-chain” with “receptor.” This developed into the “magic bullet” idea of drugs being selective and effective for their chosen cell targets. This has led to the development of many choices of molecules, such as chemotherapeutic drugs and tumour specific monoclonal antibodies with variable target specificity [63]. Conceptually, “the magic bullet” may be able to bind selectively to specific types of cells. Due to this selective binding, the therapeutic effects of a drug occur at therapeutic sites and do not cause toxic side effects at non-therapeutic sites. This is accomplished by a carrier which has a precise affinity to specific organs, tissues, or cells [64]. Nanotechnology offers an innovative chance to represent this “magic bullet”, as seen in its use for the delivery of target-specific cytotoxic drugs, radionuclides and gene-silencing oligonucleotides as effective payloads to the tumour site [63]. It is commonly acknowledged that nano-sized carriers are a necessity for effective drug targeting. Carrier systems of 200nm diameter or less are used for drug targeting because carrier systems larger than 400nm in diameter have been shown to be quickly and easily captured by the reticuloendothelial systems. For example, big carrier systems cannot circulate in the bloodstream for a sufficient time to deliver efficient quantities to therapeutic targets [64]. There are several classification of drug delivery targeting. These include passive, active, or physical. These can target organs, cells and organelles. In passive targeting nanocarrier systems, drugs delivered intravenously have a

tendency to uniformly diffuse in the body. On the other hand, tumour cells may be able to take up particles of a definite size preferentially compared with healthy cells because of a combination of permeable tumour blood vessels and defective particle screening. This can be identified as the enhanced permeation and retention (EPR) effect which is the mechanism behind passive targeting. It has been demonstrated that PEGylated NPs smaller than 100nm have reduced plasma protein adsorption on their surface and reduced hepatic filtration. NPs with a negatively charged surface will circulate longer in blood; however, NPs with a positive charged are more readily taken up by cancer cells as they have a negative surface charge [65].

In active targeting, ligands are bound to the NPs surface to enhance their uptake selectivity. These ligands can interact with target cells and can protect NPs from enzyme damage, increasing delivery efficacy. A simple form of active targeting contains a functionalizing NP with a ligand that binds to a molecule overexpressed on cancer cells. The problem with this is that healthy cells still express the same molecule, and as healthy cells significantly outnumber tumour cells, most of the NPs fail to get to their target. This concern can be moderated by using multiple ligands, or by using ligands of diverse types [65]. The methodology of active targeting is designed to raise interactions between NPs and cells and enhance internalization of drugs without changing the total biodistribution. There are several factors affecting the active targeting strategy. These include NP architecture, the ligand conjugating chemistry, the types of ligand available, administration route, non-specific binding of proteins during the NP's journey through the bloodstream, physicochemical properties, and the choice of the targeting ligand. The interactions of ligand-functionalized NP systems with their target antigen are improved by the multivalent nature of the NP architecture and several copies of the ligand increase the avidity of the NP for its target. Actively-targeted NPs need to be in close proximity to their target antigen to identify and interact with it. That fundamental characteristic is revealed as a key test to the development of actively-targeted NPs [66].

With the aim of delivering satisfactory concentrations of systemically administered

therapeutics to target tissues, NPs need to circulate in the blood stream for as long as possible. On the other hand, proteins and peptides are quickly degraded and cleared from the blood stream, requiring methods for increasing circulation time. PEG is the typically the polymer used in the drug delivery field, as a result of its long history of safety in humans and classification as Generally Regarded As Safe (GRAS) by the FDA. The success of protein PEGylation as an approach for making longer circulating and, therefore, more effective intravenous therapies led to research of NP PEGylation for systemic uses in the early 80s and 90s [67]. Doxil® was the first FDA approved PEGylated NP product in 1995. As a result of its hydrophilic nature, PEG chains attached to NPs create a hydrated cloud with a big excluded volume that sterically prevents NPs from interacting with nearby NPs and/or blood components [68]. These particles are able to avoid clearance by cells of the MPS, therefore, increasing both circulation times and drug uptake by target cells. Therefore, these permitted NP carriers persist in the bloodstream to reach or recognize their therapeutic site of action [69]. Semete et al. (2012) investigate the effect of surface coating PLGA NPs with different concentration of polymeric surfactant (PEG and Pluronic F127). They demonstrated that the percentage of PEG and Pluronic coating particles detected in plasma was higher than that of uncoated particles, showing that systemic circulation time can also be increased with oral formulations [70]. Nissinen et al. (2016) developed a specific dual PEGylation (DPEG) for mesoporous silica and found that DPEG coating increased the circulation half-life from 1 to 241 minutes [71]. Saneja et al. (2017) developed betulinic acid (BA) loaded poly(lactide-co-glycolide)- monomethoxy polyethylene glycol nanoparticles (PLGA-mPEG NPs) and showed that these NPs can extend the circulation of BA, remarkably enhancing its half-life by ~7 times [72]. Oh and Park (2014) showed that cationic gold NPs were taken by the cells and retained for a relatively long time, possibly as a result of their intracellular agglomeration. However, the PEGylated gold NPs migrated in the cytoplasm in the form of individual particles and left the cells quickly as the PEG coating stopped interactions between gold NPs and intracellular proteins [73].

An alternative methodology to reduce non-specific clearance of NPs is to coat them with a biomimetic coating containing cell membranes – derived from erythrocytes or leukocytes – in an effort to stimulate self-recognition of the NP. This self-recognition approach depends on the interactions of anti-phagocytic ligands; one of which is mediated through CD47–SIRP/ (signal-regulatory protein alpha), sending ‘do not eat me’ signals. Lastly, the extravasation of NPs into chosen tissues may also be effected by the margination effect, in which small spherical NPs cross the circulation by accumulating within the centre of the blood vessel, regulating their contact with endothelial surfaces [67].

1.4.4. Nanoparticles in the Market and in Clinical Trials:

Around two thirds of the nanoparticles on the market or in clinical trials are focused on oncology nanomedicine therapeutics [74]. The benefit of using NPs in drug delivery for cancer cells is the ability to target delivery to the tumour and their capacity to hold thousands of drug molecules, as well as their capability to overcome solubility, stability and resistance issues [75]. Liposomal doxorubicin (Doxil™/Caelyx™) was the first anti-cancer nanomedicine accepted by the FDA in 1995 to exploit the improved permeability and retention (EPR) effect. Further nanomedicines accepted for clinical use in cancer treatment include: Myocet™, DaunoXome™, Depocyt™, Abraxane™, Genexol- PM™ and Onivyde™. Nanoparticles used in cancer therapeutics can be generally divided into five central types: liposomes, polymeric conjugates, polymeric nanoparticles, polymeric micelles and others. Most of the approved nanoparticles drugs have been designed to exploit the idea of the EPR effect with a lesser subcategory of nanomedicines developed by modifying nanomedicine behaviour with additional ligand-mediated targeting (e.g., BIND-014 (BIND Therapeutics;) and MM-302 (Merrimack Pharmaceuticals)). Generally, EPR-based therapeutics are intended to increase efficiency and tolerability by altering the pharmacokinetics and bio-distribution of the drug. They can produce sustained exposure of therapeutic levels of drug at the target. By Accomplishing the ‘right target’ and ‘right exposure’, some nanomedicines have a considerably

improved therapeutic index compared to current therapy and supports a new innovative treatment approach (e.g., AZD2811 nanoparticle (AstraZeneca)) [74]. There are several investigations into the delivery of siRNA or mRNA in NPs for therapeutic uses and most of these systems are liposome based. For example, SGT-53 has restored function of the human suppressor gene p53 by delivering a plasmid containing the wildtype p53 sequence. The potential consequences of this technology are huge because p53 dysfunction is a common feature in cancers. Furthermore, there are several research groups focusing on encapsulating and delivering chemotherapeutics in NPs, mostly liposomes. For instance, VYEXOS/ CPX-351 is a combination therapy, a synergistic combination of two anticancer drugs (cytarabine and daunorubicin). Other systems used polymeric or micelle formulations of established chemotherapeutics and treatments. For instance, there are diverse paclitaxel or docetaxel micelle formulations currently in clinical trials. A number of other nanoparticle cancer therapies are aimed to treat cancer in non-standard methods. JVRS-100 is a cationic liposome incorporating noncoding plasmid DNA to stimulate the immune system to fight against the host's cancer. Stimulation of the immune system is through the CpG motifs contained in the DNA, in combination with the adjuvant effects from the liposome [76]. The safety and toxicity of these products needs to be well understood before marketing can occur to avoid any unknown side effects. Therefore, investigations must be carried out to understand and predict how NPs will disturb or interact with biological systems. This will require the improvement of existing assays, or the development of new assays which are not interfered with by the NPs themselves. NPs may interact with numerous categories of cells, organs, and tissues on the way from the site of administration to the planned target. They can effect coagulation, complement activation, immune system compatibility, phagocyte activation, and other unwanted responses [77]. **Tables 5 and 6** show the nanomedicines currently on the market and those currently in development.

Table 5: Examples of marketed nanomedicines

Nanoparticle type	Drug	Product name/company	Indication
Liposomes	Doxorubicin	Myocet™/Teva UK	Metastatic breast cancer
		Doxil™/Janssen	Ovarian cancer (secondary to platinum based therapies) HIV-associated Kaposi's sarcoma (secondary to chemotherapy) Multiple myeloma (secondary)
	Vincristine	Marqibo™/Spectrum Pharmaceuticals	Acute lymphoblastic leukaemia
	Daunorubicin	DaunoXome™/Galen	HIV-related Kaposi's sarcoma
	Cytarabine	Depocyt™/Pacira Pharmaceuticals	Lymphomatous meningitis
	Irinotecan	Onivyde™/Merrimack Pharmaceuticals	Metastatic pancreatic cancer (2nd line) Gastric cancer
	Mifamurtide	MEPACT/Millennium	Treatment for osteosarcoma (primary following surgery)
Polymeric conjugates	Asparaginase	Oncaspar™ (PEG)/Baxalta	Acute lymphoblastic leukaemia
Polymeric micelles	Paclitaxel	Genexol-PM™/Samyang Biopharmaceuticals	Breast cancer Non-small cell lung cancer Ovarian cancer
Other	Paclitaxel	Abraxane™/Celgene	Advanced breast cancer Advanced non-small cell lung cancer Advanced pancreatic cancer
Iron-replacement nanoparticle therapies			
colloid	Iron dextran	CosmoFer/INFeD/Ferrisat (Pharmacosmos)	Iron deficient anaemia
		DexFerrum/DexIron (American Regent)	Iron deficient anaemia
	Iron gluconate	Ferrelecit (Sanofi)	Iron replacement for anaemia treatment in patients with chronic kidney disease
	Iron sucrose	Venofer (American Regent)	Iron replacement for anaemia treatment in patients with chronic kidney disease

	Iron polyglucose sorbitol carboxymethylether	Feraheme (AMAG)/ Rienso (Takeda)/ Ferumoxytol	Iron deficiency in patients with chronic kidney disease
	Iron carboxymaltose	Injectafter/Ferinject (Vifor)	Iron deficient anaemia
	10% Iron isomaltoside 1000 colloid	Monofer (Pharmacosmos)	Treating iron deficiency and anaemia when oral methods do not work or when iron delivery is required immediately
	5% Iron isomaltoside 1000 colloid	Diafer (Pharmacosmos)	Iron deficient anaemia
Nanoparticle imaging agents			
colloid	Iron dextran	Feridex I.V. (AMAG)/ Endorem	Imaging of liver lesions
	Iron carboxydextran	Resovist (Bayer Schering Pharma)/ Cliavist	Imaging of liver lesions
	Iron dextran	Ferumoxtran-10/ Combidex/Sinerem (AMAG)	Imaging lymph node metastases
Nanoparticle vaccines			
Liposome	Liposome with hepatitis A virus	Epaxal (Crucell)	Hepatitis A vaccine
	Liposome with trivalent-influenza	Inflexal V (Crucell)	Influenza vaccine
Particle anesthetics			
Liposomal	Liposomal propofol	Diprivan	Induction and maintenance of sedation or anaesthesia
Nanoparticles for fungal treatments			
Liposomal	Liposomal amphotericin B	AmBisome (Gilead Sciences)	Cryptococcal Meningitis in HIVinfected patients Aspergillus, Candida, and/or Cryptococcus species infections (secondary) Visceral leishmaniasis parasite in immunocompromised patients
Nanoparticles for macular degeneration			
Liposomal	Liposomal verteporfin	Visudyne (Bausch and Lomb)	Treatment of subfoveal choroidal neovascularization from age-related macular degeneration,

			pathologic, or ocular histoplasmosis
--	--	--	---

Adapted from [74, 76].

Table 6: Examples of nanomedicines in clinical development

Nanoparticle type	Drug	Product name/company	Indication	Phase	
Cancer therapy					
liposomes	Doxorubicin	ThermoDox™/Celsion	Temperature-triggered doxorubicin release: Breast cancer recurrence at chest wall (microwave hypothermia) Hepatocellular carcinoma (radiofrequency ablation) Liver tumours (mild hypothermia) Refractory solid tumours (magnetic resonance high intensity focused ultrasound)	Phase I/II Phase III Phase I Phase I	
		2B3-101/2-BBB Medicines BV	Brain metastases Glioma	Phase II	
	Irinotecan	Onivyde™/Merrimack Pharmaceuticals	Gastric cancer	Phase II	
	Liposomal formulation of cytarabine: daunorubicin (5:1 molar ratio)	VYEXOS CPX-351 (Celator Pharmaceuticals)	leukaemias	Phase II Phase II Phase I Phase II Phase IV Phase III	
	Cisplatin	Lipoplatin/Regulon		Non-small cell lung cancer	Phase III
			SPI-77/ALZA Pharmaceuticals	Ovarian cancer	Phase II
			Aroplatin/Aronex Pharmaceuticals	Malignant mesothelioma	Phase II
	Oxaliplatin	MBP-426/Mebiopharm	Gastrointestinal adenocarcinoma	Phase II	

Paclitaxel	LEP—ETU/Insys	Breast cancer	Phase II
	EndoTAG-1/MediGene	Breast cancer	Phase II
	PNU-91934/MSKCC	Esophageal cancer	Phase II
SN-38	LE-SN38/Neopharm	Metastatic colorectal cancer	Phase II
Irinotecan: Floxadine 1:1 ratio	CPX-1/Celator	Colorectal cancer	Phase II
Pegylated liposomal mitomycin-C	PROMITIL (Lipomedix Pharmaceuticals)	Solid tumours	Phase I
FUS1 (TUSC2) encapsulated liposome	Oncoprex (Genprex)	Lung cancer	Phase I/II
Liposomal eribulin mesylate	Halaven E7389-LF (Eisai)	Solid tumours	Phase I
¹⁸⁸ Re-N,N-bis (2-mercaptoethyl)-N0,N0-diethylethylenediamine pegylated liposome	¹⁸⁸ Re-BMEDA-liposome	Advanced solid tumours	Phase I
Mitoxantrone liposome	Mitoxantrone Hydrochloride Liposome (CSPC ZhongQi Pharmaceutical Technology)	Lymphoma and breast cancer	Phase I Phase II Phase I Phase II Phase II
Cationic liposome incorporating plasmid DNA complex for immune system stimulation	JVRS-100	Leukemia	Phase I
Liposomal curcumin	Lipocurc (SignPath Pharma)	Solid tumours	Phase I/II
Liposomal formulated cisplatin with specific degradation-controlled drug release via phospholipase A2 (PLA2)	LiPlaCis (LiPlasome Pharma)	Advanced or refractory tumours	Phase I
HER2-targeted liposomal doxorubicin (PEGylated)	MM-302 (Merrimack Pharmaceuticals)	Breast cancer	Phase I Phase II/III
Paclitaxel Liposome	LIPUSU® (Nanjing Luye Sike Pharmaceutical Co., Ltd.)	Advanced solid tumours, or gastric, breast cancer	Phase IV Phase IV Phase II
Lipid particle targeting polo-like kinase	TKM-080301 (Arbutus Biopharma)	Hepatocellular carcinoma	Phase I/II

	1 (PLK1) for delivery of siRNA			
	siRNA liposome for EphA2 knockdown	siRNA-EphA2-DOPC	Solid tumours	Phase I
	Proprietary single-stranded DNAi (PNT100) encapsulated in lipid nanoparticles	PNT2258 (ProNAi Therapeutics)	Lymphomas	Phase II Phase II Phase II
	Growth factor receptor bound protein-2 (Grb-2) antisense oligonucleotide encapsulated in neutral liposomes	BP1001 (Bio-Path Holdings)	Leukemias	Phase I
	DsiRNA lipid nanoparticle for NYC oncogene silencing	DCR-MYC (Dicerna Pharmaceuticals)	Solid tumours, multiple myeloma, lymphoma, or hepatocellular carcinoma	Phase I Phase I/II
	AtuRNAi liposomal formulation for PKN3 knockdown in vascular endothelium	Atu027 (Silence Therapeutics GmbH)	Pancreatic cancer	Phase I/II
	Cationic liposome with anti-transferrin receptor antibody, encapsulating Wildtype p53 sequence	SGT-53 (SynerGene Therapeutics)	Glioblastoma, solid tumours, or pancreatic cancer	Phase I Phase I Phase I Phase II
	RB94 plasmid DNA in a liposome with anti-transferrin receptor antibody	SGT-94 (SynerGene Therapeutics)	Solid tumours	Phase I
	Double-stranded RNA mimic of miR-34 encapsulated in liposomes	MRX34 (Mirna Therapeutics)	Liver cancer	Phase I
	Anti-EGFR bispecific antibody minicells (bacteria derived nanoparticles) with a miR-16 based microRNA payload	TargomiRs (EnGeneIC)	Mesothelioma and non-small cell lung cancer	Phase I
Polymeric conjugates				
	Paclitaxel	Opaxio™ (Polyglycerol adipate)/CTI Biopharma	Ovarian cancer Non-small	Phase III maintenance

			cell lung cancer (women)	Phase II
	Irinotecan	NKTR102 (PEG)/Nektar	Metastatic breast cancer	Phase III
	Camptothecin	CRLX101 (nanoparticle)/Cerulean	Renal cell carcinoma (3rd/4th line) Ovarian cancer (2nd/3rd line)	Phase II
		XMT1001 (Fleximer™)/Mersana	Gastric cancer (2nd line) Non-small cell lung cancer (2nd/3rd line)	Phase II
	Diaminocyclohexane (DACH) Platinum	AP 5346 (Hydroxypropylmethacrylate)/ProLindac™	Ovarian cancer	Phase II
	Docetaxel	DEP™ (G5 PEG-Polylysine)/StarPharma	Advanced cancers	Phase I
		CriPec™ docetaxel (nanoparticle)/Cristal Therapeutics	Solid tumours	Phase I
Polymeric NPs	AZD2811 (AZD1152 hydroxyquinazoline pyrazol anilide; Aurora-B Kinase Inhibitor)	AZD2811 (Accurin™) nanoparticle/AstraZeneca	Advanced solid tumours	Phase I
	Cyclodextrin based nanoparticlecamptothecin conjugate	CRLX101 (Cerulean)	Ovarian, renal cell, small cell lung, or rectal cancers	Phase II Phase I/II Phase I Phase II Phase II
	Cyclodextrin based nanoparticledocetaxel conjugate	CRLX301 (Cerulean)	Dose escalation study in advanced solid tumours	Phase I/II
Polymeric micelles	Paclitaxel	NC-4016/NanoCarrier™	Advanced solid tumours or lymphomas	Phase I
		Genexol-PM (Samyang Biopharmaceuticals)	Head and neck or	Phase II Phase II

			breast cancer	Phase IV
	Docetaxel micelle	Docetaxel-PM DOPNP201 (Samyang Biopharmaceuticals)	Head and neck cancer and advanced solid tumours	Phase II Phase I
		CriPec (Cristal Therapeutics)	Solid tumours	Phase I
Other	Irinotecan	HA-irinotecan HyACT™/Alchemia	Colorectal cancer Lung cancer	Phase II Phase III
	Tumour Necrosis Factor (TNF)	CYT-6091/CytImmune	Non-small cell lung cancer	Phase II
	Albumin-bound	ABI-009 (Aadi with Celgene)	Bladder cancer, PEComa, or pulmonary arterial hypertension	Phase I/II Phase I Phase II
		ABI-011 (NantBioScience)	Solid tumours or lymphomas	Phase I
	Hafnium oxide nanoparticles stimulated with external radiation to enhance tumor cell death via electron production	NBTXR3 PEP503 (Nanobiotix)	Locally advanced squamous cell carcinoma	Phase I
Gene therapy				
liposomes	siRNA lipid nanoparticle conjugated to Vitamin A	ND-L02-s0201 (Nitto Denko)	Hepatic fibrosis	Phase I
	Lipid particle containing three RNAi therapeutics that target three sites on the HBV genome	ARB-001467 TKM-HBV (Arbutus Biopharma)	Hepatitis B	Phase II
	Lipid nanoparticle RNAi for the knockdown of disease-causing TTR protein	Patisiran ALN-TTR02 (Alnylam Pharmaceuticals)	Transthyretin (TTR)-mediated amyloidosis	Phase III Phase II Phase III
Other therapy				
liposomes	Sphingomyelin and cholesterol liposomes for toxin neutralization	CAL02 (Combioxin SA)	Pneumonia	Phase I
	Liposomal Prednisolone (PEGylated)	Nanocort (Enceladus in collaboration with Sun Pharma Global)	Rheumatoid arthritis and hemodialysis	Phase II Phase III

			fistula maturation	
	Liposomal formulation of α -GalCer	RGI-2001 (Regimmune)	Mitigating graft versus host disease following stem cell transplant	Phase I/II
	F-butane encapsulated in a lipid shell	Sonazoid	Contrast enhanced ultrasound for imaging hepatocellular carcinoma, skeletal muscle perfusion, or for estimating portal hypertension	Phase II Phase IV
Polymeric micelles	PEG, iron, and amifostine micelle Transferrin-mediated chelation for amifostine release	RadProtect (Original BioMedicals)	Dose escalation and safety for acute radiation syndrome	Phase I

Adapted from [51, 74].

1.4.5.Challenges Facing Mucosal Nanoparticles Drug Delivery:

The mucosal barrier can be found in the respiratory, gastrointestinal and reproductive tracts as well as the nostrils, eyes and mouth. Mucus is essential for protecting the cellular epithelia from chemical and mechanical damage [78]. There are several physiological barriers in mucosal delivery, including the environment with varying pH and numerous enzymes, which challenges the bioactivity of agents. Furthermore, the intact epithelium and the sticky mucus layer are considered as the absorption and permeation barrier, respectively [79]. Mucus is a dynamic semipermeable barrier which allows the exchange of nutrients, water, gases, odorants, hormones, and gametes, whereas being impermeable to most bacteria and many pathogens. Mucus is constantly secreted and shed or digested. Therefore, NPs drugs need to move ‘upstream’ via the unstirred layers of mucus adhering to the cells on the epithelium surface or penetrate a mucus ‘blanket’ before it is shed. The balance between the rate of secretion and the rate of degradation and shedding will determine the thickness of the mucus. On the other hand, by constantly secreting fresh mucus, the unstirred layer is continually and rapidly replaced. Accordingly, NPs drug delivery need to migrate upstream to reach the epithelium [80]. There are two main layers of the airway mucus barrier: the periciliary layer (PCL, 10 μ m thick) overlying the cells and surrounding the cilia, and the mucus gel (60 μ m thick) sitting on top of the PCL [15]. The PCL lacks gel forming mucins, however, it does have membrane bound mucins expressed on the cilia surface and the epithelial cell apical surfaces [81]. During particles inhalation, they become attached to the mucus gel layer and are then cleared from the lungs by the action of the cilia moving the mucus layer up and out of the lungs [15]. In gastrointestinal tract, an effective NPs drug delivery needs to pass through three obstacles in adequate quantities to produce a biological effect. These include the digestive barrier in the lumen, the mucus barrier, and the epithelial barrier [81]. Nanoparticles drug systems need locally sustained and have controlled drug release, deep tissue penetration, and protection of cargo therapeutics at both extracellular and intracellular

levels. The drug formulations need to have mucoadhesive properties to improve the therapeutic efficacy of many drug across the mucus layers. Mucoadhesion can be known as an attractive interaction at the interface between a pharmaceutical dosage form and a mucosal membrane. In addition to that, NPs should be able to cross at least the outermost layers of the mucus barrier quickly to escape mucus clearance. NPs have to escape adhesion to mucin fibres and be small enough to escape significant steric inhibition by the dense fibre mesh [78]. The pore sizes of mucus gels are around 100-200nm while those in the lung membrane bound mucin layer are around 30nm; therefore, only NPs with similar to or less than mucus pore size may potentially penetrate without modification of these layers [15]. Inhaled NP drugs need to overcome the same primary defence mechanisms which prevent all inhaled insults from engagement with and adsorption by lung epithelial tissue and the mucus gel barrier (**Figure 4**). For $\leq 100\text{nm}$ NPs, diffusion is regular (i.e. Brownian) and fast, simply passing through the mucus gel barrier before clearance. Larger NPs maybe represent major challenges over mucosal drug delivery in which they are similar to or larger than the pores within the mucus gel network. Diffusion is not simple Brownian motion and usually much less quick [82]. It is essential for effective mucosal delivery, NPs need to penetrate the mucus layer with minimum damage to the mucus layer. Furthermore, NPs need to stay unchanged by extracellular secretions [15]. There are two goals desirable in mucosal drug delivery: 1) To ensure drug passage through the mucus barrier to the epithelium before drug elimination from the respective organ by mucus clearance; and 2) To ensure carrier particles accomplish a recommended arrival time and drug uptake schedule at the epithelium. This can be achieved if one can control (one-sided) the diffusive passage times of drug carrier particles, from deposition at the mucus interface, through the mucus barrier, to the epithelium [82].

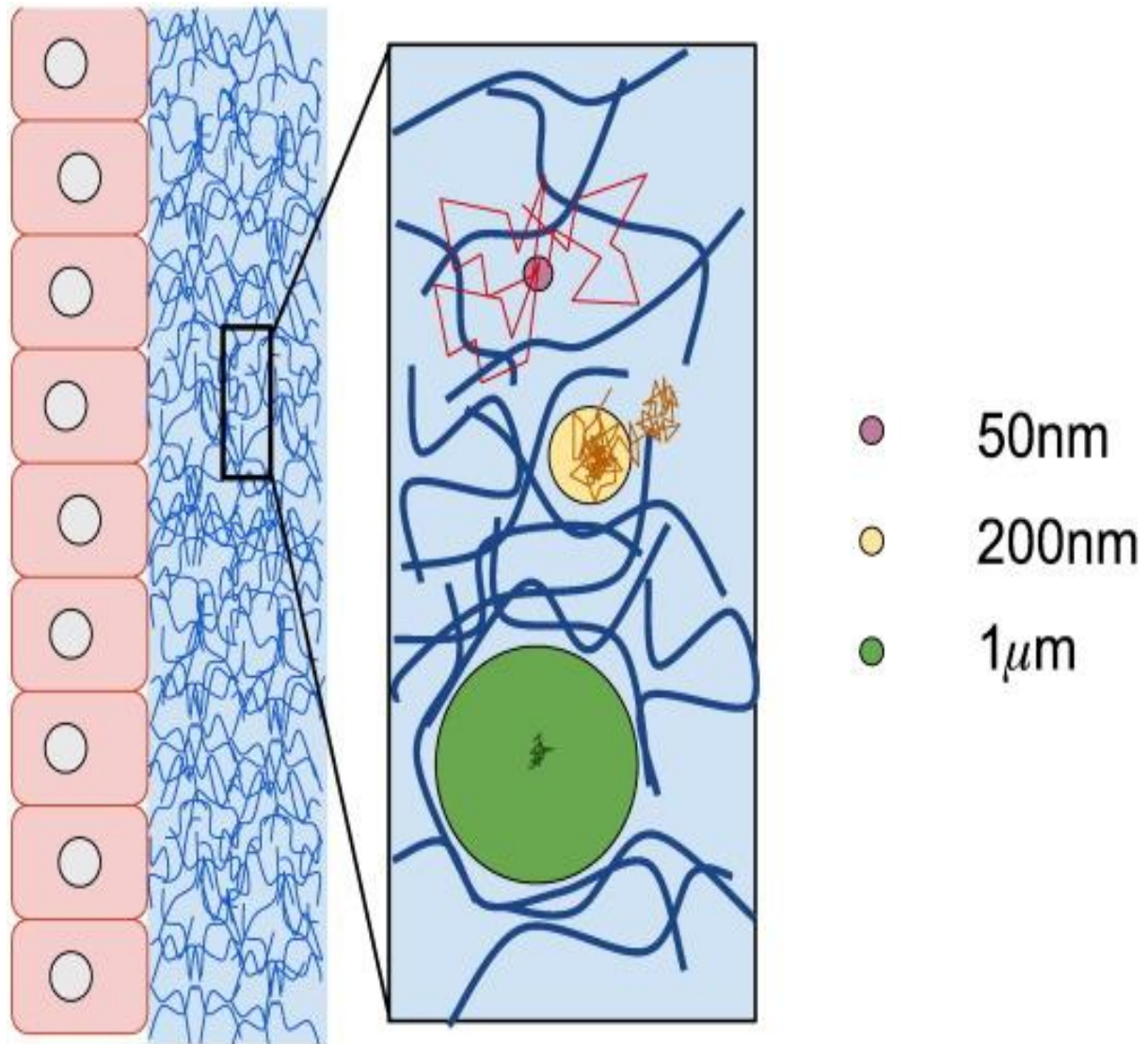


Figure 4: The effect of particle size on the nature (Brownian vs, non-Brownian) of diffusive motion in mucus barriers. Class 1: small molecules and nanoparticles $\leq 100\text{nm}$ which do not chemically bind to the mucus mesh are slightly affected by the mucus microstructure and quickly move by Brownian motion through the barrier. Class 2: Muco-inert particles of size related to mucus pores experience steric interactions with the mesh and entropic fluctuations from the mucus gel microstructure. Their increments are not only decreased compared with freely diffusing smaller particles, but they are associated, violating Brownian motion. Class 3: Muco-inert particles larger than the mucus pores (e.g. 500nm to $1\mu\text{m}$) experience the full range of entropic fluctuations from the mucus microstructure. These particle increments are similarly correlated, replicating elastic memory of the mucus gel, and show transient, anomalous, sub-diffusive behaviour. Adapted from [82].

1.4.6. The Release of Drug from Nanoparticles:

Biodegradable NPs are gaining support based on their capability as a sustainable carrier for site specific delivery of vaccines, genes, drugs and other biomolecules in the body. They help in enhanced biocompatibility, superior drug/vaccine encapsulation and are suitable release profiles for numerous drugs, vaccines and biomolecules used in a variety of applications in the field of medicine. There are several biodegradable nanoparticles, these include poly-D-L-lactide-co-glycolide (PLGA), polylactic acid (PLA), poly- ϵ -caprolactone (PCL), chitosan, poly-alkyl-cyano-acrylates (PAC) and gelatin. A high loading ability for the NP drugs is considered to be one of the most desired qualities of successful drug delivery. The amount of polymer carrier needed for drug delivery in the body could be reduced by the high loading capacity of NPs. There are two methods of loading drugs into NPs: by incorporating the drug at the time of NP production, and by adsorbing the drug after the formation of the NP. These two methods allow several advantages such as the encapsulation of the drug in the polymer, dispersion of the drug in the polymer, adsorption of the drug onto the surface of the NPs and the chemical binding of the drug to the polymer. The chemical structure of both the drug and the polymer, as well as the conditions of the drug loading can be influenced by the amount of drugs bound to the NPs and the type of interaction between the drugs and the NPs. The drug release mechanism is also an essential factor during drug formulation. Ordinarily, the drug release rate can be determined by drug diffusion through the polymer matrix, solubility of the drug, desorption of the surface bound/adsorbed drug, NP matrix erosion/degradation, and the combination of the erosion diffusion process. Moreover, drug release may be influenced by the size of the NPs and the loading effectiveness of the drug. The drug loading efficiency is important to control the initial burst and the sustained release of the NP drug. It should be noted that larger particles have a smaller initial burst release than smaller particles. The release mechanism is predominately by diffusion when the diffusion of a drug is faster than the matrix erosion. The fast initial release or burst of drug is mostly due to weakly bound or adsorbed vaccine/drug

on to the surface [83].

Andersen et al. (2009) developed a DNA origami method in three dimensions by creating an addressable DNA box (42 X 36 X 36 nm³) in size that can be opened in the presence of externally supplied DNA (keys). They were able to functionalize the lid of the DNA box with a dual lock–key system consist of DNA duplexes with sticky-end extensions to offer a ‘toehold’ for the displacement by externally added ‘key’ oligonucleotides. They found that the addition of key oligonucleotides leads to the opening of the lid, causing a decline in the efficient fluorescence resonance energy transfer (FRET) efficacy as the distance between the two dyes increases. They also investigated the kinetics of the opening process. They demonstrated that both keys are required for a full decrease in the FRET signal, indicating that a closed box can be programmed to open in response to at least two external signals. The box lid can be made to close again in the existence of specific signals. Therefore, the lid of the DNA box has the possibility to react to complex combinations of oligonucleotide sequences, for instance, cellular messenger RNAs or micro RNAs. The opening mechanism of the DNA box works in natural environments which lets biologically active components such as enzymes, to be packaged, offering control of access to their relevant substrates [84]. Consequently, the box can be programed to open and release the cargo at a specific site.

There are several advantages for using magnetic NPs in drug delivery. These include the ability to target a specific site (e.g. tumour), reducing the systemic distribution of cytotoxic compound, and improving uptake at target site, leading to effective treatment at lower doses. When the magnetic carrier is concentrated at the tumour or other target in vivo, the therapeutic agent is released from the magnetic carrier, either by enzymatic activity or via changes in physiological conditions (for example pH, osmolality, or temperature). This results in improved uptake of the drug by the tumour cells at the target sites. Magnetic targeting is dependent on the attraction of magnetic NPs to an outer magnetic field source. [85]. Riedinger et al.(2013) investigated the thermal decomposition of a thermo-sensitive molecule (azobis[N-(2-

carboxyethyl)-2-methylpropionamide]). Fluoresceineamine (FA) was bound to the azo molecule at the iron oxide nanoparticle (IONP) surface, functionalized with poly (ethylene glycol) (PEG) spacers of different molecular weights. They found that by oscillating the magnetic field at the target site, a significant local heating occurred with a temperature increase of up to 45 °C. This led to the decomposition of the NP and drug release. In addition to that, they replaced FA with the chemotherapeutic agent doxorubicin (DOX) in the same NP arrangement. They demonstrated that the alternating magnetic field (AMF) triggered distance- dependent release of the drug in a cytotoxicity assay on KB cancer cells [86].

1.5.. Cytotoxicity:

1.5.1. Cytotoxicity of Nanoparticles:

Although nanoparticle cytotoxicity in relation to the airways has been studied, different cells have been cultured, with varying incubation conditions and different assays published. These studies also contain different nanoparticle concentrations and exposure times, and overall it is hard to conclude whether the experimental cytotoxicity is physiologically relevant [38]. This section examines the cytotoxicity of several classes of nanoparticles currently being developed in vitro using lung epithelial cell models for drug delivery. A summary of the experimental setups and results for these nanoparticles are provided in **Table 7**.

An example of this is the work of Tomoda et al. 2009. They prepared poly (lactide-co-glycolide) (PLGA) nanoparticles loaded with the anticancer drug, TAS-103, in the form of nanocomposite particles as an inhalable agent for the treatment of lung cancer. They also aimed to deposit the nanocomposite particles effectively deep in the lungs and evaluate cytotoxicity against adenocarcinomic human alveolar basal epithelial cells (A549) cells. They found that the sizes of 5% and 10% TAS-103 loaded PLGA were 201 and 212 nm, respectively. Furthermore, they also showed that there was no difference in cytotoxicity between 5% and 10% TAS-103 loaded PLGA nanocomposite particles [87].

As previously discussed (section 1.4.2. Factors Affecting Drug Delivery with

Nanoparticles: the Role of Particles Size and Shape), it should be noted that smaller nanoparticles will penetrate deeper into the lung [21]. Therefore, they should have used smaller sized nanoparticle to ensure physiological relevance. It is also important to allow time for the plated cells to form tight junctions and pre-incubation of the plates for only 3h – as in this study – is not long enough.

The coating of nanoparticles has been shown to be important to avoid cell death. For example, Baoum et al. 2010 examined poly (D, L-lactide-co-glycolide) (PLG) nanoparticles ability to transfect A549 cells. They demonstrated a minimum cytotoxic effect of cationic coating material [88].

Burgess et al. 2010 prepared a novel nano-sized delivery vehicle composed of phospholipid (PL) and apolipoprotein A-I, NanoDisk (ND), to which they added amphotericin B (AMB) as a payload (ND-AMB). They investigated whether ND-AMB compared to other formulations preserved lung cell integrity in vitro as AMB can be toxic to mammalian cells and reduce lung function when inhaled. AMB, a potent antifungal agent, has been employed as an inhalable therapy for pulmonary fungal infections. They found that Calu-3 cells incubated with AMB/Deoxycholate (DOC) were significantly less viable than controls incubated with PBS alone $16.1 \pm 5.6\%$, $n=3$ ($p < 0.0001$), assessed by MTT viability. This was also shown by LDH release which was significantly increased ($p < 0.0001$). However, cells exposed to the ND- vehicle alone (i.e. ND-empty of content), were fully protected from the cytotoxicity of AMB/DOC and were indistinguishable from control cells by MTT and LDH release. They also showed that the viability of cells exposed to ND-AMB was not significantly different from the control, while LDH release from cells treated with ND-AMB was lower than AMB/DOC alone ($p < 0.0001$). In addition, treatment with ND-AMB did not significantly affect MTT or LDH levels versus AMB/DOC. ND-empty, ND-AMB or ND-AMB, in the absence of AMB/DOC, did not reduce viability or promote LDH release. They concluded that ND-AMB and ND-empty, but not ND-AMB, are able to protect against cell death [34].

Bains et al. 2010 investigated surfactant-coated micro emulsion pDNA nanoparticles to explore the potential of adapting a formulation process for pulmonary gene delivery. The statistical analysis for the study showed no significant loss in cell viability ($p>0.05$) between blank, untreated cells and cells treated with the washed, aerosolised pDNA formulation based on the MTT assay. A significant reduction in cell viability ($p<0.05$) was observed when dioleoyl trimethylammonium propane (DOTAP) liposomes, the transfection agent, were added to the cell culture medium. Statistical analysis showed a significant reduction ($p<0.05$) in cell viability when cells were treated with 80 pressurised metered dose inhalers (pMDI)-aerosolised doses, compared with 9 doses of the same formulation; this demonstrates the sensitivity of the MTT assay [89].

Alpha-1 antitrypsin deficiency is a cause of significant lung disease in some patients, which can lead to the need for lung transplantation. Pirooznia et al. 2012 encapsulated Alpha-1 antitrypsin in PLGA nanoparticles. Alpha 1- antitrypsin (α 1AT) is a 54 kDa glycoprotein which belongs to the superfamily of serpins and inhibits different proteases. α 1AT protects the lung from cellular inflammatory enzymes, especially elastase, therefore, it is known as the human neutrophil elastase inhibitor. In the absence of α 1AT, the neutrophil elastase released by lung neutrophil are not inhibited, leading to elastin breakdown and the loss of lung elasticity. This causes degradation of the lung tissue resulting in pulmonary complications such as emphysema and chronic obstructive pulmonary disease (COPD) in adults. α 1AT is not only an anti-inflammatory protein but also an immune system regulator, regulating lymphocyte proliferation and cytotoxicity, as well as mediating monocyte and neutrophil functions. Besides an anti-apoptotic function in lung epithelial cells in-vitro, α 1AT has a broad anti-inflammatory effect in humans. The aim of the above study was to prepare a wide range of particle sizes as a carrier for protein-loaded nanoparticles to deposit in different parts of the respiratory system, particularly in the deep lung. The sizes generated ranged from 1 μ m to 100nm. Various lactide to glycolide ratios of the copolymer were used to obtain different

release profiles of the drug which covers extended and rapid drug release in one formulation. They found that the viability of CorL105 cells (a human lung epithelial cancer cell line) treated with different concentrations of free and loaded nanoparticles remained unchanged and cells were more than 80% viable. In addition, the morphology of cells before and after treatment with nanoparticles was unchanged [43]. The problem with this study is that the cells used do not form fully attached layers in culture and, as such, do not represent a true lung epithelium.

Ungaro et al. 2012 designed and developed a pulmonary delivery system for antibiotics such as tobramycin (Tb), based on spray dried lactose/PLGA nano-embedded microparticles (NEM) engineered at both nanosize and microsize level. They demonstrated that MTT measured metabolic activity showed a nanoparticle dose dependent fall with calcium silicate (CS)/ alginate / PLGA particles being the most cytotoxic at 1 mg/ml causing 82% cell death but showed similar cytotoxicity to the other nanoparticles at 0.5 mg/ml ranging between 20-40% cell death, using A549 cells. Interestingly the presence of the antibiotic in the NPs reduced cytotoxicity [90].

Solid tumours have an acidic environment and lysosomes inside the cell are acidic compared to the rest of the cytoplasm. This may be useful for nanotechnology based therapies; for example, if the nanoparticles can swell in response to pH changes, their cargo could be released. In another example, crosslinked nanoparticles made of acrylate based hydrophilic polymers where the hydroxyl groups are masked by pH-labile protecting groups in 2, 4, and 6 –trimethoxybenzaldehyde. They are stable at pH 7.0 but at pH 5.0 the hydroxyl groups are exposed (masking groups removed) making the nanoparticles hydrophilic which causes swelling and cargo release [91]. Boylan et al. 2012 formulated DNA containing nanoparticles that respond to changes in pH, resulting in gene transfer via a nucleoli-independent pathway. The nanoparticles were formed by a complex of polyethylene glycol (PEG), poly-L-histidine and poly-L-lysine forming a triblock copolymer system, PEG-CH12K18. They used transformed human bronchial epithelial cells BEAS-2b cells, seeded

and incubated overnight [92]. These cells are lung epithelial-like, however, they only represent an epithelial population before confluency. As once confluent they undergo squamous differentiation and, as such, are not a reliable model for lung epithelial cell toxicity studies (Data from ECACC general cell collection). They carried out cytotoxicity tests of the DNA nanoparticles made with PEI, PEG-CH12K18, or PEG-CK30 at various DNA doses using the MTT assay. The PEI DNA nanoparticles produced the highest cytotoxicity, with a 50% reduction in metabolic activity at the highest dose 10 μ g/well. Cells incubated with either PEG-CH12K18 DNA nanoparticles or PEG-CK30 DNA nanoparticles still had more than 90% of their metabolic activity intact across all doses tested. Unlike PEG-CK30 DNA nanoparticles which enter cells and traffic to the nucleus via a nucleoli mediated pathway – BEAS-2b cells do not have surface nucleoli – PEG-CH12K18 DNA nanoparticles formulated at pH 7.5 entered cells via clathrin-coated pits, where the poly-L-histidine moieties appeared to have a proton sponge effect, due to their buffering capacity and this results in escape from lysosomes via rupture [92].

Murata et al. 2013 attempted to increase peptide absorption by lung cells by encasing the peptide in liposomes with surface modifications. They bound wheat germ agglutinin (WGA) – a lectin that interacts with alveolar epithelial cells – to carbopol (CP), a mucoadhesive polymer. They then studied the toxicity of CP-WGA surface modified liposomes in A549 cells using the MTS assay, a related assay to MTT. They found that CP–WGA solution and CP–WGA modified liposomes did not induce significant cytotoxicity. The cell viability of A549 cells did not change after treatment with CP–WGA solution or CP–WGA-modified liposomal suspensions at 0.1 and 0.3% w/v the levels used in their pharmacological experiments [93].

Jiang et al. 2013 produced three types of nanoparticles from poly (ϵ -caprolactone) (PCL) and d- α - tocopheryl polyethylene glycol 1000 succinate (PLA-PCL-TPGS) for oral delivery of anti-lung cancer agents. The three types of nanoparticles were thiolated chitosan-modified PCL nanoparticles, unmodified PLA-PCL-TPGS nanoparticles, and thiolated

chitosan-modified PLA-PCL-TPGS nanoparticles. In this study they used A549 cells as a cancer model and attempted to produce formulations that would increase cytotoxicity. They found that PLA-PCL-TPGS nanoparticles modified by thiolated chitosan enhanced the cellular uptake and cytotoxicity with A549 cells. In other words, there is a relationship between cellular uptake and cytotoxicity. The more nanoparticles inside the cells, the more they will interfere with the cell metabolism and a thiolated molecule could change the reduction/oxidation potential of the cell. They produced a thiolated chitosan-modified PLA-PCL-TPGS nanoparticle loaded with paclitaxel, an anticancer drug used for lung cancer chemotherapy. They tested all three nanoparticle formulations loaded with paclitaxel and showed greater decreases in cancer cell viability compared to the current clinical dosage form Taxol[®], and the 5% thiolated chitosan-modified PLA-PCL-TPGS nanoparticles (TNP) performed better than the unmodified PLA-PCL-TPGS nanoparticles (UNP). The advantages in cancer cell viability of the TNP > UNP > the Taxol[®] formulation was dependent on the incubation time. This may be due to the controlled release manner of the nanoparticle formulation. The advantages in cancer cell viability of the TNP > UNP > the Taxol[®] formulation is also dependent on the drug concentration. From cell viability data, an IC₅₀ can be calculated and the differences in cytotoxicity of the TNP > UNP > Taxol[®] can be quantitatively analysed by constructing a dose–response curve [94].

Kim et al. 2013 set up a study to investigate the lung delivery potential of nanoparticles made from a conjugate of vascular endothelial growth factor receptor 1 (Flt1) peptide-hyaluronate acid (HA) and to assess in vitro cytotoxicity using a cell viability assay based on cellular dehydrogenase activity (similar to MTT) in A549 cells with HA receptors. They showed that these nanoparticles do not show any cytotoxicity with cell viability of over 98% up to the concentration of 20 µg/mL, whereas polyethylenimine (PEI) nanoparticles showed cell viability lower than 10% at concentrations of PEI above 20 µg/mL. The concentration of these Flt1 peptide-HA conjugate nanoparticles could be increased to a concentration of 600

µg/ml without a significant reduction in cell viability (over 95%) [95].

Lee et al. 2012 attempted to develop a long acting anti-diabetic inhalation system by preparing deoxycholic acid-modified glycol chitosan (DOCA-GC) nanogels containing palmityl acylated exendin-4 (Ex4-C16) and investigated its cytotoxicity against A549 and Calu-3 cells. Below 0.1 mg/ml, DOCA-GC nanogels did not show significant cytotoxicity (90~97% cell viability) over a 12 hour incubation period, based on an MTT assay. DOCA-GC nanogels were slightly more cytotoxic to both cell types at over 0.3 mg/ml. However, the authors did not test the results statistically [36].

Arunraj et al. 2013 developed a delivery system to treat non-small cell lung cancer showed that Doxorubicin chitin-poly (caprolactone) composite nanogels (Dox-Chitin-PCL) had a dose dependent cytotoxicity toward A549 cells using the MTT assay. The exact mechanism of action of Dox is complex and unclear, though it is thought to interact with DNA by binding across the double helix. This will inhibit the action of topoisomerase II, thereby inhibiting replication. Chitin-PCL CNGs showed low levels of cytotoxicity with more than 80% of the cells viable at 120µg/ml. However, as the concentration of Dox containing nanoparticles increased, there is a dose dependent toxicity. Free Dox showed a significantly enhanced toxicity compared to the drug loaded nanogels. The decreased toxicity of drug loaded nanogels could be due to the slow release of the cargo [96].

Mohammadi et al. 2011 were investigating nanoparticles as vectors for gene delivery to lung epithelial cells. They prepared chitosan–DNA nanoparticles and chitosan–DNA–fibronectin attachment protein of mycobacterium bovis (FAP-B) nanoparticles (polyplexes), and investigated cell viability using A549 cells and the MTT assay. An average cell viability of over 97% was obtained with naked DNA and chitosan – DNA nanoparticles, and chitosan – DNA – FAP-B nanoparticles. There was no significant decrease in viability found for A549 cells treated with polyplexes when compared to naked DNA. Chitosan–DNA nanoparticles and chitosan–DNA–FAP-B nanoparticles carried lower cytotoxicity than the

commercial carriers like Turbofect transfection reagents [97]. It should be noted that the authors used complete media with serum during stimulation of the cells with nanoparticles. This may result in aberrant results due to interaction of nanoparticles with proteins in the media.

Grabowski et al. 2013 studied toxicity of PLGA nanoparticles with surface modifications against alveolar cells. They used three different PLGA nanoparticles (233-247 nm) which were produced using different components (polyvinyl alcohol, chitosan, or Pluronic® F68). The produced nanoparticles were neutral, positively or negatively charged NPs, respectively. They found that low concentration ($\leq 1\text{mg/ml}$) of PLGA/PVA nanoparticle (neutral) showed no effect on cell viability in the MTT, LDH, trypan blue or propidium iodide assays. In contrast, low concentration of PLGA/CS nanoparticles showed around a 30% loss of viability with the MTT assay but no change with other assays. They also found that higher concentrations ($\geq 1\text{mg/ml}$) showed $\sim 40\%$ loss of viability for both PLGA/PVA and PLGA/CS with the MTT and trypan blue assays but no loss of viability with LDH or propidium iodide assays [45]. There is a problem with the interpretation of this data as high and low levels of nanoparticles are not defined consistently; high is defined as $>1\text{mg/ml}$ or $> 0.1\text{mg/ml}$ and low is defined as $< 1.0\text{mg/ml}$ or $< 0.1\text{mg/ml}$.

Feliu et al. 2015 produced a key paper through their studies using next generation sequencing to measure changes in gene expression that appear at levels of nanoparticles that do not cause effects on classical cell viability assays. They found that cationic poly(amidoamine) dendrimers (PAMAM-NH₂) elicited acute cytotoxicity in primary human bronchial epithelial cells but PAMAMs-OH (neutral) did not. In addition, PAMAM-OH is only cytotoxic at 50 and 100 μM at 48 hours, while PAMAM- NH₂ is cytotoxic at 0.5 μM and above at both 24 and 48 hours. With the A549 cells, PAMAM-OH is not cytotoxic and PAMAM-NH₂ is between 5 and 100 μM at 48 hours but not at 24 hours. Together, the data shows that the cationic PAMAMs exhibited stronger toxicity than PAMAMs with neutral surface charge. When the authors tested the effects on gene expression at a nanoparticle level of

0.1 μ M (non- cytotoxic level), they showed a NF- κ B dependent cell cycle arrest [98]. Consequently when considering nanotoxicity more sensitive tests of cell changes may need to be applied.

Lee et al. 2013 prepared inhalable glycol chitosan-coated PLGA nanoparticles containing palmitic acid-modified exendin-4 (Pal-Ex4) (chitosan Pal-Ex4 PLGA NPs). Exendin-4 is a glucagon-like peptide 1 receptor agonist which increases insulin secretion and decreases glucagon secretion. They found that both chitosan-coated PLGA NPs and non-coated PLGA NPs appeared to be cytotoxic to A549 cells at concentrations over 0.03 mg/mL (~80% viability) as measured by a modified MTT assay. Thus, the cytotoxicity seemed not to be solely dependent on whether it was coated with chitosan. Empty PLGA NPs did not show significant cytotoxicity (~95% cell viability) at 12 hours at a concentration of 0.03 mg/mL [99].

1.5.2. *The Use of Nanoparticles to Improve the Effectiveness of Cytotoxic Drugs:*

Some studies actively aim to increase cytotoxicity, while most studies are trying to produce NPs with reduced cytotoxicity. For example, Zhao et al. 2013 studied three types of nanoparticle formulations from commercial PCL and synthesized TPGS-b-(PCL-ran- PGA) diblock copolymer for oral delivery of anticancer agents, comprising DDAB-modified PCL nanoparticles, unmodified TPGS-b-(PCL-ran-PGA) nanoparticles and DDAB-modified TPGS-b-(PCL-ran-PGA) nanoparticles. The role of DDAB is to increase cell surface residency time. In vitro cell viability studies using A549 cells showed advantages of the DDAB-modified TPGS-b-(PCL-ran-PGA) nanoparticles over commercial Taxotere®, an anti-mitotic agent. All three nanoparticle formulations performed better in decreasing the cancer cell viability compared to the current clinical dosage form Taxotere®. The 5% DDAB-modified TPGS-b-(PCL-ran-PGA) nanoparticles (CNP) were more effective than unmodified TPGS-b-(PCL-ran-PGA) nanoparticles (BNP). This is demonstrated by the fact that A549 cell viability after 24 hours exposed to 10 μ g/mL drug concentration was 44% for Taxotere®, and 29% for 5%

DDAB-modified TPGS-b-(PCL-ran- PGA) nanoparticles (CNP). In addition, compared with Taxotere[®], the cytotoxicity was increased by 38% ($p < 0:05$, $n = 6$) and 19% ($p < 0:05$, $n = 6$) for 5% DDAB-modified TPGS-b-(PCL-ran-PGA) nanoparticles (CNP) after 48 h and 72 h exposure to 10 $\mu\text{g/mL}$ of the drug. This increase in cell killing most likely results from the effects of the TPGS and DDAB components in increasing cellular uptake. The advantages in cancer cell viability is dependent on the incubation time and may result from the controlled release. This time dependent effect on cell killing by the nanoparticles is clearly demonstrated by the release characteristics of docetaxel with only 13.5%, 18.2% and 23% released for 5% DDAB-modified TPGS-b-(PCL-ran-PGA) nanoparticle formulation (CNP) after 24 h, 48 h and 72 h, respectively. Also, the breakdown of the copolymer could release the TPGS components, which have additive antitumor activities in the presence of antitumor drugs, thereby increasing cancer cell death. In addition, DDAB has been shown to trigger caspase-3-mediated apoptosis. Therefore, DDAB may also increase cancer cell death [100].

Chittasupho et al. 2014 developed a nanoparticle delivery system for doxorubicin, an effective anti-cancer agent whose use is limited by toxicity. They produced an LFC131 peptide conjugated to sodium carboxyl methyl cellulose coated poly (DL-lactic-coglycolic acid) (PLGA) nanoparticles. The target for LFC131 is CXCR4, a chemokine receptor which is involved in metastasis of cancers. The cytotoxicity, measured by the MTT assay, of doxorubicin-loaded LFC131 conjugated nanoparticles (LFC131-DOX NP) in A549 cells increased in a dose dependent fashion. DOX-NP and LFC131-DOX-NP caused a significant reduction (40% compared to the control) in cell viability at the highest concentration tested (2.5 mg/ml), which was equivalent to 0.25 and 0.14 mg/ml of DOX entrapped in DOX-NP and LFC131-DOX NP, respectively. DOX alone reduced cell viability by 60% of the control at 0.5 mg/ml [44]. This data demonstrated that encapsulation of doxorubicin does not reduce its cytotoxic effects on cancer cells but could allow targeted delivery and prevent/reduce systemic effects seen in vivo.

Table7. Cytotoxicity studies of nanoparticles involving lung epithelial cells (in vitro)

NP type	Cell type	assay	reference
TAS-103-loaded PLGA nanoparticles 201-211.8nm	A549	MTT	[87]
i. PLG nanoparticles ~200nm. ii. PEI nanoparticles.	A549	MTS	[88]
ND-AMB	Calu-3	i. MTT. ii. LDH.	[34]
surfactant-coated micro emulsion pDNA nanoparticles	A549	MTT	[89]
Chitosan–DNA nanoparticles 227±43 and 279±27 nm.	A549	MTT	[97]
i. PEG-CH ₁₂ K ₁₈ based DNA nanoparticles 325±11 nm. ii. PEG-CK ₃₀ based DNA nanoparticles 300±11 nm. iii. EI based DNA nanoparticles 40±3.2 nm.	BEAS-2B	MTT	[92]
DOCA-GC nanogels ~250nm	i.A549. ii. Calu-3.	MTT	[36]
Encapsulation of Alpha-1 antitrypsin in PLGA nanoparticles range of 100 nm to 1µ	Cor L105	MTT	[43]
PLGA based nanoparticles containing PVA or CS with alginate. 278-350nm.	A549	MTT	[90]
i. PLGA chitosan coated nanoparticles 695.7 ± 62.7. ii. PLGA nanoparticles 594.7± 33.3nm.	A549	MTT	[99]
PLGA containing PVA or CS. 200-400nm	A549	1. MTT. 2. LDH. 3. Trypan blue. 4. Propidium Iodide	[45]
i. Chitin-PCL CNGs 70±20nm. ii. Dox-chitin-PCL CNGs 240±20nm.	A549	MTT	[96]
i. Flt1 peptide-HA conjugate nanoparticles. ii. PEI nanoparticles.	A549	WST-1. EL-cytox	[95]
i. 5% thiolated chitosan-modified PCL nanoparticles (CNP) 203.56 ± 4.35. ii. Unmodified PLA-PCL-TPGS nanoparticles (UNP) 198.46 ± 2.49.	A549	MTT	[94]

iii. 5% thiolated chitosan-modified PLA-PCL-TPGS nanoparticles (TNP) 206.15 ± 3.66 . iv. 0% thiolated Chitosan-modified PLA-PCL-TPGS nanoparticles (DNP) 219.33 ± 4.25 .			
CP-WGA surface-modified liposomes 400nm.	A549	MTS	[93]
i. 5% DDAB-modified PCL nanoparticles (ANP) 235.52 ± 9.97 . ii. TPGS-b-(PCL-ran-PGA) nanoparticles (BNP) modified with a cationic surfactant didodecyldimethylammonium bromide (DDAB) 249.45 ± 3.58 . iii. 5% DDAB-modified TPGS-b-(PCL-ran-PGA) nanoparticles (CNP) 228.33 ± 2.01 . iv. 0% DDAB-modified TPGS-b-(PCL-ran-PGA) nanoparticles (DNP) 222.25 ± 4.26 .	A549	MTT	[100]
Doxorubicin-loaded LFC131 conjugated nanoparticles. 300nm	A549	MTT	[44]
i. PAMAM-OH 5.6 ± 0.9 nm. ii. PAMAM-NH ₂ 4.1 ± 0.2 nm. iii. L-PAMAM-OH 1.0 ± 0.2 nm. iv. L-PAMAM-NH ₂ 4.4 ± 0.3 nm.	1. PBECs. 2. A549	1. LDH. 2. Alamar Blue Assay.	[98]
GAG PLGA nanoparticles 100-150nm.	A549	i.MTT. ii.LDH.	[101]

Table 7 continues

Concentrations	Exposure conditions	Exposure duration (hours)	Results	Reference
1, 3, 10, 30, and 10nM	i. 96 well plates. ii. Pre-incubated for 24h.	24	i. Although ED ₅₀ of free drug was more than 30 nM, the ED ₅₀ of nanocomposite particles was approximately 10 nM. ii. There is almost no difference observed in cytotoxicity between 5% and 10% TAS-103-loaded PLGA nanocomposite particles.	[87]
0.1, 1, 10, 100, 1000, and 10000 µg/ml	i. 96 well plates. ii. Pre-incubated for 24h.	24	i. Minimum cytotoxic effect of cationic coating material (IC ₅₀ ~1190– 2450 µg/mL). ii. Branched PEI complexes showed significant cytotoxicity at low concentration (IC ₅₀ ~ 35 mg/mL)	[88]
75µg/ml	i. 24 well plates. ii. Pre-incubated for 48h.	18	i. Calu-3 cells incubated with AMB/DOC were significantly less viable than controls incubated with PBS alone 16.1±5.6%, n=3 (p < 0.0001), assessed by MTT viability and LDH release, which was significantly increased 11.3±1.2-fold, n=3 (p < 0.0001). ii. Cells with ND-empty were fully protected from the cytotoxicity of AMB/DOC and were indistinguishable from control cells by MTT and LDH release. iii. The viability of ND-AMB was not significantly different from control while LDH release from cells treated with ND-AMB was lower than AMB/DOC alone 3.7±0.90-fold, n=3 (p < 0.0001). iv. Treatment with ND-AMB+ did not significantly affect MTT or LDH levels versus AMB/DOC. ND-empty, ND-AMB or ND-AMB+ in the absence of AMB/DOC did not reduce viability or promote LDH release.	[34]
15µg/flask	i. T25 flask. ii. 50% confluency	42	i. Statistical analysis showed no significant loss in cell viability (p>0.05) between blank, untreated cells and cells treated with the washed, aerosolised pDNA formulation. ii. A significant reduction in cell viability (p<0.05) was, however, observed when DOTAP was added to the cell culture medium.	[89]

			iii. Statistical analysis showed a significant reduction ($p < 0.05$) in cell viability when cells were treated with 80 pMDI-aerosolised doses, compared with 9 doses of the same formulation.	
1 μ g/well	i. 96 well plates. ii. Pre-incubated for 24h.	48	i. Average cell viability of over 97% was obtained with naked DNA and chitosan–DNA nanoparticles and chitosan–DNA–FAP-B nanoparticles. ii. No significant decrease in viability was found for A549 cells treated with polyplexes when compared to naked DNA. iii. Chitosan–DNA nanoparticles and chitosan–DNA–FAP-B nanoparticles carried lower cytotoxicity than the commercial carriers such as Turbofect transfection reagents.	[97]
0.2, 2, 5, or 10 μ g DNA/well	i. 96 well plates. ii. Pre-incubated for 24h.	48	i. PEI DNA nanoparticles induced the greatest cytotoxicity, with a 50% reduction in metabolic activity at the highest dose ($P < 0.01$). ii. Cells incubated with either PEG-CH ₁₂ K ₁₈ DNA nanoparticles or PEG-CK ₃₀ DNA nanoparticles retained greater than 90% of their metabolic activity across all DNA doses tested. iii. Unlike PEG-CK30 DNA nanoparticles which enter cells and traffic to the nucleus via a nucleoli mediated pathway, PEG-CH12K18 DNA nanoparticles formulated at pH 7.5 enter cells via clathrin-coated pits, where the poly-L-histidine moieties appear to have a proton sponge effect, resulting in escape from lysosomes.	[92]
0.01~1.0 mg	i. 96 well plates ii. Pre-incubated for 12 hour	6 or 12	i. At below 0.1 mg/ml the nanogels were not cytotoxic. ii. At 0.3 mg/well and above, there was an increase in cytotoxicity but this was not tested statistically.	[36]
0 to 1.5 mg/ml	i. 96 well plates ii. Pre incubated for 24 hour	24	i. The viability of cells treated with different concentrations of free and loaded nanoparticles remains unchanged and cells retained more than 80% of their viability. ii. The morphology of cells before and after treatment with nanoparticles was similar.	[43]

1 mg/ml and 0.5 mg/ml	i.96 well plates ii.Pre incubated for 24 h	24	CS/ alginate / PLGA particles were the most cytotoxic at 10 mg/ml causing 82% cell death but showed similar cytotoxicity to the other nanoparticles at 0.5 mg/ml ranging between 20-40% cell death	[90]
0.003–0.3 mg/mL	i.96 well plates ii.Pre incubated for 24 h	12	i. Both chitosan-coated PLGA NPs and non-coated PLGA NPs gave around 80% viability and were cytotoxic to A549 cells at concentrations of over 0.03 mg/mL. ii. PLGA NPs did not exhibit significant cytotoxicity (~95% cell viability) at 12 hours post-administration at a concentration of 0.03 mg/mL, regardless of the presence of a chitosan-coating.	[99]
From 0.005 to 3 mg/mL	i. 96 well plates for MTT and LDH. ii. 6 well plates for trypan blue and propidium iodide. iii. re-incubated for 24h.	i. 24 hours for MTT and LDH. ii. 48 hours for trypan blue and propidium iodide.	i. Low concentration (≤ 1 mg/ml) of PLGA/PVA nanoparticle showed no effect on cell viability in the MTT, LDH, trypan blue or propidium iodide assays. ii. Whereas low concentration of PLGA/CS nanoparticles showed around 25% loss of viability with MTT assay but no change with other assays. iv. Higher concentration (≥ 1 mg/ml) showed ~ 25% loss of viability for both PLGA/PVA and PLGA/CS with the MTT and trypan blue assays but no loss of viability with LDH or propidium Iodide assays.	[45]
24, 48, 72, 96 and 120 μ g/mL	i. 96 well plates ii. 90% confluency	24	i. Empty chitin-PCL CNGs had little effect on the cells with over 80% viability retained at all doses. ii. Doxorubicin containing chitin-PCL-CNG nanoparticles showed a dose dependent cytotoxicity.	[96]
up to 600 μ g/mL	i. 24 well plates. ii. Pre-incubated for 24h.	24	i. Flt1 peptide-HA conjugate nanoparticles showed a cell viability over 98% up to the concentration of 20 μ g/mL, whereas PEI exhibited a cell viability lower than 10% at the concentration of PEI higher than 20 μ g/mL. ii. Flt1 peptide-HA conjugate nanoparticles showed a cell viability over 95% up to the concentration of 600 μ g/mL	[95]

0.25, 2.5, 12.5, and 25 µg/ml	i. 96 well plates. ii. Pre-incubated overnight.	24, 48, and 72.	i. The advantages in cancer cell viability of the TNP > UNP > the Taxol® formulation is dependent on the incubation time. ii. The advantages in cancer cell viability of the TNP > UNP > the Taxol® formulation is also dependent on the drug concentration. iii. The TNP showed better IC50 values and better in vitro therapeutic effects for A549 cells than commercial Taxol®.	[94]
150µl of 1-3 mg/ml	96 well plates	2	i. Cell viability of A549 cells was almost unchanged after treatment with CP-WGA solution or CP-WGA-modified liposomal suspensions at the concentrations used in subsequent experiments. ii. In contrast, a positive control solution containing the nonionic water-soluble surfactant Triton X-100 at 0.1% (w/v) significantly reduced the viability of A549 cells.	[93]
0.25, 2.5, 12.5, and 25 µg/mL	i. 96 well plates. ii. Pre-incubated for overnight.	24 , 48 and 72	The modified nanoparticles were more cytotoxic than unmodified based on IC50.	[100]
0.02–2.5 mg/ml	96 well plates 80% confluent	6 hours, then removed NPs and incubated with media for 18 hour	i. LFC131- DOX NP and DOX NP showed cytotoxicity to A549 cells, a reduction in cell viability was observed in a dose dependent manner. ii. DOX-NP and LFC131-DOX-NP caused a significant reduction (60% of control) in cell viability at the highest concentration tested (2.5 mg/ml), which is equivalent to 246.5 and 140 µg/ml of DOX entrapped in DOX-NP and LFC131-DOX NP, respectively. iii. ree DOX reduced cell viability to 39% of the control at concentration of 500 µg/ml. iv. In addition, cell sensitivity to doxorubicin was greatly increased when the cells were treated with LFC131-DOX NPs and DOX NPs compared with free DOX at concentrations of 30–120 µg/ml doxorubicin entrapped in NPs.	[44]

0.1, 0.5, 1, 5, 10, 50, and 100 μM	96 well plates	24 and 48	<p>i. PAMAM-OH forms a neutral nanoparticles and PAMAM-NH₂ forms a positively charged nanoparticles. PAMAM-NH₂ is more cytotoxic to PBEC.</p> <p>ii. PAMAM-OH is only cytotoxic at 50 and 100 μM at 48 hours.</p> <p>iii. AMAM- NH₂ is cytotoxic at 0.5 μM and above at both 24 and 48 hours.</p> <p>iv. ith the A549 cells PAMAM-OH is not cytotoxic and PAMAM- NH₂ is between 5 and 100μM at 48 hours but not at 24 hours.</p>	[98]
100, 200, 300, 400, 500, and 600 $\mu\text{g/ml}$	<p>i. 96 well plates.</p> <p>ii. Pre-incubated for 24h.</p>	24	<p>i. Moderate decrease in viability with MTT assay.</p> <p>ii. LDH: minimal increase in ~ 10-20% loss of cell viability cellular toxicity</p>	[101]

PLGA= poly (D, L-lactide-co-glycolide). PLG= poly (D, L-lactide-co-glycolide). PEI= poly (ethylenimine).pDNA=plasmid DNA. siRNA= small interfering RNA. PEG-CH₁₂K₁₈ = PEG maleimide 12 histidines – 18 lysines forming a tripolymer. ND-AMB=- NanoDisk- Amphotericin B. LFC131= a peptide inhibitor of CXCR4-ligand binding. PAMAM-NH₂= cationic poly (amidoamine) dendrimers. PLGA= poly (lactide-co-glycolide). PLA-PCL-TPGS= self-synthesized d- α - tocopheryl polyethylene glycol 1000 succinate. PCL= Poly (ϵ -caprolactone). HA= hyaluronic acid. DOCA-GC= deoxycholic acid-modified glycol chitosan. WGA= wheat germ agglutinin, a ligand that specifically interacts with alveolar epithelial cells. CP= carbopol, a mucoadhesive polymer. α 1AT= Alpha 1- antitrypsin, belongs to the superfamily of serpins and inhibits different proteases. TAS-103= the anticancer drug 6-[2-(dimethylamino) ethyl] amino]-3-hydroxyl-7H- indeno[2,1-c]quinolin-7-one dihydrochloride. GPs= gelatin nanoparticles. CDDP = cisplatin. bEGF= biotinylated-EGF. GP-PT = the anticancer activities of CDDP-incorporated in GPs. GP-Pt-bEGF= the anticancer activities of GP-Pt with bEGF modification. DDAB= didodecyldimethylammonium bromide. TPGS= Vitamin E d- α -tocopheryl polyethylene glycol 1000 succinate. Chitin-PCL CNGs= chitin-poly (caprolactone) composite nanogels. Dox-chitin-PCL CNGs = Doxorubicin chitin-poly (caprolactone) composite nanogels. Calu-3 = Human airway submucosal epithelial cell line. PVA= polyvinyl alcohol. A549 = adenocarcinomic human alveolar basal epithelial cells) cancer cells. BEAS-2B= human bronchial epithelial cells. PBECs= primary human bronchial epithelial cells. Cor L105 = human epithelial like lung cell line. MTS= the 3-(4, 5-dimethylthiazol-2-yl)-5-(3-carboxymethoxyphenyl) - 2-(4-sulfophenyl)-2H-tetrazolium. MTT= the colorimetric 3-[4, 5-dimethylthiazol-2-yl]-2, 5-diphenyl tetrazolium bromide. LDH=cytosolic enzyme lactate dehydrogenase. WST-1=Cell Proliferation Reagent.

1.6. Nanoparticles as Promoters of Inflammation:

1.6.1. The Use of Nanoparticles to Modulate Immunological Responses:

It is not possible to comprehensively measure inflammation *in vitro* due to the involvement of multiple cell types *in vivo*, but there is the possibility to measure markers of pro-inflammatory signalling and the gene expression involved in inflammation. The most common technique for measuring pro-inflammatory responses is to measure cytokine and/or chemokine protein production by cells. The measurements include assays of cytokines such as tumour necrosis factor alpha (TNF α), interleukin (IL), IL1 α , IL1 β , IL6, IL8 and so on. One of the most frequent assay methods used is enzyme linked immunosorbent assay (ELISA) which is able to measure cytokines. In addition to ELISA, cytokine mRNA expression can be measured as an indicator of changes at the gene expression level using the polymerase chain reaction (PCR) technique. It should be noted that mRNA content is not absolutely reflective of the protein production because of posttranscriptional modification, changes in protein stability and mRNA stability [20].

Grabowski et al. 2013 investigated three different modified PLGA NPs; polyvinyl alcohol, chitosan, or Pluronic[®] (F68) which formed respectively neutral, positively or negatively charged NPs. They found that the inflammatory response from A549 cells, evaluated by measurement of the cytokines IL-6, IL-8, MCP-1, and TNF- α , was low for all NPs. There were some differences, especially for negative PLGA NPs which produced a higher inflammatory response, related to a higher uptake of these negative nanoparticles. IL-6, IL-8, and MCP-1 levels were in a dose response and peaked at 1 μ g/mL lipopolysaccharide (LPS, positive control). Other tested cytokines could not be detected. At a concentration of 0.1mg/ml PLGA/PVA, PLGA/CS and polystyrene NPs exposure, the cytokine levels were between the levels of cytokines produced by non-treated cells and LPS treated cells. PLGA/PF68 NPs induced higher cytokine secretions than other NPs, with values equivalent or above LPS-

treated cells [45].

1.7. Permeation of Mucus:

Although human mucus is not easy to obtain, an alternative mucus source can be used from animal's sources (especially if it is obtained immediately after death). The most useful method to isolate the mucin, while still retaining the ability to function with relevant physiological properties is by isolation in the presence of proteolytic inhibitors. After that, purification is by a CsCl equilibrium density gradient avoiding any chaotropic agents that could denature the protein: protein, carbohydrate: carbohydrate and protein: carbohydrate interactions which are essential for gel formation. Another approach is using cell models secreting mucus, allowing a dynamic mucus barrier to be used and allowing permeation and uptake of labelled particles to be measured. This can also allow simultaneous cytotoxicity studies. It should be noted that care should be taken with labelled particles because adding the label may seriously alter the particle properties. Caco-2, HT29MTX co-cultures and HT29MTX have been used to produce a measurable mucus layer in cell culture. However, these cell cultures have several limitations. Firstly, the thickness *in vivo* reported for the total mucus bilayer in the small intestine is 170, 133 and 480 μm in the duodenum, jejunum and ileum, respectively, while the mucus thickness reported for co-culture after 16 days was 2-10 μm . Secondly, the mucus appears in blobs above the goblet cells with thinner areas above the Caco-2 cells, rather than the continuous layer observed physiologically. Thirdly, HT29-MTX cells are derived from a colonic adenoma with altered gene expression with down regulation of MUC 2 production [15]. Mucus permeation studies can be measured by a transwell-snapwell system and transwell diffusion studies. In the transwell-snapwell system, permeation studies across freshly excised tissue are usually accomplished with using chambers. The mucus layer is surrounded with two penetrable filters linked to the snapwell ring and incorporated between the donor and the acceptor compartments, allowing particles to permeate through the mucus. Therefore, this

system is based on a donor and acceptor compartment detached by a fundamental compartment which contains a vertical layer of mucus. However, because of the separation of the mucus layer from the donor chamber the transwell/snapwell diffusion system has an additional barrier for particles compared to the in vivo situation. In other words, direct exchange of particles with the mucus layer is avoided by the penetrable filter and so the simulation of the in vivo situation is restricted. In transwell diffusion studies, one of the systems to assess mucus diffusion is the side by side[®] diffusion device containing one donor and one receiver as well as a custom membrane holder. The membrane holder is located between the two compartments, containing the mucus separated between two drug penetrable membranes. The transwell diffusion system represents a novel method involving a two compartment system. A 24 well plate comprises the acceptor compartment and an additional 24 inserts make up the donor compartments. The two compartments are separated from each other by a membrane covered with 50 mg of fresh mucus. One of the main advantages of using this newly established method is that it allows the use of samples introduced straight on to the surface of the mucus, simulating much closer the in vivo situation; therefore, the direct interaction between mucus and a drug delivery system can be assessed. This system also allows rapid comparison of different samples. In addition to that, permeation of particles can be investigated within different purified mucus samples, different mucus layer locations or at different pH values at the same time [102].

1.8. Rheology of Mucus:

The selective barrier function of mucus is very tightly regulated by its biochemical composition. Physically mucus behaves as a non-Newtonian gel, which can be characterised by its response to shear rate and shear stress. The important physical characteristics of mucus can be studied by advanced rheological characterization, and this has produced some understanding of mucus physiology and disease pathology. The interaction of nanoparticles

with mucus and its effect on mucus rheology is, therefore, an important consideration since mucus is the first barrier that nanoparticles may encounter. It is also important to consider the effect of non-mucin components during the investigation of rheological properties of mucus gels. Mucus gels can be considered as viscoelastic and plastic. They can deform under load and return to their original shape during loading removal. However, these gels may be deformed in a long-lasting manner under excess load. There are many methods to investigate the rheological properties of mucins. These include solution viscosity measurements, as well as analysis of native and reconstituted gels using creep compliance methods, spinability, magnetic rheogoniometry, nuclear magnetic resonance (NMR), light scattering, and cone and plate mechanical spectroscopy [103].

Viscosity measurements of mucin solution can give information about the size and shape of mucins, as well as interactions among and within mucin molecules, especially the interactions preceding gel formation. As the viscosity of purified mucins increases, the concentration of mucins increases until the solution forms a gel. Solution viscosity measurements can be helpful in investigating potential muco-adhesives and mucin polymeric structure. From a methodological viewpoint, correct storage of samples is essential since the properties of mucus can be altered by incorrect freezing, degradative enzyme activity or dehydration. Spinability is the simplest methods but the least accurate for investigating viscoelasticity, and is based on drawing out a thread of mucus and recording the length achieved before it breaks. It only gives information about the tensile strength of the gel. However, it has been linked to at least one biological function (the ability of cilia to move mucous blankets using frog palates, giving a relative transport rate). NMR has been used to measure gel strength and relies on measuring the line width of the signal from a water proton to give a measure of viscosity. Dynamic laser light scattering has also been used to assess rheological properties of mucins and give information about G' (storage or elastic modulus)

and G'' (loss or viscous modulus). Dynamic and transient testing are the most reliable methods to assess the physical behaviour of mucous gels. In these two methods, a stress is applied to the gel and the resulting strains or rate of strain is measured. Creep testing, which is a transient method, has been used widely to measure the rheological behaviour of mucus secretions and reconstituted mucin gels. Two methods of dynamic testing have been used: magnetic rheogoniometry, and conventional cone and plate mechanical spectroscopy. Magnetic rheogoniometry is based on the photoelectric analysis of the motion of a small steel ball in a mucus sample. However, mucus is non-homogeneous and the small ball may be in an area of weak gel or strong gel and give a misleading report on overall gel strength. Conventional cone and plate mechanical spectroscopy is, therefore, regarded as the most reliable and informative method for the rheological characterization of mucus [103].

1.9. The Aims of the Thesis:

The aim of my thesis is to assess the safety profile of different novel NPs when interacting with mucosal barriers in vitro. In chapter three, I investigated the role of inflammation and cytotoxicity. I also studied the effect of cell density of Calu-3 cells on the CellTiter blue assay and the influence of nanoparticles on a standard curve for IL-8. In chapter four, I measured the potential cytotoxicity of self-nanoemulsifying drug delivery systems (SNEDDS) and assessed the mucus permeation behaviour of SNEDDS within a novel mucus diffusion model utilizing standardized Transwell diffusion plates.

Chapter Two: Methodology and Materials

2.1. Cell Cultures:

2.1.1. *Primary Bronchial Epithelial Cells (PBEC):*

Cell cultures were carried out as described previously [27, 28]. Epithelial cells were retrieved from a bronchoscopy of lung transplant recipients. Ethical approval had been obtained from the Local Research Ethics Committee and all patients gave informed consent. After the bronchoscopy and short-term storage (approximately 2 hour) of the brushings, the samples were suspended in transport media (5ml sterile PBS, 5ml RPMI with 10% FCS) and centrifuged for 7 minutes at 200xg. The cell pellet was suspended in 2ml of clonetics bronchial epithelial cell basal medium (Clonetics BEBM, (Lonza), San Diego, CA, USA) together with bronchial epithelial cell growth medium (BEGM) single quots (Clonetics), 50 U/ml penicillin, 50 mg/ml streptomycin (Sigma, UK), 50 mg/ml gentamycin and 50 µg/ml amphotericin B (Lonza, USA). Then the cells were transferred into T25cm² Flasks pre-coated with a 1% collagen solution (Vitrogen 100, cohesion, Palo Alto, CA, USA) and placed in a CO₂ incubator (37 °C and 5% CO₂). After the first 48 hours, another 3ml of supplemented medium was added with a subsequent exchange (3ml) every 48 hours until the cells reached 90% confluency. Once the cells reached confluence, PBECs were passaged using 3ml trypsin which was neutralized using an equal volume of Roswell Park Memorial Institute Media (RPMI) supplemented with 10% foetal calf serum (FCS). After that, the cells were put in 10ml of culture medium and transferred to vitrogen (Cohesion) coated T75cm² Flasks, 24 well plates (40,000 cells/ well) or 96 well plates (20,000 cells/ well). The cells were then cultured until they reached 90% confluency. I performed experiments on epithelial cells from different transplant patients (first passage “PI”, and second passage “PII”). All of these steps were carried out under strict sterile conditions in a laminar flow hood. The major difficulty at this

stage involved infections developing in the cells. Some problems were faced with innate infection from patient derived organisms resistant to the antibiotics in the growth medium because of the nature of many of the cells gained (e.g. early post-transplant brushings obtained from the recipients). There were also occasional problems with infection introduced during culturing regardless of following a strict sterile technique. Infected cells were bleached and discarded from the study. The brushings produced 4×10^4 cells with ~90% of the cells being epithelial cells and the rest being made up of neutrophils, macrophages and lymphocytes [27].

A few cells types (including primary) did not optimally attach to standard tissue culture plastic or glass unless it was coated with a suitable substrate, mimicking the natural environment of the cells [104]. *In vivo* airway epithelial cells are attached to a basement membrane which includes collagen. The primary airway cell cultures were, therefore, carried out on collagen coated tissue culture containers, as previously described by our lab [27, 28].

Confluency is a measure of the density of cells in a culture dish or a flask and refers to the coverage of the dish or flask by the cells [105]. It is useful to determine when to passage cells or when to induce a perturbation such as a cell stimulus or challenge [106]. Cell lines must be maintained in the exponential growth phase for the best culture results. In other words, they must be sub-cultured on a regular basis before they reach 100% confluence when they enter a stationary growth phase. If the cells are around 70% to 90% confluent (i.e cover 70-90% of the flask), they need to be sub-cultured [107]. Examples of cell confluency are given in **Figure 5**. It is hard to count Calu-3 in images because they grow in clusters. Therefore, the degree of confluency was assessed by an estimation of confluency.

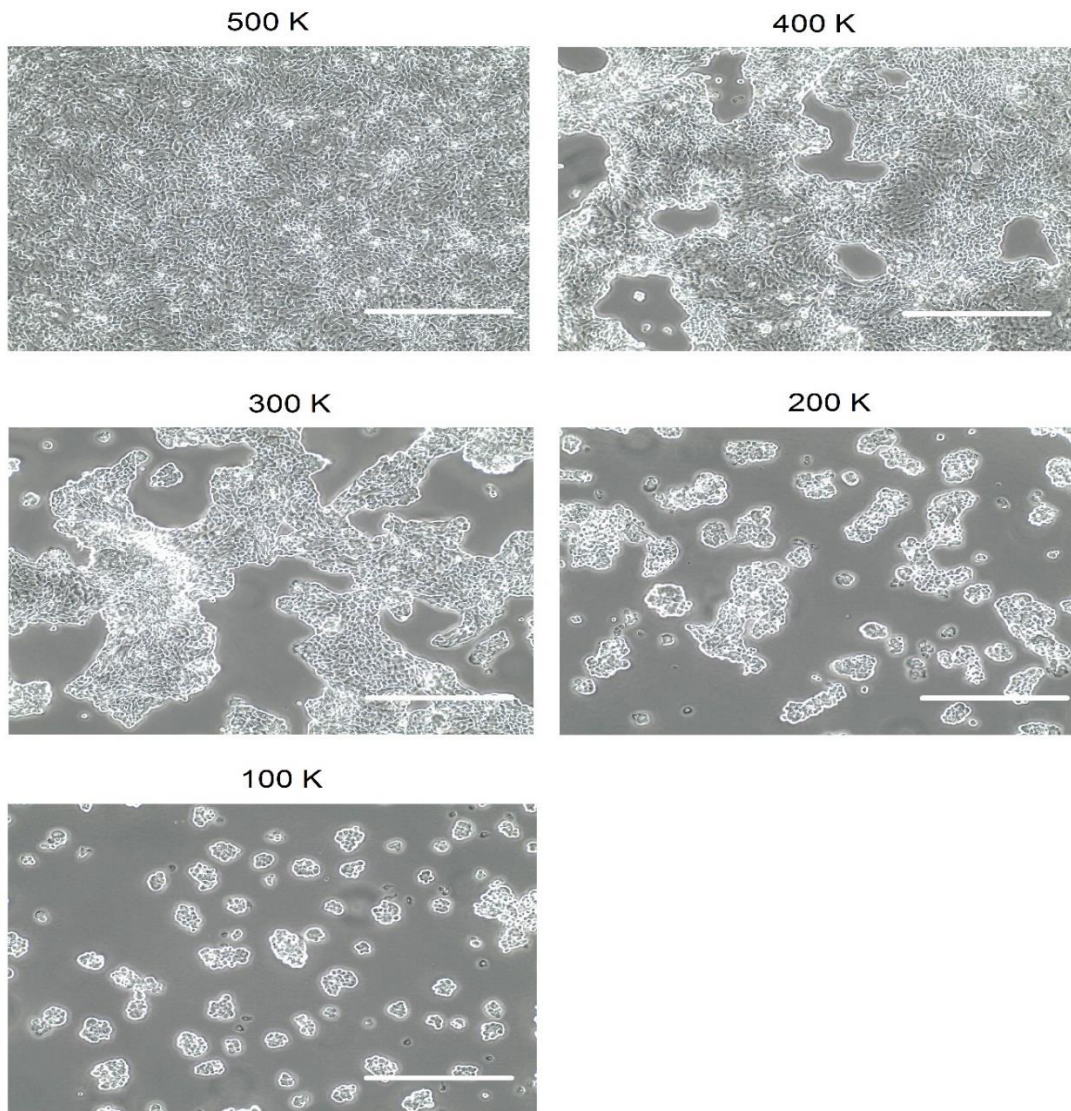


Figure 5. Images taken when 100% confluency reached for 500K in Calu-3 cells. 80% confluency of 400K cell density. 60% confluency of 300K cell density. 40% confluency of 200K cell density. 20% confluency of 100K cell density. Scale bar 500 μ m.

2.1.2. Calu-3:

The Calu-3 cells are an adenocarcinoma cell line which was developed by Jørgen Fogh in 1975 using a pleural effusion from a lung cancer patient. Calu-3 cells express CFTR lysozyme, lactoferrin and the serous cell markers [108]. They are deficient in the dense granules that characterize serous cells in vivo. They also secrete mucus in around 25% of the cells and in an air-liquid interface culture, they contain translucent mucin granules. These are 1-2 μm in diameter and have the mucins MUC5AC and MUC5B characteristic of airway goblet cells and submucosal glands [109]. Despite this, Calu-3 cells lack normal chromosomes 1, 13, 15 and 17 [110]. Calu-3 cells were grown in Dulbecco's modified Eagle's medium (DMEM) supplemented with 50 mg/ml penicillin and streptomycin, MEM non-essential amino acids, 100 U/mL penicillin/streptomycin, 100 $\mu\text{g}/\text{mL}$ GlutaMAX equivalent to 2mM l-glutamine (all from Invitrogen, Carlsbad, CA) and 10% fetal bovine serum (Hyclone, Logan, UT). The cells were maintained at 37 °C in an incubator with 90% humidity and 5% CO₂. After they had grown to 90% confluency, cells were trypsinized and seeded into 24 (50,000 cells/ well) or 96 (20,000 cells/ well) well plates for cytotoxicity and inflammation studies. Experiments were performed with cells of passage numbers 25–45.

The Calu-3 cells (Calu-3 (ATCC® HTB-55™)) are a lung adenocarcinoma derived cell line produced from a metastatic site. The American Type Culture Collection (ATCC) protocol for culture of Calu-3 cells does not recommend the use of coated tissue culture ware so the Calu-3 cells were cultured on non-coated tissue culture flasks, following the ATCC protocol [111].

2.2.Nanoparticles:

2.2.1. Nanoparticle Characterizations:

I have used three different poly nanoparticles (DL-lactide-co-glycolide in a 50:50 molar ratio) (PDLG) (NP1-3). These were received in suspension from Nanomi (Nanomi B.V Oldenzaal, Netherlands) and three different poly (lactic-co-glycolic acid) (PLGA) (NP4-6) received in dry powder form from Aristotle University of Thessaloniki (AUTH, Greece) (**Table 8**). In addition, the two polystyrene nanoparticles used in this study were obtained as dispersion in DI water from Corpuscular Company (New York, NY). The primary sizes as initially received were 52 and 100nm based on photon correlation spectroscopy and/or laser diffraction provided by the company. All of these nanoparticles were tested in Chapter 3.

Table 8. Physiochemical characterizations of NPs used in this study.

Nanoparticle Types	Identification Name	Concentrations as Received	Fluorescent Marker	Suspended in	Colour	Size nm	Zeta Potential mV
NP1	PDLG 5002A	1.7mg/ml	Lumogen red 305	Water	Light pink	160	N/A
NP2	PDLG 5002B	3mg/ml	Lumogen red 305	Water+0,5% pluronic F108 (w/w)	Light pink	122	N/A
NP3	PDLG 5002	0.7 mg/ml	Lumogen red 305	Water	Light pink	160	N/A
NP4	PLGA-trypsin	15.34 mg	0.93% w/w trypsin	Lyophilized powder	White	329	-1.17
NP5	PLGA-papain	15.04 mg	10.8% w/w papain	Lyophilized powder	White	388	3.16
NP6	PLGA-bromelain	15.04 mg	5.13% w/w bromelain	Lyophilized powder	White	549.5	-5.28

It should be noted that each NP 1-3 was loaded with 0.1% w/w fluorescent dye and 0.02% (w/v) of sodium azide have been added to the samples. PDLG: poly DL-lactide/glycolide copolymer, PLGA: poly (lactic-co-glycolic acid). Trypsin: a serine protease from the proteases of mixed nucleophile (superfamily A) which can be found in the digestive systems of many vertebrates to hydrolyse proteins. Papain: a cysteine protease of the peptidase C1 family, used to tenderize meat and as a food supplement to help digestion. Bromelain: a proteolytic extract derived from the stems of pineapples and constituted an unusually complex mixture of different thiol-endopeptidase and other not yet completely characterized component such as phosphatases, glucosidases, peroxidases, cellulases, glycoproteins and carbohydrates. N/A=not available.

Table 9 shows the self nanoemulsion drug delivery systems (SNEDDS) that were used in chapter 4. These nanoparticles were prepared by Aristotle University of Thessaloniki, Greece.

Table 9. Characterizations of nanoparticles.

Nanoparticles	Size	Lipids	Chromophore
SNEDDS-a	35nm	Cremophor EL, lauroglycol FCC, and labrafil M1944CS.	Lumogen
SNEDDS-b	15nm	Transcutol P, cremophor RH 40, and ethanol.	Lumogen
SNEDDS-c	15nm	Transcutol P, cremophor RH 40, and PEG 400.	Lumogen

2.2.2. Dispersion Protocol for Nanoparticles:

The nanoparticles were vortexed for 10 seconds at maximum speed on a whirlmixer and then placed in a sonication bath (220-240V, 50-60 Hertz, 2000 Watts, module U300H, Module number F0001602, 03/7/2012, Ultrawave LTD, Cardiff) for 5 minutes at 25°C. This was followed by vortexing for 10 seconds at maximum speed. All the materials used to prepare the stock and working concentration were sterilized and prepared in a laminar flow cabinet.

2.3.Sandwich ELISA:

The sandwich ELISA for measuring IL-8 was carried out as described in the commercial human CXCL8/IL-8 DuoSet kit (Catalogue number DY208, R&D systems). In summary, 96 well plates were coated with 100 μ l of capture antibody solution and the plate was sealed and incubated overnight at room temperature. After 24 hours, the solution was disposed of. The plate was washed with 400 μ l of washing buffer two times followed by an extra wash of PBS twice. 300 μ l of blocking buffer was added to the plate and plate was sealed and incubated for 1 hour at room temperature. Then the plates was washed with washing buffer and PBS two times. After that, 100 μ l of serial dilutions of IL-8 standard were added to the plate (ranging from 2000 to 31.25 pg/ml of standard solution). At the same time, the samples were added to the plate. Both the standard solution and the samples were incubated for 2 hours at room temperature. The plate was then washed with washing buffer and PBS two times. 100 μ l of detection antibody was added to the plate and the plate was sealed and incubated for 2 hours at room temperature. The plate was then washed two times with washing buffer and PBS. 100 μ l of horseradish peroxidase solution was added to the plate and the plate was sealed and incubated for 30 minutes at room temperature. The plate was then washed twice with washing buffer and PBS. Then 100 μ l of substrate solution was added to the plate and it was sealed and incubated for 20 minutes at room temperature. 50 μ l of stop solution was then added to the plates. The samples were quantitated within 30 minutes by subtracting readings at 540nm from the readings at 450nm. Standard NPs curves were done to detect the interference of NPs with the ELISA. A concentration of 250 μ g/ml NPs (20 μ l of working concentration of NPs) was added to 80 μ l of standard IL-8 in each well. Therefore, the total concentration of IL-8 NPs standard was 50 μ g/ml in the total volume of 100 μ l.

2.4. Cell Viability:

2.4.1. CellTiter Blue:

The viability of a population of cells *in vitro* can be determined using a variety of experimental methods. One parameter used to define cell viability is whether or not metabolic processes remain active. Viable cells must carry out metabolic reactions to generate the energy required to maintain homeostatic processes including synthesis of critical components and maintenance of membrane potential. When cells lose membrane integrity *in vitro*, their ability to carry out metabolic processes ceases. In other words, they die [112]. The methods to monitor and track cell viability essentially fall into two categories: those that detect changes in cell membrane integrity and those that function based on the ability of a viable cell to incorporate or metabolize a particular substrate [113]. One method for monitoring cell viability is the conversion of indicator dyes to form a measurable end product. The CellTiter-Blue™ Cell Viability Assay – a buffered solution containing highly purified resazurin – depends on the capacity of living cells to convert a redox dye (resazurin) into a fluorescent end product (resorufin). The assay affords a homogeneous, fluorometric technique for assessing the number of viable cells in multiwell plates. Viable cells maintain the capability to metabolise resazurin into resorufin. However, nonviable cells quickly lose metabolic capability and, therefore, do not produce a fluorescent signal. Resazurin penetrates cells in where it is reduced to the fluorescent resorufin, as a result of the action of redox enzymes. After that, the fluorescent resorufin will diffuse into the surrounding medium. Resazurin is dark blue and has slight fundamental fluorescence until it is reduced to resorufin, which is pink and very fluorescent [112]. It is also possible to measure resazurin and resorufin levels using absorbance. The absorbance maximum of resazurin is 605nm, and the reduced resorufin has a maximum at 573nm. Therefore, a subtraction of absorbance 570nm-600nm was done in this thesis to get the accurate value of how much resazurin had been reduced to resorufin by the cells as fluorescent analysis was not

available. The assay was designed for use as an endpoint assay rather than as a kinetic method of monitoring cell growth. The reagent should be added near the end of the period of exposure to the compound being tested [112]. The advantages of this assay are summarized in **table 10**.

The CTB assay was purchased from Promega (catalogue number G8082). This assay relies on cell reduction reactions to convert resazurin to resorufin which fluoresces at 590nm. In addition, when using non-fluorescent measurements, resazurin absorbs at 605nm and resorufin absorbs at 573nm. Cells were incubated in 100µl of culture medium and 20 µl of cellTiter blue reagent was added. The plates were shaken for 10 seconds and then incubated at 37°C for 1-4h, before being shaken for 10 seconds. Absorbance was then read at 570nm, and the 600nm value was subtracted from the 570nm value to correct for any background interference. Standard curves were constructed using mixtures of live and methanol killed cells in the ratios of live:dead: 100:0, 75:25, 50:50, 25:75, and 0:100 (positive control).

Table 10: The Advantage of using CellTiter-Blue assay.

Advantage	Comments
speed	Cell washing, removal of medium, and multiple pipetting steps are not required.
	The assay is suitable for manual use as well as for high-throughput automated screening assays.
	The homogeneous add-incubate-measure format reduces the number of handling steps
Allows Your Choice of Assay Format and Method of Detection.	Can be used with 96- or 384-well formats, and data can be recorded using fluorescence or absorbance.
Allows You to Perform More than One Assay on the Same Sample	The reagent is relatively non-destructive to cells during short-term exposure; it is possible to use the same culture wells to do more than one type of assay.
Safe	The reagent is generally nontoxic to cells, allowing extended incubation periods in some situations.
	Requires no scintillation cocktail, radioactive waste disposal (unlike [³ H]-thymidine incorporation assays) or use of hazardous solvents (required for MTT-based assays).
It can be stopped	The fluorescence/ absorbance generated in the CellTiter-Blue [®] Assay can be stopped and stabilized by adding 3% SDS.
Purified	The resazurin supplied with the CellTiter-Blue [®] Cell Viability Assay is purified to ensure that there will be no significant background from residual levels of resorufin in the Reagent.

Adapted from [114].

2.4.2. MTT:

The in vitro mitochondrial dehydrogenase activity was evaluated using the 3-[4,5-dimethylthiazol-2-yl]-3,5-diphenyl tetrazolium bromide (MTT) test, adapted from the protocol previously described [115] and purchased from Sigma. The MTT assay is one of the most common cell viability assays. This assay determines mitochondrial function by evaluating the activity of mitochondrial enzymes such as succinate dehydrogenase [39]. MTT is assumed to be entirely reduced into its formazan intracellularly. The quantity of formazan formed is directly related to the number of metabolically active cells in the culture which can be measured spectrophotometrically when dissolving the formazan in an organic solvent. Reduction of the water-soluble MTT salt by metabolically active cells causes the formation of MTT-formazan crystals. Reduction of MTT in isolated cells is considered as a display of “cell redox activity” [116]. The MTT assay produces a coloured product – a purple formazan – which can be measured by light absorbance at an exact wavelength. The absorbance value results describe both the cell number and the functional viability of those cells [39]. The cells were seeded into 96 well plates and pre-incubated until 90% confluency. Cytotoxicity studies were done after 24 hours of nanoparticles exposure. Then the cells were washed with PBS twice. The cells then received 10 μ l of MTT solution per well. After 3h incubation at 37°C, I added 100 μ l of MTT solubilisation solution (10% triton X-100, 0.1M HCl in anhydrous propan-2-ol) to dissolve the formazan crystals per well. Measurements were performed at wavelengths of 570nm and background at 690nm. The recorded value was A_{570nm}-A_{690nm}. Cells killed with methanol were considered as 100% dead cells.

2.5.Light Microscopy:

Pictures were taken immediately after stimulation with NPs and after 24 hour of exposure. The microscope used was an EVOS XL core transmitted light microscope from Advanced Microscopy Group (AMG) Company. The pictures (phase contrast) were taken on 100, 200 and 400x magnification.

2.6.Cleaned Porcine Intestinal Mucus:

Porcine mucus was prepared in house from freshly scraped pig stomachs as described previously [117]. In brief, 1g of mucus (wet weight) was added to 5ml of sodium chloride (0.1M) and stirred for one hour at 4°C. The sample was centrifuged at 9000rpm (10,400g) at 10°C for 2 hours. After this, the supernatant and granular material at the bottom were discarded. The pellet was re-suspended in half the volume of sodium chloride (0.1M) used for the first extraction. The re-suspended pellet was stirred for 1 hour at 4°C. Then it was centrifuged at 9000rpm (10,400g) at 10°C for 2 hours. Finally, the supernatant was discarded. The cleaned mucus was used immediately or stored frozen until required.

2.7.Rheology:

Rheology was carried out as described previously [117]. 4.5g of cleaned porcine small intestinal mucus was loaded onto 40 mm serrated parallel plates, with gap of 1000 μ m. Excess mucus was removed from the side of the plates using a clean nylon spatula and the samples were covered to prevent dehydration and sample loss. The rheology was analysed using a Kinexus Pro (Malvern Instruments, UK). The sample was allowed to equilibrate and stabilise at 37^oC for 5 minutes before any experiments were performed. The initial experiment was a non-destructive amplitude sweep set at 1Hz, starting at 0.01% complex shear strain to calculate the linear viscoelastic region (LVER). The end of the LVER was determined as the shear strain that caused the G' to deviate from the initial reading by more than 10%. The LVER was used as the fixed amplitude in the second experiment, the frequency sweep with cross over. The frequency sweep was set to run between 0.1 and 10 Hz. The final series of tests were destructive amplitude sweeps. The complex shear strain was set to start at 0.1% up to a maximum of 1000%; however, the test was stopped once the mucus gel became a viscous liquid, which was generally before the test reached a complex shear strain of 600%. This test was repeated three times. The G', G'' and phase angle were measured within LVER for each repeat as well as the complex shear strain of the breakdown point for each repeat.

2.8. Permeation Studies:

The permeation studies were carried out as described previously [118]. In brief, 50 mg of porcine mucus was used in 24 well transwell plates (Greiner-BioOne, Kremsmünster, Upper Austria, Austria). The basolateral chamber was filled with 500µl of 0.1M phosphate buffer at pH 6.8 and the apical chamber was filled with 250 µl of fluorescent labelled SNEDD formulation diluted 1:100 in the buffer as shown on **Figure 6**. The 24 well plate was then covered with a plate lid and incubated at 37°C on a shaking board (Vibramax 100; Heidolph Instruments, Schwabach, Bavaria, Germany). At 0, 1, 2, 3, 4, 5 and 6 hours, samples of 100 µl were removed from the basolateral (acceptor) compartment and replaced with the same volume of the buffer. The samples were measured in 96 well plates at an excitation wavelength of 480nm and an emission wavelength of 520nm (Fluostar Galaxy, Ortenberg, Hesse, Germany). The amount of SNEDD permeation was calculated as compared to the control value. In other words, permeation measurements of each formulation were performed without mucus to determine the 100% control value. A further control to measure the background level of fluorescence and, therefore, 0% of SNEDD permeation was performed. 250µl of the buffer used for the SNEDD suspension was added to the apical chamber without the SNEDDs. This was to determine background fluorescence released from the mucus.

Figure 7 illustrates how the time course of permeation was assessed. Diffusion experiments were carried out without mucus to allow determination of the amount of fluorescent labelled particles that penetrate the membrane and reach the acceptor side. The percentage of penetrated particles was calculated using the following equation:

$$\text{Percentage of permeation} = \frac{[(\text{fluorescence of test NP} - \text{fluorescence of 0\% control}) / (\text{fluorescence of 100\% control at 6 hours} - \text{fluorescence of 0\% control})] * 100.}$$

The percentage of permeation can be calculated for the nanoparticle at each hour interval compared to the 100% control at 6 hours.

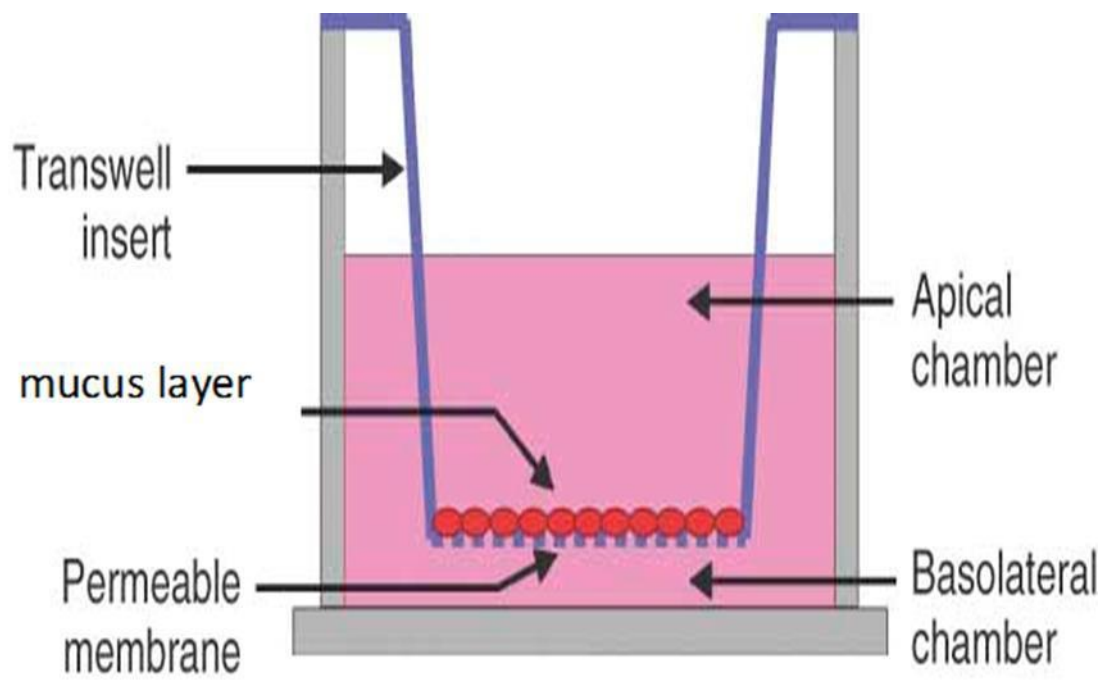


Figure 6. Transwell inserts covered with mucus and particle suspension.

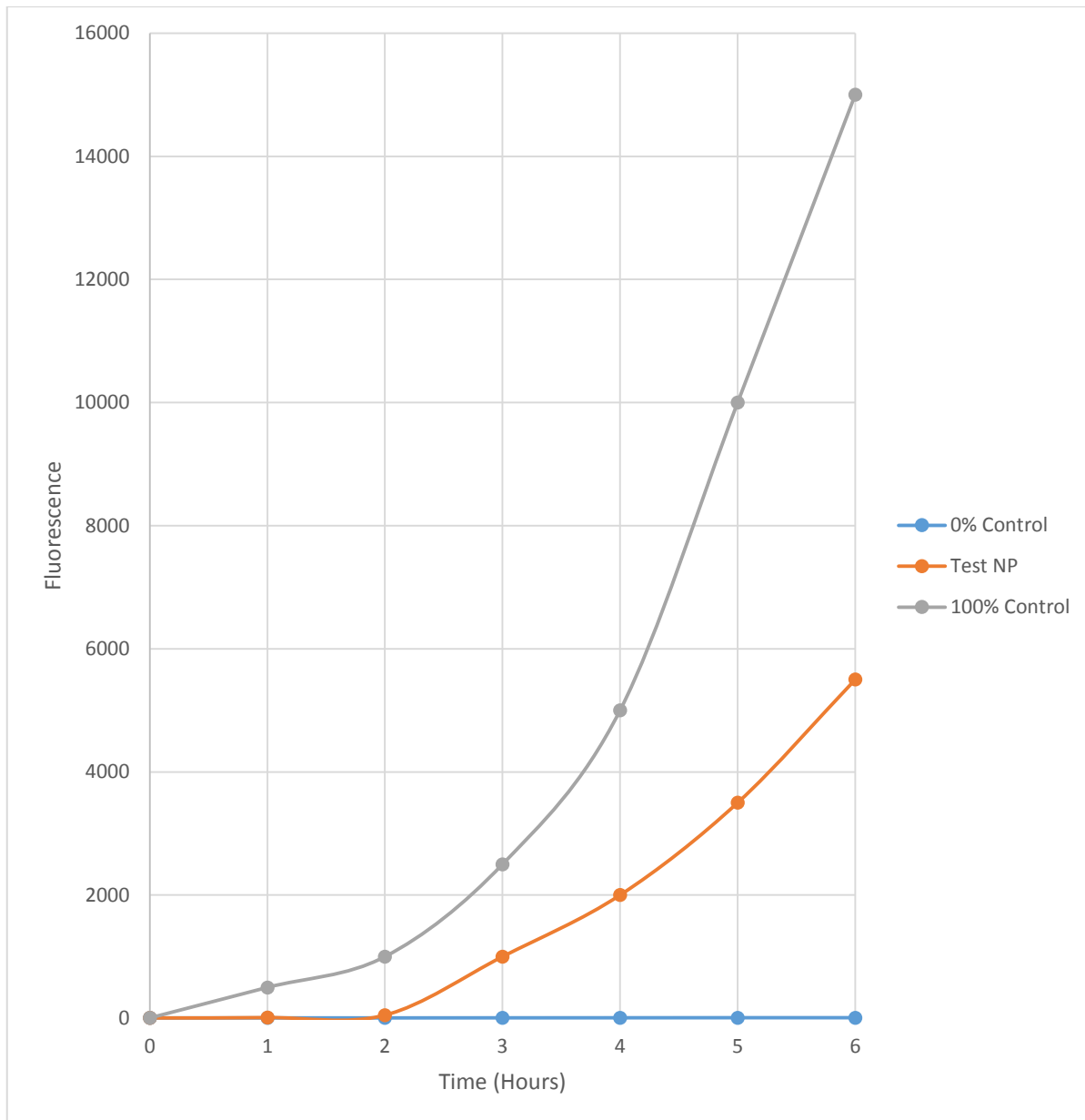


Figure 7: Time course of permeation. 0% control refers to test the permeation of mucus only (no NPs tested). Test NP refer to test the permeation of NPs through the mucus. 100% control refer to test the permeation of NPs without mucus.

2.9. Statistics:

Statistical testing is composed of two types: parametric and nonparametric methods. Parametric methods are used where data follows a normal distribution. Nonparametric methods are employed when the probability distribution cannot be defined. T test is a parametric statistical method used to compare the means of two groups. It is also known as the Student's T test and is a statistical analysis technique developed by William Sealy Gosset in 1908 as a means to control the quality of dark beers. T tests are used when the data in question fulfils the conditions of normality, equal variance and independence. They can be divided into two types: independent and paired. The independent or unpaired T test is used when the two groups under comparison are independent of each other. The paired t test is used when the two groups under comparison are dependent on each other. It can be considered as a type of T test for a single sample since it tests the difference between two paired results [119].

Bar charts with error bars are the most common way of describing sample means with associated error [120]. There are two main purposes for the use of error bars. They indicate the spread of data by displaying the standard deviation around the mean [121]. Error bars can also indicate the reliability of the mean by showing the standard error of the mean (SEM) [121, 122]. Standard deviation (SD) defines the difference of the “observed data” calculated as the average distance from each observation to the sample mean. If the data is normally distributed, 95% of the observations should fall in the range of the mean $\pm 2SD$. The standard error of the mean defines the precision of the sample mean calculated. The SEM is defined as (SD/\sqrt{n}) where n indicates the sample size and \sqrt{n} is the square root of n . The SEM can be related to a statistical significance; 95% confidence intervals (CI) can be derived from SEM values ($95\%CI = \text{mean} \pm 2SE$) [122].

All the statistics were performed using Prism 6 from GraphPad software. Paired T tests were used to analyse differences between the viability of cells and IL-8 levels without NPs and

cells with NPs using human primary lung epithelial cells. Correlation analysis was used to analyse the differences produced by the cell density of Calu-3 cells using the CellTiter Blue assay. Unpaired T tests were used to analyse the permeation of SNEDDS at 6 hours. $P \leq 0.05$ were considered statistically different.

Chapter Three: Nanoparticles and Lung Epithelial Cells

3.1. Abstract:

3.1.1. Introduction:

The aim of this study was to evaluate the safety profile of different novel nanoparticles when interacting with human primary lung bronchial epithelial cells in vitro. More specifically, I was investigating the role of inflammation and cytotoxicity.

3.1.2. Methods:

Primary bronchial epithelial cells (PBEC, passage I and II) and the human airway epithelial cell line (Calu-3) (passage 22-40) were cultured in 24 and 96 well plates. Three different formulations of NPs were used to measure IL-8 production by cells as a marker of inflammation (measured by sandwich ELISA). The Celltitire blue assay (CTB) was used to test cell viability. The effect of cell density on CTB were investigated (500k, 400k, 300k, 200k, 100k, 50k, 42k, 33k, 25k, 17k and 8.3k) in 24 well plates.

3.1.3. Results:

After 24 hours of exposure, the viability of cell exposed to 52nm polystyrene nanoparticles showed no statistical difference between cells with nanoparticles and cells without nanoparticles. The cell density in 24 well plates had a major effect on the CTB assay when the cell seeding density decreased. Calu-3 cells grown in 96 wells plated at 20K density demonstrated that the CTB may not be sensitive enough to test the viability of cells in 96 well plates. In addition to my cytotoxicity results, IL-8 was shown to be slightly increased in human primary cells when stimulated with different concentrations of the nanoparticles. However, IL-8 increased significantly when cells were cultured with the same proportion of sterile water as the nanoparticles were delivered in (a control for osmolarity).

3.1.4 Conclusion:

I have found that CTB may not be sensitive enough to test the viability of cells with NPs. Therefore, other assay systems need to investigate. Furthermore, I have also shown that these NPs do not cause a significant increase in IL-8 production in primary human airways bronchial epithelial cells. Any apparent increase in IL-8 with NPs may have been because of osmotic shock.

3.2.Introduction:

The European Science Foundation (ESF) identified the five main areas in which nanomedicine is used: (i) analytical tools, (ii) nano-imaging, (iii) nanomaterials and nanodevices, (iv) novel therapeutics and drug delivery systems and (v) clinical, regulatory and toxicological issues [5]. Currently, nanotechnology is used for molecular imaging to achieve clearer diagnosis with better-quality images. Nanotechnology is also being used in biomarker-based proteomics and genomics technologies. These applications may allow clinicians to accurately diagnose disease at the very early stages, allowing more effective therapy [123]. Furthermore, the use of nanotechnology in drug delivery has been shown to enhance bioavailability, have minimal side effects and have decreased toxicity to other organs, as well as being less expensive. This can be administered in many ways such as vascular injections or inhalation [124].

The increasing use of nanoparticles (NPs) in different areas has raised broad concerns about their safety [125]. Due to their small size, NPs have unique properties compared with bulk material, as they have a having larger surface area per unit mass ratio and, therefore, potentially larger biological reactivity and also quantum effects potentially leading to novel hazards [126]. In addition, NPs may interfere with traditional cytotoxicity tests because of their large surface area and chemically active surfaces, producing false positives or false negatives in assessments of toxicity, making it difficult to compare toxicity data. Possible interactions from particles are: (1) the particle optical properties could interfere with light absorption or fluorescence methods used for detection, (2) chemical interactions between the particles and the assay components, and (3) binding of assay molecules to the particle surface [127]. At the present time, a range of assays are used which measure cell viability through enzyme activity; for example, (3-(4, 5-dimethylthiazol-2-yl)-2, 5-diphenyltetrazolium bromide [MTT] measures the activity of NADH dependent enzymes, thus measuring cell metabolic activity of NADH-dependent cellular oxidoreductase enzymes. The CellTiter-Blue assay which relies on the

reduction of resazurin to resorufin or ATP level as in the CellTiter-Glo assay. However, little has been reported about the interactions between nanoparticles and the compounds used in these assays. The levels of interference in these assays requires further investigation [128]. For instance, Belyanskaya et al. 2007 found that the interference of single walled carbon nanotubes (SWCNTs) with the MTT assay can be influenced by surfactants used to suspend the SWCNTs. Moreover, depending on the purification procedure of SWCNTs, they are able to reduce MTT to its MTT-formazan form in the absence of cells or enzymes. It has been suggested that careful assay validation and controls are needed to avoid a potential bias in concluding results of cytotoxicity studies. Belyanskaya et al. reported that the amount of interference can be based on three factors: (1) the assay protocol, (2) surfactant interactions and (3) the chemical structure of the SWCNT. They concluded that extreme caution should be used when interpreting cell viability data without the appropriate controls in place [116]. In another study, Hoskins et al. 2012 investigated magnetic nanoparticles [MNPs] 100nm in diameter coated with poly (ethylenimine) [MNP-PEI] and poly (ethylene glycol) [MNP-PEI-PEG] to provide a subtle difference in their surface charge and their cytotoxicity. This was analysed by three standard cell viability assays: 3-(4,5- dimethylthiazol-2-yl)-5-(3-carboxymethoxyphenyl)-2-(4-sulfophenyl)-2H-tetrazolium [MTS], CellTiter Blue and CellTiter-Glo in human neuroblastoma (SH-SY5Y) and mouse macrophage (RAW 264.7) cells. They found that in comparison to trypan blue manual counting, the MTS and Titer-Blue assays overestimated the viability while the Titer-Glo also showed a small but non-significant overestimation. For example, at 25µg/ml MNP-PEI nanoparticles, RAW 264.7 cells were all dead when measured using trypan blue, whereas cellTiter Blue showed ~400% viability and MTS showed ~150% viability. Their findings show that when interpreting cell viability data from commercial assays on novel nanoparticles, caution should be applied. Their data strongly suggested that analysis of nanotoxicity needs a different approach to conventional toxicity studies used for cytotoxic compounds and other molecules. Their results also

demonstrate that cell viability measurements must be allied with analysis of other cellular processes when determining the cytotoxicity and biocompatibility of nanoparticles [128]. Kroll et al. 2012 demonstrated that 24 engineered nanoparticles interfered with classic cytotoxicity assays using A549 cells in a concentration, particle and assay-specific dependent manner. They observed a concentration dependent interference of all 24 engineered NPs with the optical measurements used to determine the oxidative stress (dichlorofluorescein, DCF), cellular metabolic activity (MTT) and cell viability (*lactate dehydrogenase*, LDH). These results suggest that each in vitro test system has to be evaluated for each nanoparticle type to assess nanoparticle cytotoxicity [129]. Verifying cytotoxicity data with at least two or more independent test systems has been suggested earlier [130] but still may not be sufficient to eliminate inaccurate results and incorrect interpretations [129]. Darolles et al. 2013 found that Co_3O_4 nanoparticles interfere with CellTiter blue at high doses above 1250 $\mu\text{g}/\text{mL}$ using BEAS-2B cells. They modified the assay protocol by introducing a centrifugation step to remove the nanoparticles before reading the luminescence. The results from this assay agreed with those from a clonogenic assay. They suggested that interference testing should be performed before assessing particle toxicity using in vitro tests to avoid false interpretations. In addition, in several cases of interference, the protocol could be adapted to allow the reliable use of these in vitro tests [125].

The aim of my study was to evaluate the safety profile of different novel NPs when interacting with human primary lung bronchial epithelial cells in vitro. More specifically, I am investigating inflammation and cytotoxicity. I also investigated the effect of cell density of Calu-3 cells on the CellTiter blue assay and the effect of nanoparticles on a standard curve for IL-8.

3.3. Methods:

3.3.1 Cell Cultures:

See chapter 2 for methods of primary bronchial epithelial cells and Calu-3 cells.

3.3.2. Nanoparticles:

The two polystyrene nanoparticles NP7 and NP8 (PNP; catalogue number 100111-10, 100121-10, respectively) were obtained from the Corpuscular Company (New York, NY). The primary sizes as initially received were 52 and 100nm respectively, based on photon correlation spectroscopy and/or laser diffraction provided by the company. Furthermore, I have used three different poly (d-lactide-co-glycolide) (PDLG) (NP1-3) and three different poly (lactic-co-glycolic acid) (PLGA) (NP4-6). The details of the NP7 and 8 are shown in **table 11**. The NPs were stored on the fridge at 4°C until use.

3.3.3. Dispersion Protocol:

All materials used to prepare the stock and working concentration were sterilized and prepared in a laminar flow cabinet. Nanoparticles were used on the cells immediately after preparing the working concentration. Stock concentration were disposed of. See Chapter 2 for further information.

3.3.4. IL-8 Measurement:

See chapter 2.

3.3.5. Cell Viability: see chapter 2

The CellTiter-Blue assay was used. See chapter 2.

3.3.6. Light Microscopy:

See chapter 2.

3.3.7. *Statistics:*

Details are given in chapter 2.

3.4. Results and Discussion:

3.4.1. *The Physiochemical Characterizations of the NPs:*

The characterization of the nanoparticles used is shown in **table 11**.

Table 11. Physiochemical characterizations of NPs 7 and 8 used in this study.

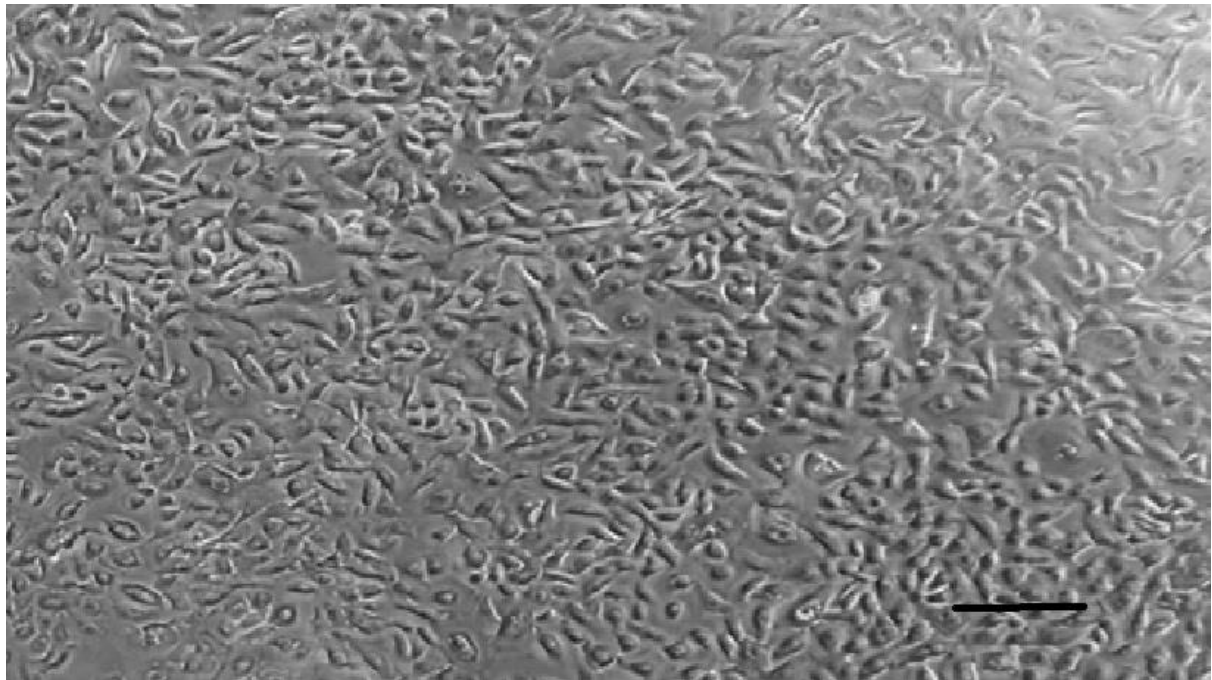
Nanoparticle Types	Identification Name	Concentrations as Received	Quantity	Fluorescent Marker	Suspended in	Colour	Size nm	Zeta potential mV
NP7	polystyrene nanoparticles	25 mg/ml	10 ml	N/A	DI water	white	52	N/A*
NP8	polystyrene nanoparticles	25 mg/ml	10 ml	N/A	DI water	white	100	N/A*

N/A* = not available.

3.4.2. Light Microscopy:

I stimulated human primary bronchial epithelial cells with 52nm polystyrene nanoparticles and took pictures of the cells after 24 hour exposure with different concentrations of NPs (**Figure 8**). There were no obvious differences in morphology between the controls (cells without NPs) and the cells with NPs. Cells exhibited the typical cobble stone appearance of viable epithelial cells and are phase bright to indicate their live appearance. There is no evidence of cells becoming fibroblastic (which would be recognised by a spindle shaped appearance).

A)



B)

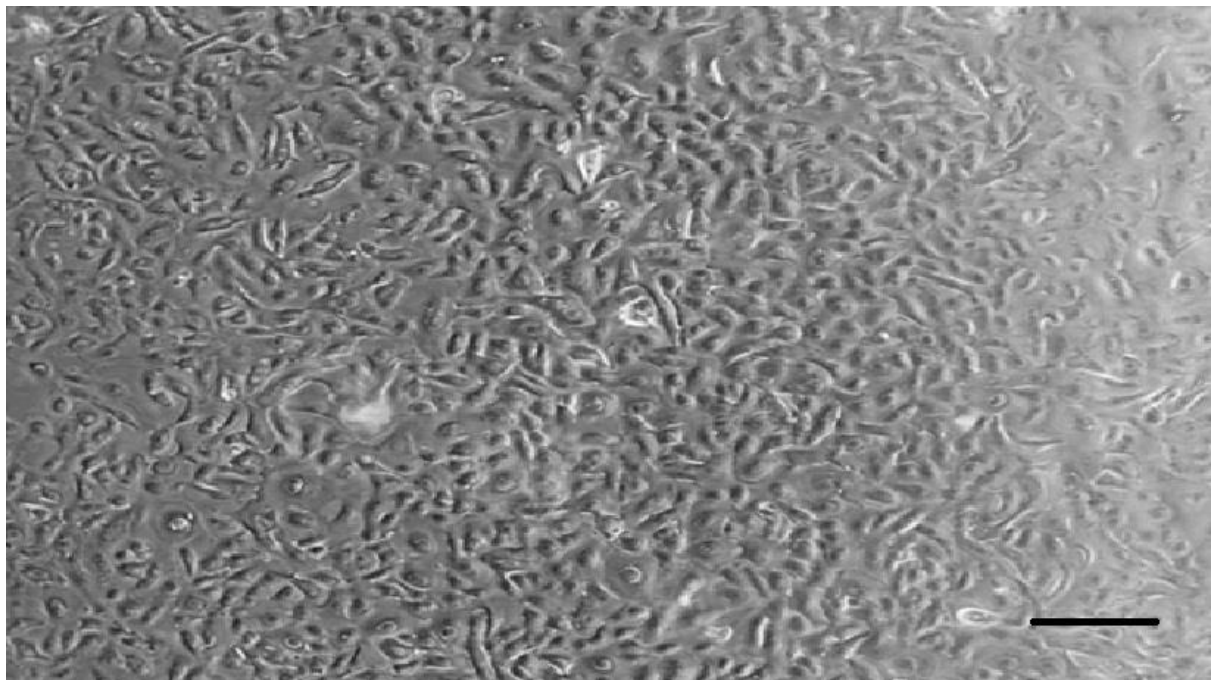


Figure 8: Primary epithelial cells A) control cells (cells treated with resting media only). B) 50µg/ml of 52nm polystyrene. Scale bar 200µm.

3.4.3. Cell Viability:

After 24 hours exposure of the 52nm Polystyrene nanoparticles (NP7) at 50 μ g/ml, I investigated the viability of cells. The results are presented in **table 12** after CellTiter blue assay incubation for 2 hours (n=7). It showed there is no statistical difference between cells without NPs and those with NPs (P value 0.06). It can be seen from **table 12** that cell viability with NPs was 100% and the cells exposed to PNP ranged from 67.8% up to 100% with a median value of 94.1. Three of the experiments (3, 4, and 6) showed cells remained 100% viable after polystyrene NP exposure, whereas experiments 1, 2, 5 and 7 showed a decrease in viability on exposure of the cells to nanoparticles (77.8, 74.3, 94.1, and 67.8, respectively). Overall, the four experiments showed a decrease in viability on exposure to nanoparticles, and the other three showed no change.

Table 12. The percentage of live cells in primary human bronchial epithelial cells after 24 hours exposure of 50µg/ml of 52nm PNP (NP7).

Number of experiment	The viability of control (cells without NPs)	The viability of cells with NPs
1	100	77.8
2	100	74.3
3	100	100
4	100	100
5	100	94.1
6	100	100
7	100	67.8

P value is 0.06. There is no significant different between the viability of cells without NPs and cells with NPs. The viability of controls (100%) cells represent the viability of cells untreated with NPs (i.e. cells treated with resting media).

As a control I investigated the interference of polystyrene NPs (PNP) (size 100nm) with the Celltiter-blue assay in the absence of cells in 96 well plates. The results are presented in **table 13** and **figure 9** after CTB incubation of 2 hours (n=5). The results were negative even with the control (resting media with CTB only). There was no colour change detected in any of the experiments. In other words, the CTB assay maintained a dark blue colour. In the absence of cells, resazurin was not converted into the end product of resorufin. When I subtracted 600nm (~maximum absorbance resazurin) from 570nm (~ maximum absorbance of resorufin), the absorbance of resorufin (product) was lower than that of resazurin (substrate). This indicated that there is no interference of PNP with the CTB assay itself in the absence of living cells. Hoskins et al. (2012) investigated the effect of magnetic NPs (MNPs) with CTB assay reagents in the absence of cells. They demonstrated that there is no significant effect on absorbance, fluorescence or luminescent readout, proposing that the increase absorbance and fluorescence were only apparent and caused by the combination of cells, assay reagents, and NPs [128].

Table 13: the OD absorbance of polystyrene NPs with CTB assay (without cells).

Experiment/ Concentration	1	2	3	4	5	Average	Standard deviation
Control	-0.07	-0.29	-0.1	-0.14	-0.14	-0.15	0.09
25 µg/ml	-0.07	-0.23	-0.12	-0.14	-0.16	-0.15	0.06
50 µg/ml	-0.12	-0.16	-0.14	-0.15	-0.15	-0.14	0.02
100 µg/ml	-0.08	-0.21	-0.06	-0.16	-0.13	-0.13	0.06

Control experiment refer to resting media only (no NPs) incubated with CTB assay.

PNP with CTB

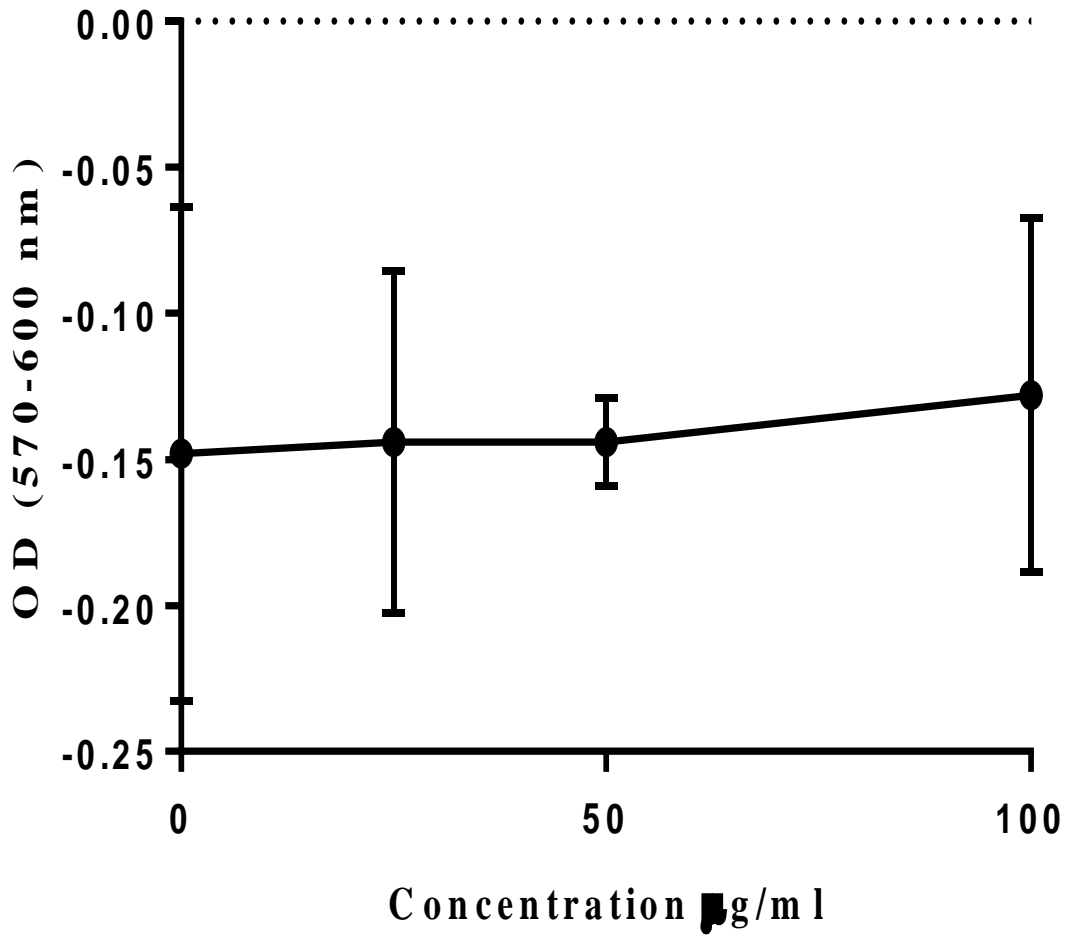


Figure 9: the OD absorbance of polystyrene NPs with CTB assay (without cell culture).

Three primary human lung epithelial cells cultures were exposed to three different PDLG nanoparticles (NPs 1-3) (**Table 8**) for 24 hours in 24 well plates. In each experiment (**Table 14**), cells were washed with PBS twice before applying the assay to avoid possible interference with the assay. In PDLG 5002A NPs, the viability of 100 μ l and 200 μ l were 90.6% and 95.5% of alive cells. When I stimulated the cells with the same concentration of deionized water, the results of 100 μ l and 200 μ l were 100% and 82.1% of alive cells. In PDLG 45002B, all the concentrations tested of NPs and deionized water remained 100% alive cells. In PDLG 5002, all the concentration tested remained 100% alive, except for 100 μ l of deionized water (82.3% of alive cells). In addition to this, I noticed that some of the OD values were higher than 100% alive cells. For example, the OD values of 100 μ l and 500 μ l of PDLG 45002B were 0.8 and 0.9 which were higher than the controls cells with an OD value of 0.6 (cells without NPs). Even with the deionized water, the OD value of 100 μ l and 500 μ l (0.9 and 1.1) were higher than the control cells (0.6) (cells without deionized water). These results might be due to differences in cell density. Therefore, I further investigated the effect of cell density on the CTB using Calu-3 cells in 24 well plates.

Table 14. Results of the CTB assay of three different PDLG NPs in human primary epithelial cells.

NPs	Concentration μ l	OD values of 570-600nm	Percentage of alive cells
PDLG 5002A	Control	0.9	100
	100	0.9	90.6
	100a	1.1	100
	200	0.9	95.5
	200a	0.8	82.1
PDLG 5002B	Control	0.6	100
	100	0.8	100
	100a	0.9	100
	500	0.9	100
	500a	1.1	100
PDLG 5002	Control	0.6	100
	50	0.7	100
	50a	0.7	100
	100	0.6	100
	100a	0.6	82.3

Standard curves were constructed using mixtures of live and methanol killed cells in the ratios of live: dead, 100:0, 75:25, 50:50, 25:75, and 0:100. N/A= not applicable. a= concentrations of deionized H₂O instead of NPs. Please note that these results are for triplicates of exposure of NP1-NP3 (**Table 8**) on PBEC.

3.4.4. The Effect of Cell Density on the CTB Assay:

Calu-3 cells were cultured at different seeding densities in 24 well plates to study their effect on the CTB assay (**Table 15, Figures 10-12**). In my first experiment (n=3), I cultured Calu-3 cells at different seeding densities of 500K, 400K, 300K, 200K, 100K and 50K. I applied the CTB assay only when the 500K density of Calu-3 was confluent at about 90%. It is shown that standard curves vary as the cell density decreased (**Figure 10**). **Table 16** represents correlation analysis between these cell densities. There are significant differences between 500K and 400K (3.62e-004), 500K and 300K (P value is 0.0008), 500K and 100K (P value is 0.03), and 500K and 50K (P value is 0.008). There are also significant differences between 400K and 300K (P value is 1.8e-004), 400K and 100K (P value is 0.03), and 400K and 50K (P value is 0.02). Additionally, there is a significant difference between 300K and 100K (P value is 0.02), and 300K and 50K (P value is 0.02). There is a significant difference between 100K and 50K (P value is 0.03). In the second experiment (n=3), I cultured Calu-3 cells at different densities varying from 42K, 33K, 25K, 17K and 8.3K. I applied the CTB assay when the 42K density of Calu-3 was confluent at about 90%. It is also shown that standard curves vary as the cell density decreased (**Figure 10**). **Table 17** represents correlation analysis between these cell densities. There are significant differences between all of the cell density tested (P values shown in **table 17**). Overall, it appears that seeding densities have a major effect on the CTB assay. As cell density decreased, the assay seems to lose accuracy. In higher numbers of cells, the standard curves appear to be closer to parallel due to a better signal (stronger). In lower numbers of cells, the signal of the assay is weak and becomes less accurate. The standard curves diverge as the density gets lower and the signal is affected. It should be noted that OD values in primary cells are higher than Calu-3 cells. This may be due to higher activity in primary cells, suggesting that those cells have more metabolic activity. After investigating the assay characteristics in 24 well plates, I investigated the sensitivity of the CTB assay in 96 well plates.

Table 15. Summarized results of cell density effect on the CTB assay. For each cell density, experiments were done in duplicate at least. All of the experiments were done with Calu-3 in 24 well plates.

%DC	Cell density										
	500K	400K	300K	200K	100K	50K	42K	33K	25K	17K	8.3K
100	0.06	0.05	0.05	0.06	0.04	0.05	0.01	0.02	0.01	0.01	0.03
75	0.07	0.07	0.07	0.05	0.05	0.05	0.04	0.04	0.03	0.03	0.03
50	0.1	0.1	0.09	0.04	0.05	0.06	0.08	0.08	0.06	0.05	0.05
25	0.12	0.12	0.11	0.1	0.06	0.06	0.11	0.11	0.09	0.07	0.06
0	0.14	0.14	0.13	0.13	0.08	0.07	0.14	0.13	0.1	0.08	0.06

Standard curves were constructed using mixtures of live and methanol killed cells in the ratio of live:dead: 100:0, 75:25, 50:50, 25:75, and 0:100. It should be noted that the OD values given in the table are the result of absorbance at 570 minus the absorbance at 600nm.

Table 16. Correlation analysis between cell densities of Calu-3. Cells seeded at 50K, 100K, 200K, 300K, 400K and 500K. Numbers of experiments were in triplicate.

Cell density	500K	400K	300K	200K	100K	50K
500K	N/A	3.62e-004	0.0008	0.1	0.03	0.008
400K	3.62e-004	N/A	1.80e-004	0.13	0.03	0.01
300K	0.0008	1.8e-004	N/A	0.11	0.02	0.02
200K	0.10	0.13	0.11	N/A	0.049	0.14
100K	0.029	0.03	0.02	0.049	N/A	0.03
50K	0.008	0.01	0.02	0.14	0.034	N/A

N/A= Not applicable. It should be noted that the value in the table represent the P value. P value < 0.05 is considered significant. CTB were used when 500K was at least 90% confluent.

Table 17. Correlation analysis between cell densities of Calu-3. Cells seeded at 8.3K, 17K, 25K, 33K and 42K. Numbers of experiments were in triplicate. CTB were used when all the cells were at least 70% confluent. Experiments were carried out in 24 well plates.

Cell density	42K	33K	25K	17K	8.3K
42K	N/A	0.0001	0.0006	0.0003	0.01
33K	0.0002	N/A	0.0001	0.0004	0.006
25K	0.0006	0.0001	N/A	0.0002	0.006
17K	0.0003	0.0004	0.0002	N/A	0.01
8.3K	0.012	0.006	0.006	0.01	N/A

N/A= Not applicable. It should be noted that the value in the table represent the P value. P value < 0.05 is considered significant. Numbers of experiments were in triplicate. The CTB assay was carried out when 42K cells were at least 90% confluent.

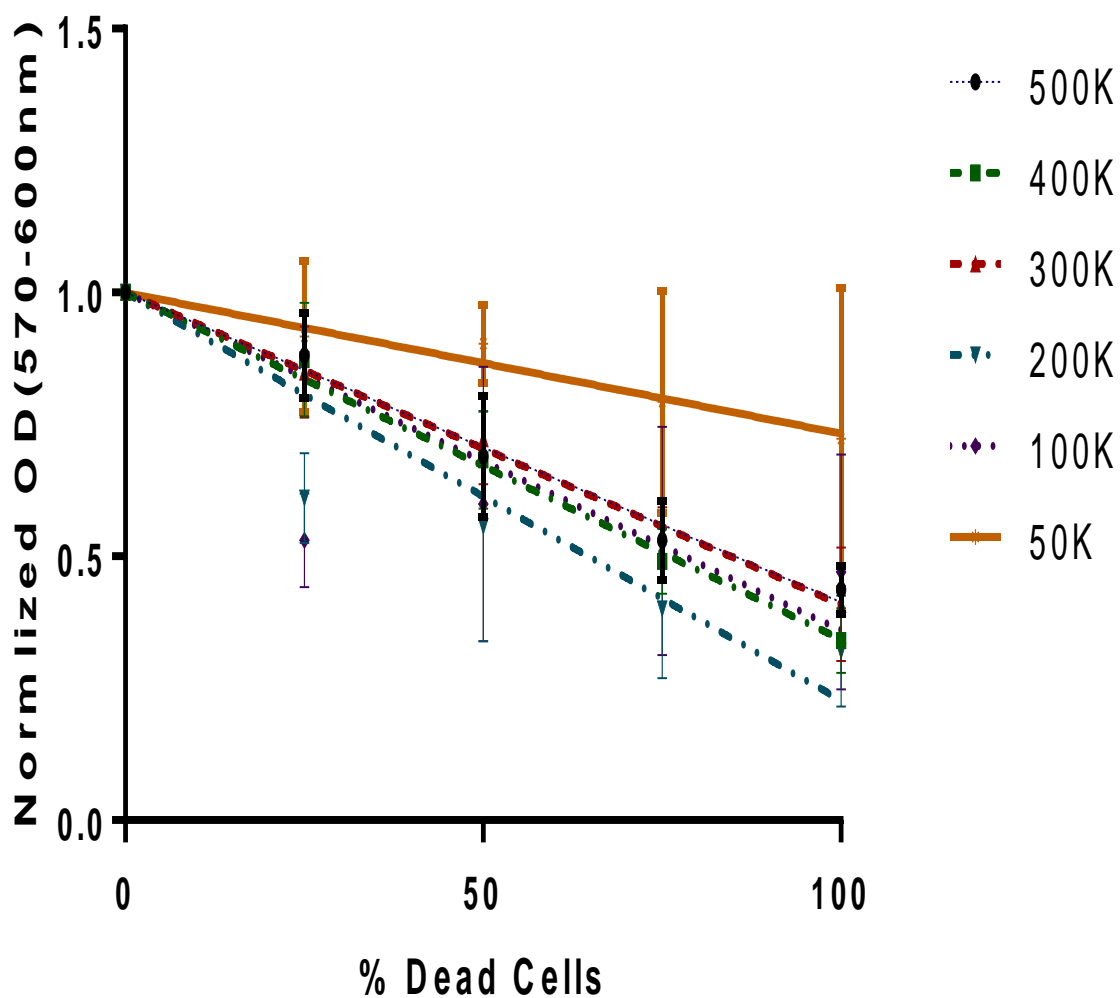


Figure 10. The effect of cell density in CTB assay in Calu-3. Cells were seeded between (serial dilutions) from 500K to 50K in 24 well plates. Numbers of experiments were in triplicate. CTB were used when 500K cells were at least 90% confluent. Standard curves were constructed using mixtures of live and methanol killed cells, in the ratios of live: dead, 100:0, 75:25, 50:50, 25:75, and 0:100. Data were normalized to 100% live cells for each condition. Then I have re-plotted to force to (0, 1) for each regression line.

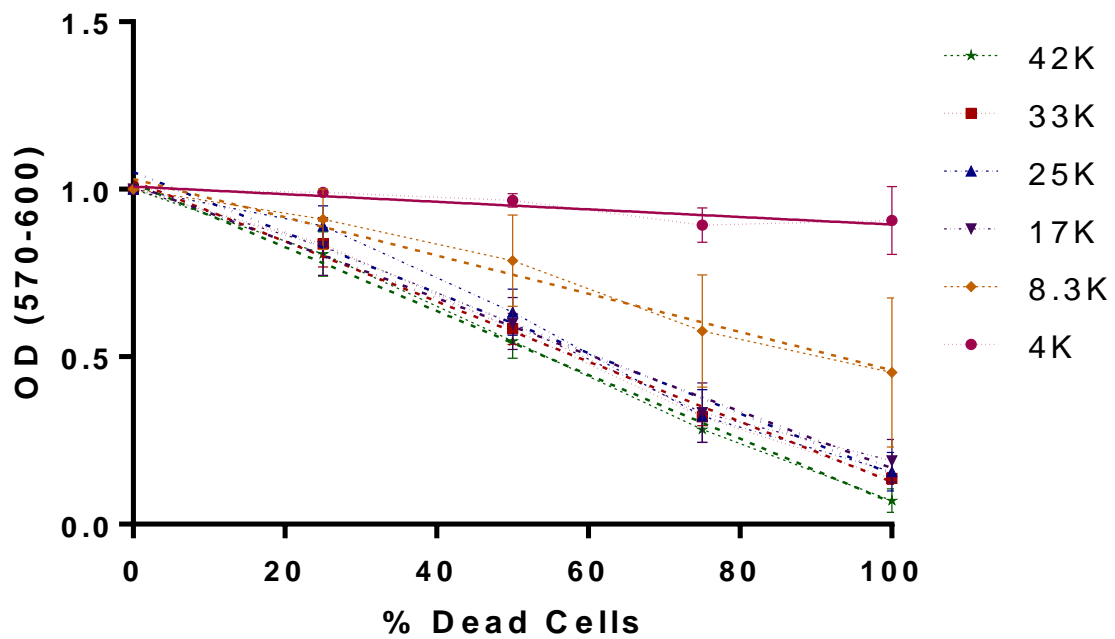


Figure 11. The effect of cell density in CTB assays in Calu-3. Cells were seeded between on serial dilutions from 42K to 8.3K in 24 well plates. Numbers of experiments were in triplicate. CTB were used when 42K cells were at least 90% confluent. Standard curves were constructed using mixtures of live and methanol killed cells, in the ratios of live: dead, 100:0, 75:25, 50:50, 25:75, and 0:100. Data were normalized to 100% live cells for each condition. Then I have re-plotted to force to (0, 1) for each regression line.

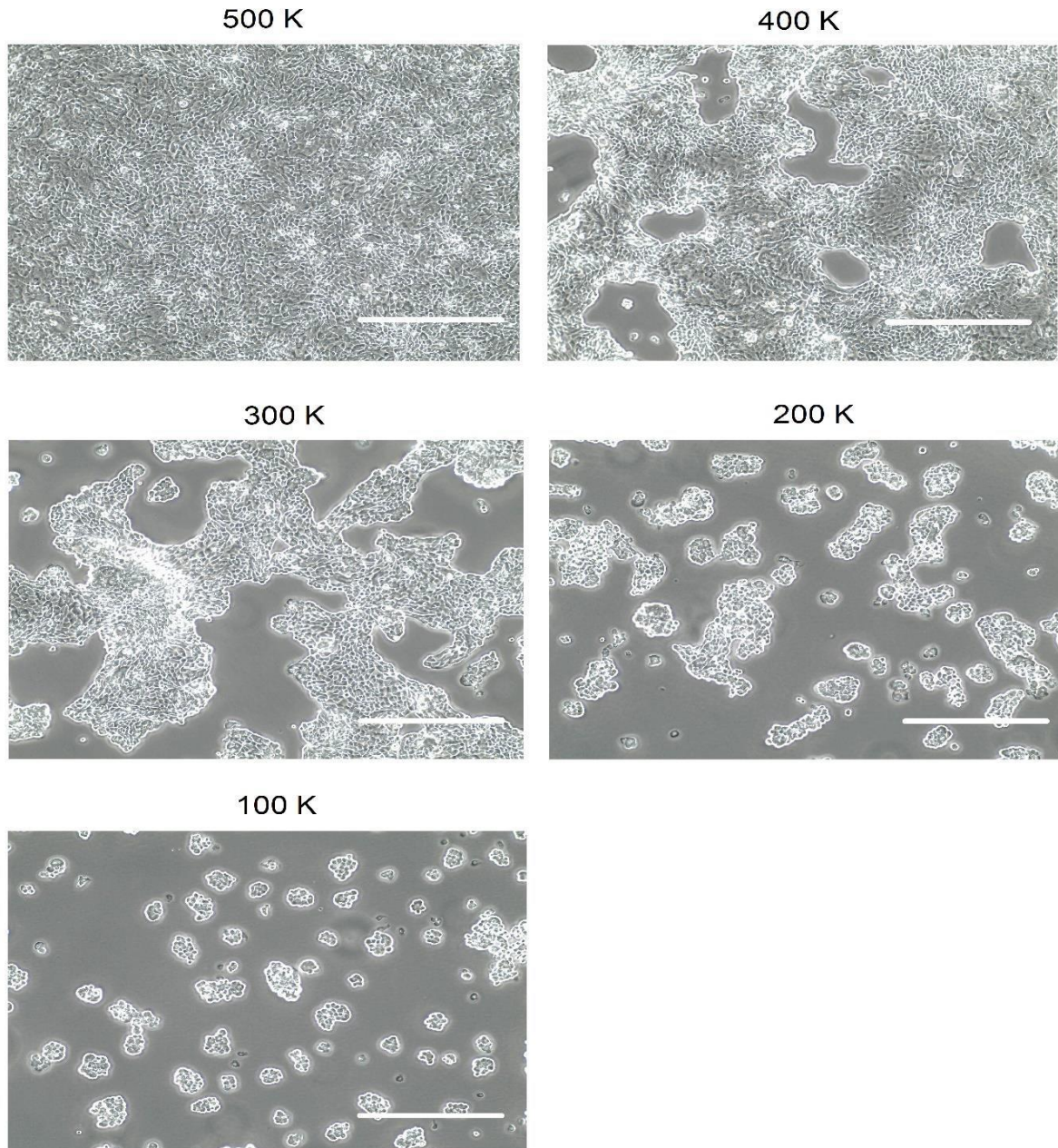


Figure 12. Images taken illustrating different confluency of Calu-3 cells. 100% confluency reached for 500K. Scale bar 500 μm . The number of cells in Calu-3 cultures is hard to count in images because they grow in clusters. Therefore, a subjective estimate of confluency has been applied instead. The degree of confluency was 80% for 400K, 60% for 300K, 40% for 200K and 20% for 100K.

3.4.5. Measuring CTB Assays using 96 Well Plates:

After studying the effect of cell density in 24 well plates, I cultured Calu-3 at a seeding density of 20K (per well) in 96 well plates and carried out a CTB assay (**Figure 13, Table 18 and 19**). I found that the CTB assay could test the percentage of live and dead cells for Calu-3 seeded at 20K cell density.

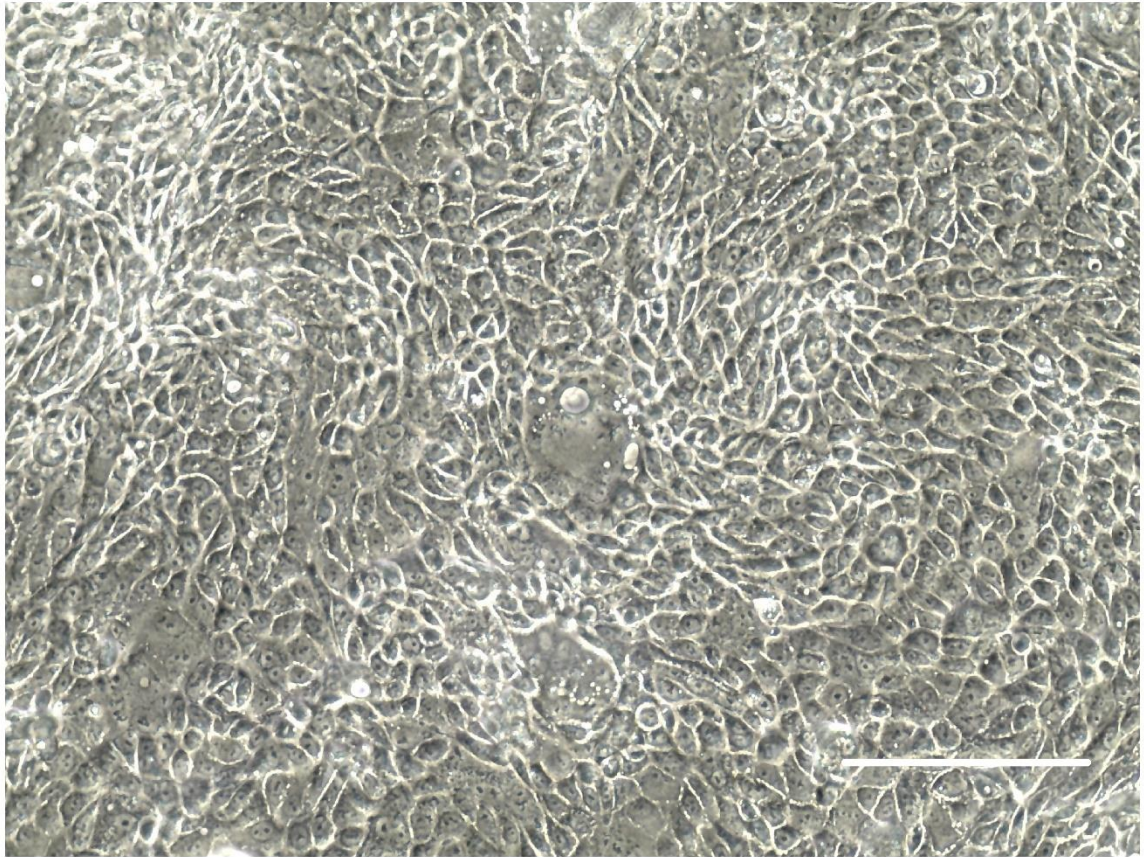


Figure 13. 100% confluent Calu-3 grown in well of 96-well plate. Seeding density 20K. Scale bar 200 μm .

Table 18. The effect of 20K cell seeding density on the CTB assay. Triplicate experiments were done in 96 well plates with Calu-3 cells.

Experiment number	Percentage of dead cells	OD value of 570-600nm at 20K density per well
1	100%	-0.16
	75%	-0.01
	50%	0.11
	25%	0.27
	0%	0.39
2	100%	-0.24
	75%	-0.03
	50%	0.19
	25%	0.41
	0%	0.41
3	100%	-0.21
	75%	-0.03
	50%	0.01
	25%	0.29
	0%	0.36

It should be noted that the value of 20K density per well is the OD value of subtraction of absorption at 570nm-600nm. Standard curves were constructed using mixtures of live and methanol killed cells in the ratios of live:dead: 100:0, 75:25, 50:50, 25:75 and 0:100.

Table 19. The average and standard division of 20K cell seeding density on CTB.

Percentage of dead cells	Mean	Standard deviation
100%	-0.2	0.04
75%	0.02	0.01
50%	0.1	0.09
25%	0.32	0.08
0%	0.39	0.03

The data are derived from **table 18**.

In addition to cell line experiments, I stimulated primary epithelial cells with three different NPs (NP4-6) (**Table 8**) for 24 hours and measure cytotoxicity in 96 well plates. I found that three types of nanoparticles interfered with the CTB assay (data not shown). In other words, my data were above the OD value of control cells.

Hoskins et al. (2012) found that magnetic nanoparticles (MNP-PEI, and MNP-PEI-PEG) seems to have consistently overestimated the viability when using the Celltitre blue assay (CTB). They assumed that interactions were happening between the assay systems with the assay reagents and the nanoparticles, causing incorrect cell viability assessment. They suggested that interference was only presents when the cells, the NPs and the reagents were present [128]. Monterio-Riviere et al. (2009) investigated single wall carbon nanotubes (SWCNT), Fullerenes (C60), Carbon black (CB), nC60 and quantum dots (QD) on human skin epithelial cell line (keratinocytes) and applied CTB and MTT assays. They found that these assays produce unacceptable results with some nanoparticles due to nanoparticles/dye interaction and/or nanoparticles adsorption of the dye/dye products. They concluded that nanoparticles interact with assay markers to cause variable results with standard toxicology assays and may not be appropriate for measuring nanoparticles cytotoxicity. This suggests that more than one assay should be required during when measuring nanoparticle cytotoxicity as well as imaging techniques such as transmission electron microscopy, to validate chemical marker-based viability assays [130]. In addition, Oostingh et al. (2011) found that the CTB assay was incorrect for detecting cell viability since the fluorescence measurement showed a false rise in the cell viability, possibly due to the physical presence of the particles rather than particle induced effects [131]. AshaRani et al. (2009) investigated silver nanoparticles (Ag-np) on normal human lung fibroblast cells (IMR-90) and human glioblastoma cells (U251). They found that CTB shows a slow drop in metabolically active cells. However, these observations show the same interference as seen with the ATP assay where the NPs produce a large absorbance without the presence of the cells [132]. Schlinkert

et al. (2014) studied differently functionalized silver (Ag) and gold (Au) on A549 cells, BEAS-2B cells and NHBE cells. They found that there is a small interference in the light emitted during the endpoint when measuring both of Ag and Au NPs with CTB assay, causing a small underestimation of the NPs induced reduction in cellular viability [133].

3.4.6. *The Effect of Nanoparticles on the ELISA Standard Curve for IL-8:*

After 24 hours exposure with 50µg/ml of 52nm PNP, IL-8 cytokines were measured via the sandwich ELISA. In **table 20** (the data was calculated on normal IL-8 standards as shown in **Figure 14a**), there is no statistical difference between cells without NPs (mean is 549) and cells with NPs (mean is 532) (P value is 0.9, n=7). Moreover, it shows that these NPs do not downregulate IL-8 production. Ruenraroengsak et al. (2012) showed a significant increase in IL-8 with 50nm unmodified polystyrene latex nanoparticles (NPs) with transformed human alveolar epithelial type 1-like cells (TT1) at 50 µg/ml [134]. Thach and Finkelstein (2012) investigated the interaction of charged polystyrene bead particles consisting of 57nm amine conjugated, 780 nm amine conjugated, 60nm carboxyl conjugated and 820 nm carboxyl conjugated with A549 cells. They found that there is a reduction in IL-8 levels [135]. However, I cannot directly compare my results to these results due to different cell cultures and different incubation times. In addition to this, I used human primary bronchial epithelial cells which are closer to humans. I also investigated if the nanoparticles interfere with IL-8 assay, and if so, how (i.e. over or underestimate). Therefore, I did an extra three standard curves to answer these questions (**Figure 14b**). It seems that 52nm PNP at a concentration of 50µg/ml does not interfere with the level of IL-8.

Table 20. Concentration of IL-8 with control (cells without NPs) and with 50µg/ml of 52nm PNP.

Experiment number	Control (without NPs, pg/ml)	With NPs (pg/ml)
1	1198	812
2	138	238
3	877	911
4	412	435
5	198	259
6	459	532
7	558	610
Mean	549	532

There is no significant difference between control and cells with NPs (paired t test two tailed, P = 0.09). Experiments were carried out in 24 well plates.

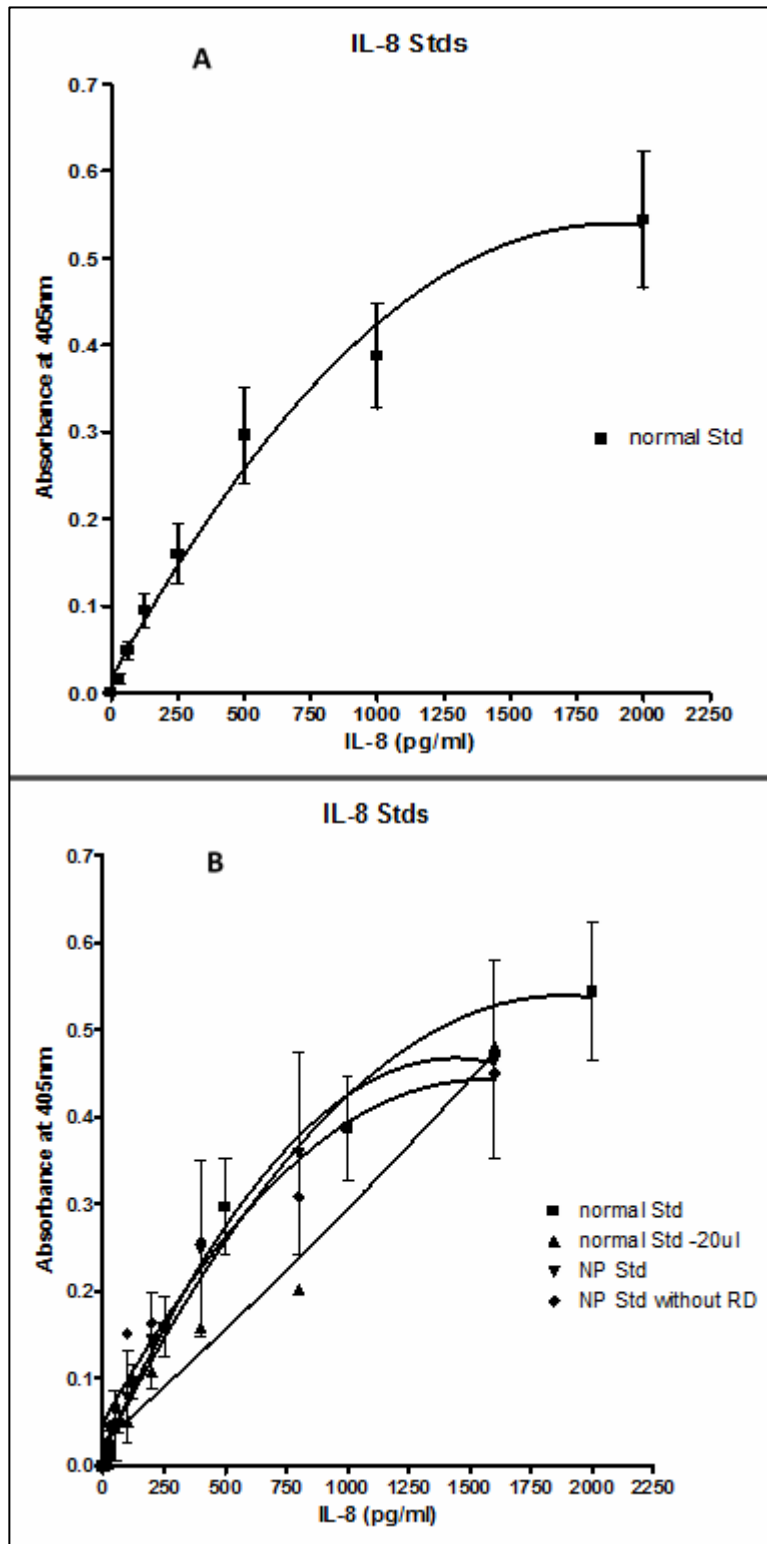


Figure 14. The standard curves of IL-8. A) Mean standards data for IL-8 ELISA. b) IL-8 normal std. normal std= normal IL-8 standard of 0-2000 pg/ml. Normal std-20 μ l= normal standard of IL-8 of 0-1600 pg/ml, NP std= nanoparticle standard 0-16000 pg/ml, NP std without RD= IL-8 standard with media with nanoparticles at a concentration of 50 μ g/ml (total concentration of IL-8 was 0-1600 pg/ml).

3.4.7. The Effect of NPs on IL-8 Levels Using Primary Human Epithelial Cells:

I stimulated epithelial cells from PHEC with three different NPs types (**Table 8**) and measured IL-8 levels using ELISA in 24 well plates (**Table 21**). I also stimulated the cells with the same concentration of deionized water as a control for osmotic shock because these NPs were made in deionized water. In PDLG 5002A NPs, there is an increase in IL-8 in both concentration tested (100 and 200 μ l) compared to untreated cells (control). When I used the same concentration of deionized water to test the osmotic effect, there was 16 fold increase in IL-8 for 200 μ l. Similarly to PDLG 5002A, PDLG 5002B NPs showed an increase in IL-8 in both concentrations tested (100 and 500 μ l) compared to untreated cells. In testing for osmotic shock, 500 μ l of deionized water showed a maximum increase of almost 19 fold compared to untreated cells. In PDLG 5002 NPs, there is only an increase at a concentration of 50 μ l. 100 μ l of these NPs show a downregulation in IL-8 production. 50 μ l of deionized water showed a slight increase in IL-8 and 100 μ l of water showed a 2 fold increase in IL-8. Overall, IL-8 release increased slightly but not significantly with the three different formulations of PDLG NPs. The maximum osmotic shock occurred at the maximum tested volume of deionized water (500 μ l).

Table 21. IL-8 concentration with three different NPs. a*= water ratio as controls in IL-8. Each NP was done in duplicate experiments on primary epithelial cells patients.

NPs types	The concentrations of 500µl in NPs solution or H ₂ O	Volume of resting media µl	IL-8 concentration pg/ml
PDLG 5002A	Untreated	500	142
	100	400	364
	100a*	400	245
	200	300	323
	200a	300	1964
PDLG 5002B	Untreated	500	142
	100	400	405
	100a	400	268
	500	0	371
	500a	0	2647
PDLG 5002	Untreated	500	154
	50	450	178
	50a	450	191
	100	400	144
	100a	400	314

The characterizations of these NPs are listed in **Table 8**. All of these experiments are done with 24 well plates. It should be noted that the total volume of nanoparticles or water or resting media is 500µl.

Chapter Four: Mucosal Drug Delivery via Self-Nanoemulsifying Drug Delivery Systems

4.1. Abstract:

4.1.1. Introduction:

The aim of this study was to evaluate the cytotoxicity of self-nanoemulsifying drug delivery systems (SNEDDS) and to assess the mucus permeation behaviour of SNEDDS within a novel mucus diffusion model utilizing standardized Transwell diffusion plates.

4.1.2. Methods:

Three different SNEDDS labelled with lumogen were produced (Aristotle University of Thessaloniki, Greece). Calu-3 cells were used to assess their cytotoxicity using the MTT assay. Permeation studies were carried out using a mucus diffusion model. The samples were measured in 96 well plates at an excitation wavelength of 480nm and an emission wavelength of 520nm. The amount of SNEDDS permeation was calculated as compared to the control value which was a permeation measurement of each formulation performed without mucus to determine the 100% maximal permeation. A further control to measure the background level of fluorescence from mucus and, therefore, 0% of SNEDDS permeation was performed. 250 μ l of the buffer used for the SNEDDS suspension was added to the apical chamber without the SNEDDS. The rheology of mucus was measured to assess the gel structure of mucus. Oscillation amplitude, oscillation frequency and amplitude sweep strain controlled were analysed in order to characterise the rheological properties of the mucus.

4.1.3. Results:

Although the plates were washed with PBS twice before applying the MTT assay, the results indicate that there is interference with the MTT assay. Despite this, SNEDDS-associated cytotoxicity was seen at the highest concentration used. The data showed that there was no size dependent permeation of mucus (15nm vs 35nm); however, the composition of the

SNEDDS (such as lauroglycol) may play a major role in their ability to permeate mucus. Also, mucus is not homogenous and this resulted in variation of the permeation data. The elastic modulus (G') is dominant over the viscous (G'') parameter indicating that the mucus was still a gel. The phase angles (δ) were between 12.3 to 19.4°. The initial breakdown stress (Pa) values were highest compared to the repeated breakdown stress in all experiments.

4.1.4. Conclusion:

SNEDDS-a was cytotoxic at high concentrations. The mucus used in these experiments behaved as a gel. I showed that the composition of the SNEDDS played an important role in determining the permeation of the mucus gel layer.

4.2.Introduction:

Mucus is a viscoelastic and adhesive gel which defend the lung airways, gastrointestinal (GI) tract, vagina, eye, and other mucosal surfaces [15, 136]. The mucus layers protect the mucosal tissues. They help in forming steric adhesive barriers which are frequently cleared and renewed. The mucus barrier generally contain negatively charged glycoproteins secreted by goblet cells and mucosal glands but not in the stomach. It is composed of mucins, which have cysteine rich subunits connected by disulphide bonds [118]. Many foreign particulates, including particle based drug delivery systems, are competently immobilized in mucus layers by the pores and/or by adhesion. The nanoparticles are then removed from the tissue within seconds to a few hours based on the location in the body, resulting in a limitation in the duration of drug delivery locally. In order to bypass mucus, nanoparticles must avoid adhesion to mucins and be small enough to penetrate the pores in the dense fibre mesh [136]. The diffusion of poorly soluble drugs via the mucus gel layer is essential to allow interaction with the epithelium and to lead to an acceptable serum concentration. Nanoemulsions are such a formulation to ensure adequate drug dissolution and are spontaneously formed in the presence of water or gastric juice [118]. Self-nanoemulsifying drug delivery systems (SNEDDS) are isotropic mixtures of oil, surfactant and co-surfactant which naturally develop an oil/water nanoemulsion when mixed with water. It has been suggested that their interactions with the mucus layer would be small because of the hydrophobic surface of the formed nanodroplets [137]. Self-emulsifying means that the formulation forms an emulsion spontaneously and this is a property of the components in the formulation and it does not require mechanical mixing. Therefore, the term derives as self- emulsifying [138]. However, this may not be the case as mucus does contain hydrophobic regions. Due to the greater surface area formed by nanoemulsions, drugs solubilized in SNEDDS have a high dissolution velocity [118].

The aim of this investigation was to assess the potential cytotoxicity of SNEDDS and

evaluate the mucus permeation behaviour of SNEDDS within a novel mucus diffusion model utilizing a standardized Transwell diffusion system.

4.3.Methods:

4.3.1. *Nanoparticles:*

Details are given in chapter 2.

4.3.2. *Nanoparticles Dispersion:*

Details are given in chapter 2.

4.3.3. *Calu-3:*

Details are given in chapter 2.

4.3.4. *MTT Assays:*

Details are given in chapter 2.

4.3.5. *Cleaned Porcine Intestinal Mucus:*

Details are given in chapter 2.

4.3.6. *Rheology of Mucus:*

Details are given in chapter 2.

4.3.7. *Permeation Studies:*

Details are given in chapter 2.

4.3.8. *Statistics:*

Details are given in chapter 2.

4.4. Results and Discussions:

4.4.1. Nanoparticles Characterization:

Nanoparticle Characterization is shown in **table 5**.

4.4.2. Cytotoxicity:

The cytotoxicity data of SNEDDS-a, -b, and -c is illustrated on **tables 22, 23, and 24** (n=5). The average percentage live cells for 2, 0.2, and 0.02 mg/ml of SNEDDS-a was 56, 93, and 97 respectively, demonstrating that SNEDDS-a are only cytotoxic at the highest concentration. The average percentage of live cells for 2, 0.2, and 0.02 mg/ml of SNEDDS-b was 88, 85, and 93 respectively, demonstrating that SNEDDS-b showed little cytotoxic at any of these concentrations. The average percentage of live cells for 2, 0.2, and 0.02 mg/ml of SNEDDS- c was 97, 97, and 98 respectively. As with SNEDDS-b, SNEDDS-c was not cytotoxic. Although the plates were washed with PBS twice before applying the MTT assay, the results show interference with the MTT assay. The fact that interference happened even after washing with PBS suggests that the nanoparticles had attached to or were taken up by the cells. This could be explained by the fact that SNEDDS are lipid and, as such, are compatible with cell membranes. Furthermore, fluorescence did not affect the cytotoxicity result. Belyanskaya et al. (2007) found that the MTT assay may be influenced by surfactants used to suspend single wall carbon nanotubes (SWCNT). They suggested that interference in the MTT assays can be influenced by (i) the surfactant used to suspend SWCNTs; (ii) the MTT method used; and (iii) the types of SWCNTs [116]. Monteiro-Riviere et al. (2007) studied SWCNT, fullerenes (C60), carbon black (CB), and quantum dots (QD) in vitro with human epidermal keratinocytes to determine their cytotoxicity with the MTT assay. They found false positive reactions due the adsorption of cell metabolized formazan by nanoparticles. They suggested that more than one assay could be required when assessing nanoparticle cytotoxicity [130]. Furthermore, Kroll et al. (2012) assessed the validity of the MTT assay using 24 well characterized nanoparticles. They demonstrated that nanoparticles

interfere with MTT assays in a concentration and assay specific dependent way, suggesting that each in vitro test system has to be assessed with each nanoparticle type to accurately determine the nanoparticle cytotoxicity. They also indicated that extra washing steps should be included and nanoparticles concentrations should be limited to non-interfering levels. They also concluded that classic cytotoxicity assays have to undergo extra development and be validated for each particle tested [129]. Hoskins et al. (2012) investigated the viability of magnetic NPs using 3-(4,5-dimethylthiazol-2-yl)-5-(3-carboxymethoxyphenyl)-2-(4-sulfophenyl)-2H-tetrazolium [MTS] in human neuroblastoma (SH-SY5Y) and mouse macrophage (RAW 264.7) cells. They showed that MTS assays have dependably overestimated the viability, suggesting that interactions were happening between the NPs and the assay system, causing an incorrect cell viability assessment [128]. Vrček et al. (2015) studied the interference of different surface coatings of silver (AgNPs) and maghemite NP (γ -Fe₂O₃NPs) with the MTT assay and found false results. They suggested that the interference was dependent on the nature and the surface characteristics of the nanoparticles and their stability in physiological media. Their results also indicated that interference was concentration and assay type dependent [139]. However, Karamanidou et al. (2015) who developed SNEDDS formulations for oral insulin delivery containing a hydrophobic ion pair of insulin/dimyristoyl phosphatidylglycerol (INS/DMPG), demonstrated that SNEDDS-c (27.2 nm) is the least cytotoxic, while SNEDDS-a (30.1 nm) and -b (36.7nm) are more cytotoxic with 2mg/ml showing around 80% of cell death in Caco-2 cells. These differences may be due to the presence of Lauroglycol FCC which was included only in SNEDDS-a and -b [140]. It should be noted that the SNEDDs in my study are different in size, oil/surfactant/co-surfactant and the cell cultures used in the Karamanidou et al. study. I demonstrated that SNEDDS- b (15 nm) and -c (15 nm) were the least cytotoxic, suggesting that size plays a rule in cytotoxicity similar to the Karamanidou et al. results. Perhaps the different in my cytotoxicity data was due to the presence of lauroglycol which was found only in SNEDDS-a.

Table 22. Cytotoxicity results of SNEDDS-a.

Experiments / Concentrations	1	2	3	4	5	Average	Standard Deviation
Untreated	100	100	100	100	100	100	0
2mg/ml	11	85	64	18	100	56	39.7
0.2mg/ml	99	100	67	100	100	93	14.7
0.02mg/ml	100	100	86	100	100	97	6.3

These values are percentage of live cells (n=5). Experiments were made using 96 well plates of Calu-3 cells. Calu-3 cells were incubated 24 hours with SNEDDS-a. Calu-3 cells were washed twice with PBS before applying MTT assay. It should be noted that SNEDDS -a contained lumogen which interferes with the MTT assay. Corrections were made by measuring this interference and subtracting it from values obtained with the cells.

Table 23. Cytotoxicity results of SNEDDS-b.

Experiments / Concentrations	1	2	3	4	5	Average	Standard Deviation
Untreated	100	100	100	100	100	100	0
2mg/ml	71	68	100	100	100	88	16.74
0.2mg/ml	61	65	100	100	100	85	20.32
0.02mg/ml	100	66	100	100	100	93	15.21

These values are percentage of live cells (n=5). Experiments were made using 96 well plates of Calu-3 cells. Calu-3 cells were incubated 24 hours with SNEDDS-b. Calu-3 cells were washed twice with PBS before applying MTT assay. It should be noted that SNEDDS -b contained lumogen which interferes with the MTT assay. Corrections were made by measuring this interference and subtracting it from values obtained with the cells.

Table 24. Cytotoxicity results of SNEDDS-c.

Experiments / Concentrations	1	2	3	4	5	Average	Standard Deviation
Untreated	100	100	100	100	100	100	0
2mg/ml	84	100	100	100	100	97	7.2
0.2mg/ml	86	100	100	100	100	97	6.3
0.02mg/ml	91	100	100	100	100	98	4.0

These values are percentage of live cells (n=5). Experiments were made using 96 well plates of Calu-3 cells. Calu-3 cells were incubated 24 hours with SNEDDS-c. Calu-3 cells were washed twice with PBS before applying MTT assay. It should be noted that SNEDDS -c contained lumogen which interferes with the MTT assay. Corrections were made by measuring this interference and subtracting it from values obtained with the cells.

4.4.3. Mucus Permeation by Nanoparticles (Permeation Study):

The results of my permeation studies are summarized in **Figures 15-18**.

Percentage of permeation = [(fluorescence of test NP–fluorescence of 0% control) / (fluorescence of 100% control at 6 hours - fluorescence of 0% control)] * 100.

The percentage of permeation of SNEDDS-a, -b, and -c after 6 hours was 41%, 40%, and 18% respectively. SNEDDS-a is not statistically different from SNEDDS-b (P=0.95) and -c (P=0.21). Moreover, SNEDDS-b is not statistically different from SNEDDS-c (P=0.07). As shown in **table 9**, SNEDDS-a is larger than b and c (35nm vs 15nm). There is no size dependency on mucus permeation because SNEDDS-a and -b have almost the same permeation but have different sizes (35nm for SNEDDS-a and 15nm for SNEDDS-b). However, my results indicate that nanoparticle composition may play a major role in determining the permeation of the mucus. This is because SNEDDS-b and -c have the same size (15nm) but are composed of different material and lipids. Both SNEDDS-b and -c have transutol and cremophor materials (Transcutol P and cremophor RH 40 lipids) but SNEDDS-b has ethanol and SNEDDS-c has PEG 400. The shape of the graphs show similar biphasic kinetics of permeation through mucus of the nanoparticles. SNEDDS-c achieves a slower rate; SNEDDS-c shows a permeation rate over the first 2 hours of ~5% per hour, but over the next 4 hours the rate slows to ~2.5% per hour. Both SNEDDS-a and -b show a faster rate of ~10% per hour over the first 2 hours and then a halving of the rate to ~5% per hour over the next 4 hours. It should be noted that there is some variation in the results. For instance, in **table 25**, experiment 3 has 1 hour permeations of 4% and 6 hour permeations of 19%. However, in experiment 4 there was 12% of 1 hour permeations and 87% of 6 hour permeations. These differences could be related to the fact that mucus is not homogenous, sample variation and different components present within the mucus. It also could contain regions of lower density or pores and this potentially accounts for these variations. Friedl et al. (2013) studied different SNEDDS formulations and

investigated their diffusion behaviour through a porcine intestinal mucus layer. They found that the permeation of SNEDDS occurred in a size dependent manner; with a 70.3% permeation for a formulation with lower droplet size (12nm) compared to only 8.3% for a formulation with a higher size (455nm) [118]. Additionally, 455nm is in the range of the pores in mucus reported as 20-500nm [15], suggesting that SNEDDS of 455nm would be excluded from most of the pores and would, therefore, not permeate the mucus layer. Friedl et al. (2013) also showed that formulation composition was an essential determinant of drug permeation as SNEDDS formulations prepared using cremophor RH40 and triacetin were found to be the most effective formulations [118]. Karamanidou et al. (2015) showed that SNEDDS-c has around 40% permeation in comparison with SNEDDS-a and -b which have around 30% permeation. They suggested that these differences may be because of possible interaction between mucus and SNEDDS, depending on the structural characteristics of the SNEDDS ingredients (e.g., oil, surfactant, co-surfactant) and their composition [140].

Table 25. SNEDDS-a percentage of permeation over 6 hour.

Experiments/ Time (hour)	1	2	3	4	Average	Standard Deviation
1	18	1	4	12	9	7.8
2	17	2	9	41	17	17
3	25	7	16	66	29	26.0
4	26	14	18	59	29	21.0
5	28	28	18	84	40	29.7
6	28	29	19	87	41	31.3

The amount of SNEDD permeation was calculated as compared to the control value. The permeation measurement of each formulation was additionally performed without mucus to determine the 100% control value. A further control containing mucus was only applied to see if it any of the background fluorescence is mucus related.

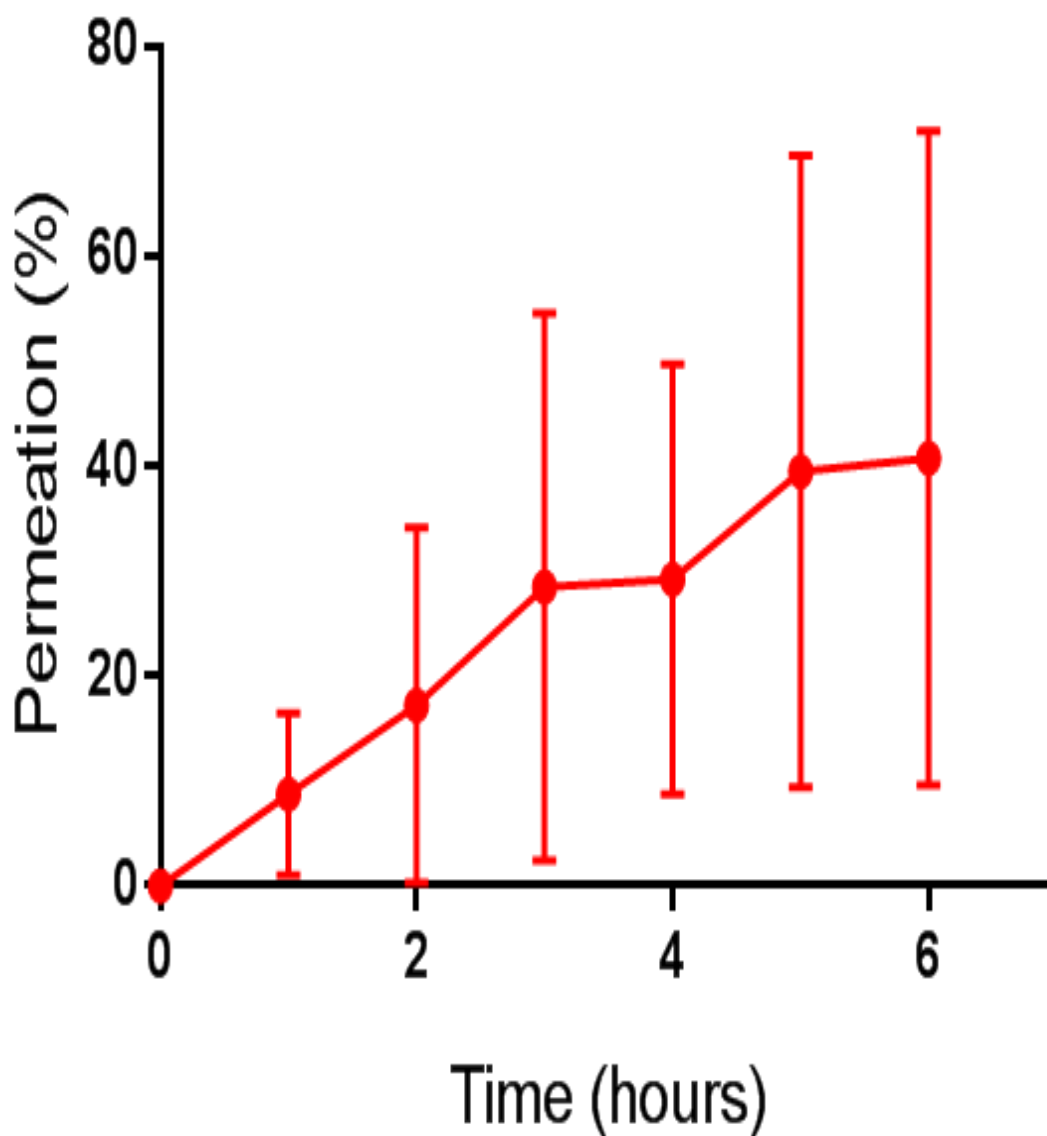


Figure 15: Permeation results for SNEDDS-a. The amount of SNEDD permeation were calculated as compared to the control value. The permeation measurement of each formulation were additionally performed without mucus to determine the 100% control value. A further control containing mucus only was applied to see if it was any background fluorescence is mucus related. 0% control refers to test the permeation of mucus only (no NPs tested). Test NP refers to a test of the permeation of NPs through the mucus. 100% control refers to a test of the permeation of NPs without mucus.

Table 26. : SNEDDS-b percentage of permeation over 6 hour

Experiments/ Time (hour)	1	2	3	4	Average	Standard Deviation
1	2.7	20	4.9	10	9	7.6
2	4	31	19	14	17	11.5
3	9	44	20	18	23	14.9
4	14	47	19	22	26	14.6
5	28	45	20	24	29	11.0
6	31	47	20	60	40	17.4

The amount of SNEDD permeation was calculated as compared to the control value. The permeation measurement of each formulation was additionally performed without mucus to determine the 100% control value. A further control containing mucus was only applied to see if it any of the background fluorescence is mucus related.

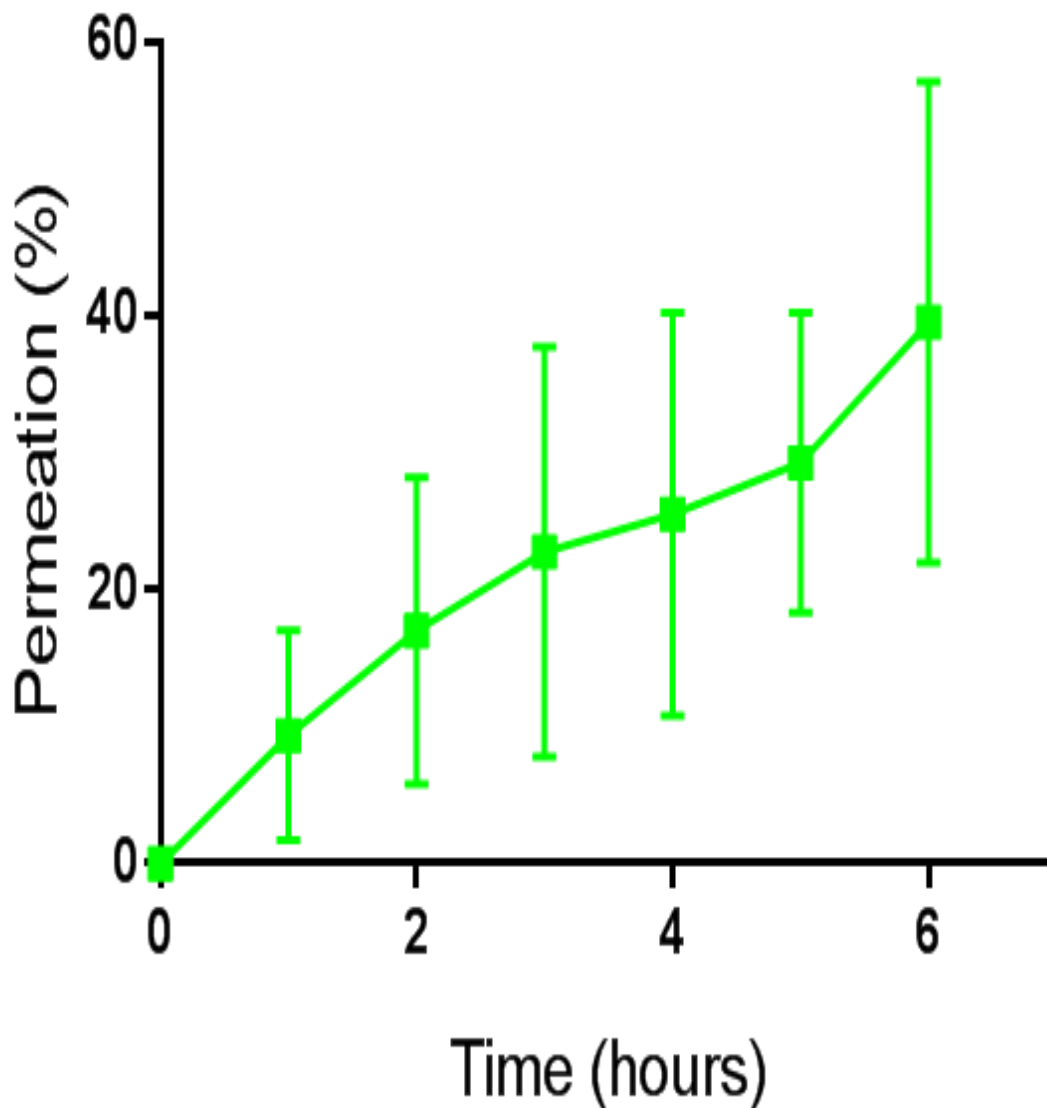


Figure 16: Permeation results for SNEDDS-b. The amount of SNEDD permeation were calculated as compared to the control value. The permeation measurement of each formulation were additionally performed without mucus to determine the 100% control value. A further control containing mucus only was applied to see if it was any background fluorescence is mucus related. 0% control refers to test the permeation of mucus only (no NPs tested). Test NP refers to a test of the permeation of NPs through the mucus. 100% control refers to a test of the permeation of NPs without mucus.

Table 27. SNEDDS-c percentage of permeation over 6 hour.

Experiments/ Time (hour)	1	2	3	4	Average	Standard Deviation
1	4	4	4	5	4	0.5
2	4	6	9	19	9	6.4
3	4	8	16	20	12	7.5
4	4	11	18	19	13	7.0
5	6	26	18	20	18	8.3
6	8	26	19	20	18	7.5

The amount of SNEDDS permeation was calculated as compared to the control value. The permeation measurement of each formulation was additionally performed without mucus to determine the 100% control value. A further control containing mucus was only applied to see if it any of the background fluorescence is mucus related.

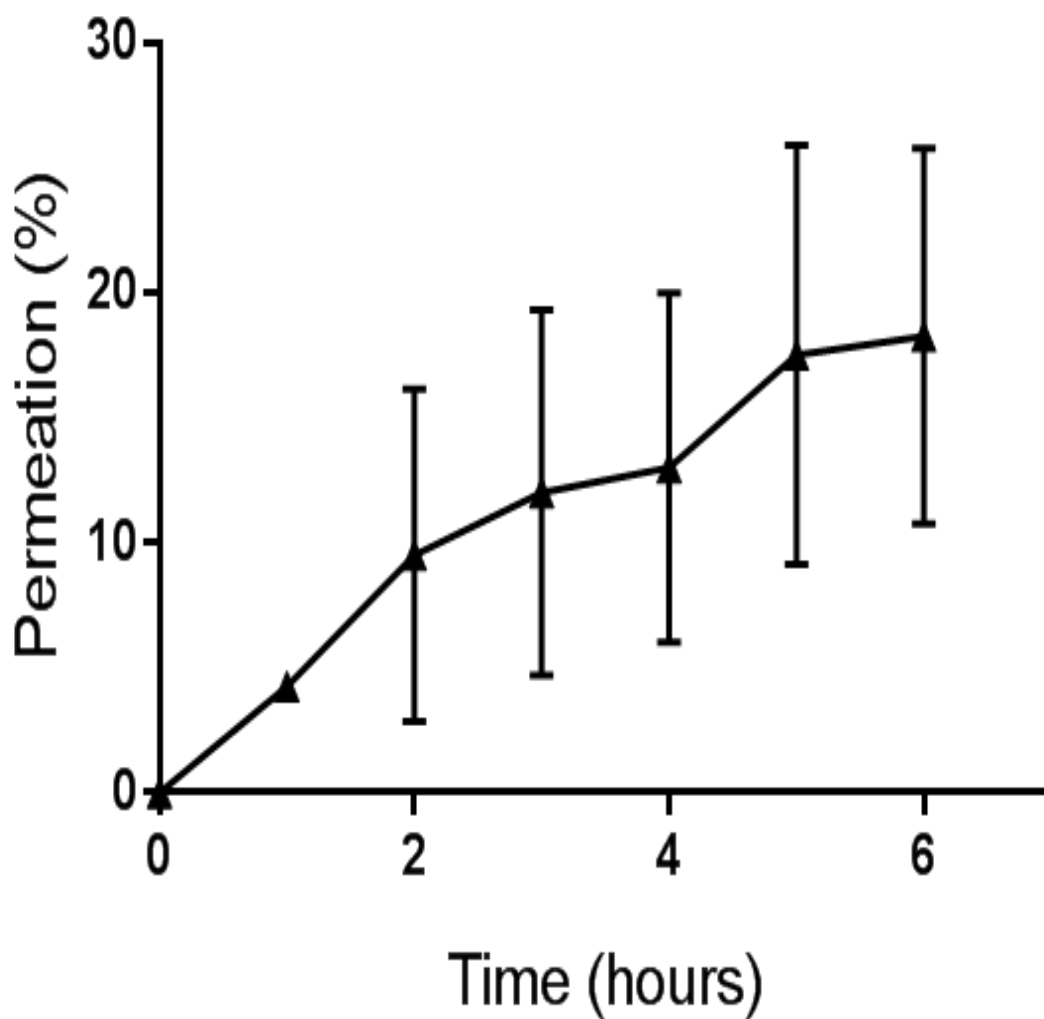


Figure 17: Permeation results for SNEDDS-c. The amount of SNEDD permeation were calculated as compared to the control value. The permeation measurement of each formulation were additionally performed without mucus to determine the 100% control value. A further control containing mucus only was applied to see if it was any background fluorescence is mucus related. 0% control refers to test the permeation of mucus only (no NPs tested). Test NP refers to a test of the permeation of NPs through the mucus. 100% control refers to a test of the permeation of NPs without mucus.

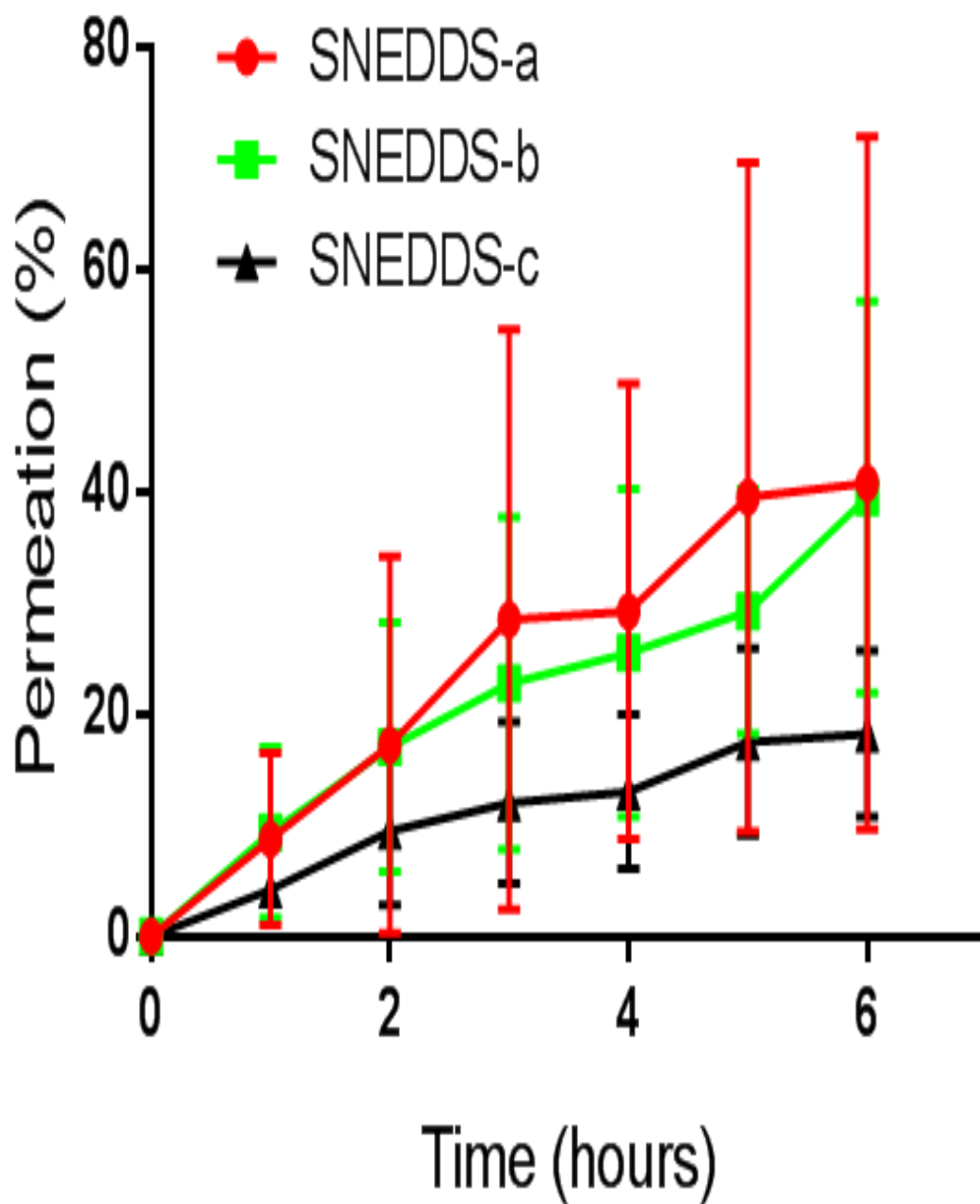


Figure 18: the permeation results of all SNEDDS together. The amount of SNEDD permeation were calculated as compared to the control value. The permeation measurement of each formulation were additionally performed without mucus to determine the 100% control value. A further control containing mucus only was applied to see if it was any background fluorescence is mucus related. 0% control refers to test the permeation of mucus only (no NPs tested). Test NP refers to a test of the permeation of NPs through the mucus. 100% control refers to a test of the permeation of NPs without mucus.

4.4.4. Rheology of Porcine Intestinal Mucus:

It was essential for the performance of valid permeation studies that the mucus used in the test system was verified to be in the gel state as this is the native state in vivo and, consequently, an understanding of this state is functionally important. Rheology is the study of the flow and deformation of materials and is a commonly used method in the study of biopolymers, encompassing viscosity, creep testing and oscillatory rheology. In the case of a pure solid, as the strain is directly correlated to the stress, maximum strain will be at the point of maximum applied stress. The stress wave and strain wave will be precisely in phase with each other and the material can be assumed to have a phase angle of 0° . In the case of a pure liquid, it is the strain rate that is directly correlated to the applied stress. The strain rate will be zero at the maximum applied stress; thus, the stress and the strain waves will be 90° out of phase with each other and, hence, have a phase angle of 90° . Many materials (including mucus) are said to be viscoelastic and they have phase angles between 0 and 90° . If the phase angle is below 45° then solid like behaviour takes over and these material are commonly reflected as gels. Accordingly, solid like behaviour ($\delta < 45^\circ$) relates to $G' > G''$. The lower the phase angle, the greater dominance of the solid like behaviour over liquid like behaviour and, hence, the stronger the gel [141].

Rheological characteristics of the porcine intestinal mucus from the small intestine are summarized in **table 28 (figure 19)**. In all experiments ($n=5$), the elastic (G') is dominant over the viscous (G''), indicating that the mucus was in a gel state. The phase angle (δ) was between 12.3 to 19.4° . In addition, my study also investigated the breakdown stress of the mucus which in the case of the mucus gel is fundamentally a function of the resistance to flow within the gel. The breakdown stress can be measured as the point at which $G' = G''$ or $\delta = 45^\circ$ [141]. I demonstrated that the initial breakdown stress (Pa) (213.9) was dominant over the repeated breakdown stress (169.3) in all experiments ($n=5$) (**Table 28**). The first breakdown is higher than the next breakdown in all my experiments. This indicates that the gel never get back to its

original structure after multiple shear strain tests. In other words, whatever the initial interactions were, when broken, they cannot reform. The most extensive rheological data of mucus gels were done by Taylor and her colleagues on gastric mucus [141-143]. Taylor (2002) found that the gel flowed ($G'' > G'$) rather than ruptured; this could yield gel fragments, in response to excess shear stress. Gel properties ($G' > G''$) could be recovered with a phase angle representative of a gastric mucus gel as the shear stress was lowered below the level that induced breakdown. This suggest gel behaviour typical of a weak gel. The first increase-decrease stress sweep initiated a loss in the value of the moduli G' and G'' at minimum stress but instantly repeating the sweep up to 10 times resulted in no further loss in the moduli at minimum stress. Taylor et al. (2002) demonstrated that there was no significant difference between the stress at the point of breakdown (187 Pa) and the stress at the point of recovery. When the shear stress is increased above that essential for gel breakdown, the mucus flows as a viscous liquid. When the shear is reduced, the gel recovers its solid dominate behaviour ($G' > G''$). This breakdown / recovery behaviour of the gel is very reproducible with continuous breakdown sweeps making very similar patterns of G' and G'' through the entire stress range for up to 10 repeats. After each successive breakdown, the material recovers to its unique phase angle and there is no significant difference between the stress at breakdown and the stress at recovery suggesting that there has been no decrease in the ability of mucus to form a gel. Mucus gels are different from the majority of biopolymer gels as it displays rheological reversibility. In other words, it is able to flow and re anneal. Many biopolymers form a strong physical gel which while not covalently linked, indicate a behaviour that is in numerous ways like covalently linked or chemical gels, although of a weaker nature. Normally, these gels will rupture in response to excessive force and after being ruptured, they retain only the properties of a broken gel. This is different to the behaviour of a physical gel or structured liquid which will usually flow in response to excess force and regain its gel properties upon rest, known as rheological reversibility [141].

Taylor et al. (2004) investigated the mucus bilayer in the pig stomach. They found that both mucus secretions showed G' dominance over G'' across the frequency range (0.1-3 Hz), indicating a true gel. They also found that the phase angle (δ) of the shear-resistant mucus was significantly ($P < 0.001$) lower than for the shear compliant mucus and was, thus, characterized as a stronger gel (15 vs 5-10). They also found that the shear resistant mucus stayed in the gel state ($G' > G''$) over a much larger variety of shear stress with a typical breakdown stress of ~ 150 Pa – two orders magnitude higher than the shear-compliant gel [142].

I found that G' , G'' , and δ were shear strain independent within the linear viscoelastic region (LVER) (**figure 19**). However, when the shear strain was increased, it showed that they are shear strain dependent. Furthermore, the gradient slopes of G' and G'' from a frequency sweep were analysed ($n=5$) as shown in **table 29** and **figure 20**. At a lower frequency, G' and G'' from a frequency sweep were generally decreased, suggesting that the gel is weakening (i.e. going to flow). At a higher frequency, G' and G'' were generally increasing, indicating that the mucus is starting to thicken again (i.e. it became more gel). The phase angle (δ) was between 10 and 25. Taylor et al. (2002) found that gastric mucus revealed very reproducible behaviour with the phase angle lying between 5 and 10. She also revealed that both G' and G'' showed only a small frequency dependence, dropping in value when the frequency was lowered. These results are similar to what I found for small intestine mucus. This suggests some impact from entanglements on the bulk properties of the gel. The gel showed no increased trend to flow at lower frequencies confirmed by the steady values for the phase angle. She showed that the gel worked as a viscoelastic solid with the elastic modulus G' being significantly higher than the viscous modulus G'' [141]. Taylor et al. (2005) also studied the frequency dependence of the rheological behaviour of three mucous system (native pig gastric mucus, purified mucin gel and mucin alginate gel). They found that a frequency dependence became clear when the effect of frequency on the stress-strain curves of purified mucus system was studied over a variety of stress sufficient to induce flow within the systems. They also showed that in all three

mucus systems the maximum stress was enough to induce a transition to viscous flow within the sample. They also reported that at 0.2 Hz, the stress/strain values for both native mucus gel and the mucin gel revealed an almost linear region followed by an increase before a more noticeable decrease. In the case of the mucin alginate gel, it showed a slightly decreased stress/strain when the applied stress increased followed by a noticeable decrease when the applied stress was increased further. These results indicated the behaviour was characteristic of a system weakening under applied stress, with the induced strain increasing more quickly than the applied stress as the applied stress increased and the system started to flow at lower frequencies. In addition, all the samples demonstrated a comprehensive linear region before an increase in stress/strain at 1 Hz. This suggested that both systems became more resistant to deformation as the applied stress was increased, with the induced strain increasing more gradually than the applied stress at higher frequencies. In other words, when the system weakens, it is likely that it will become less capable to resist deformation and the induced strain will rise at a considerably larger rate than the applied stress and, consequently, stress/strain will decrease. Stress/strain increases as the applied stress increases, suggesting that the capacity of the gel to resist deformation increased as the applied stress increased (i.e., the gel undergoes stress hardening). They assumed that the system is capable of adsorbing and storing energy, especially at higher frequencies, therefore, reducing the amount of energy existing to induce strain within the network and additionally weaken the gel. This stored energy can be rearranged into the network when the stress is removed and solid like properties are recovered. They also suggested that the energy may be stored by changes in the packing of mucin molecules within the system or by conformational changes within the mucin molecules. Increasing the applied stress could force the molecules to adopt high energy conformations or packing structures which then return, freeing their stored energy, when the stress is removed. This model is companionable with the frequency dependent behaviour because at lower frequencies, the relaxation time is longer and thus statistically less elements could be

stuck in high energy conformations or structures. They also suggested that at lower frequencies where the value of stress/strain decreases with increasing stress, there is significant weakening and the system keeps the capacity to store a substantial amount of energy, suggesting that at least a definite degree of rheological reversibility. This could reflect the lubricating capability of bottle brush structures, for example, the glycosylated regions present on the mucin molecules [143].

The above arguments suggest that mucus gels have some degree of frequency dependency. The small intestine gel showed frequency dependency over the ranges tested. Between 0.1 and 1 Hz, there was a decrease in G' and G'' followed by an increase over 1-10 Hz. The G'' increase was greater than the increase in G' , indicating a tendency to flow. This change at high frequency is demonstrated by an increase in δ , indicating a weaker gel. This biphasic behaviour could be explained by the gel forming interactions which have time to break and make at low frequency but at a higher frequency, they do not have time to reform.

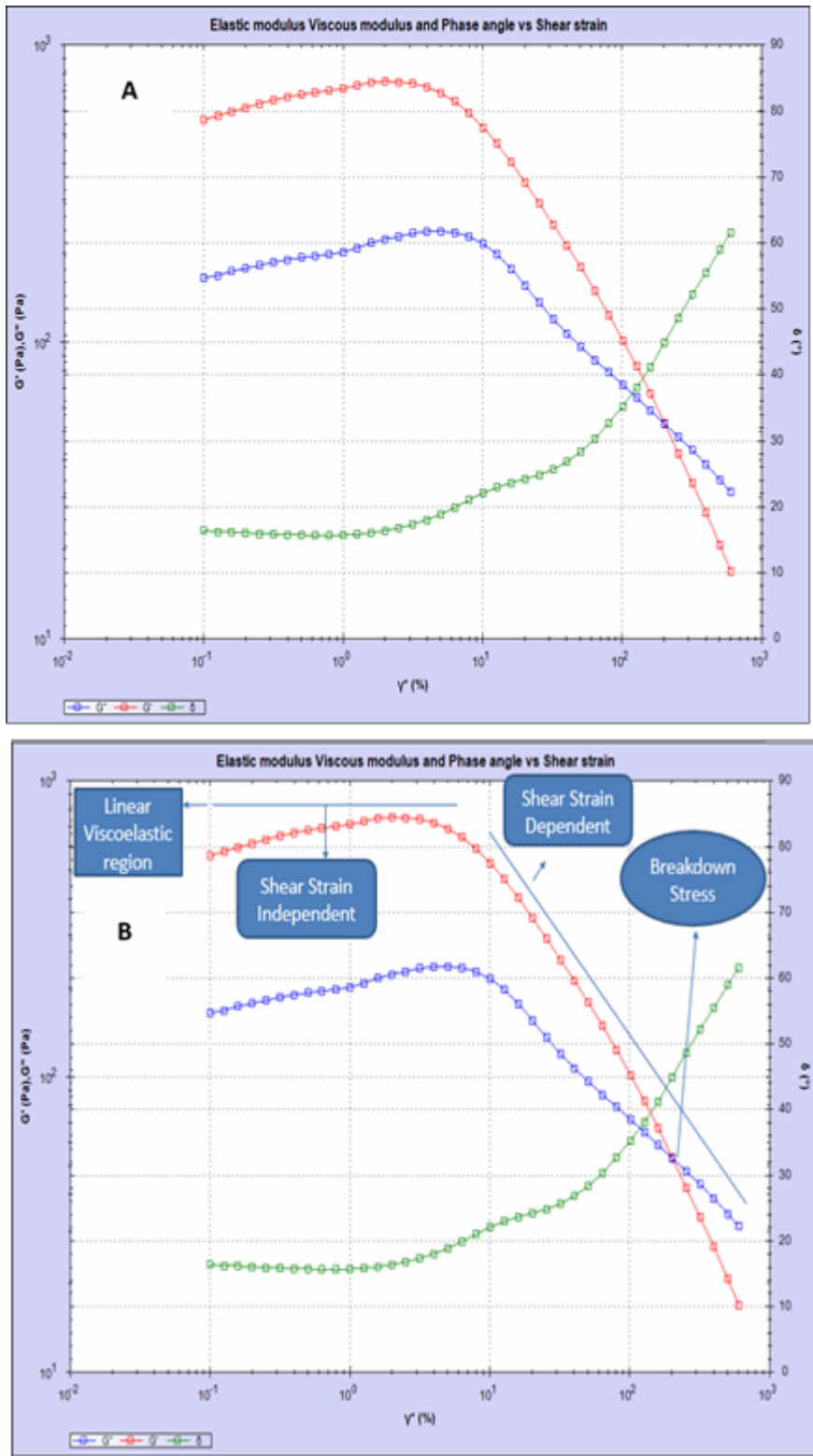


Figure 19. Amplitude sweep of cleaned porcine intestinal mucus. Amplitude sweep was run at 1 Hz. a) An example of one experiment of mucus. b) An example showing linear viscoelastic region (LVER), breakdown stress, shear strain independent region of mucus and shear strain dependent region of mucus.

Table 28. Rheological characteristics of the porcine intestinal mucus from the small intestine.

Samples	Linear viscoelastic region				Breakdown stress (Pa)	
	Shear Strain %	G' (Pa)	G'' (Pa)	δ°	Initial	Repeated
1	10	204.9	71.9	19.4	201.5	126.8
2	15.9	100.3	29.5	16.4	201.7	159.2
3	12.6	145.7	46.5	17.7	253.4	179.8
4	5	141.2	30.8	12.3	159.8	155
5	10	153.4	44.1	16.1	253.2	226.1
Average	10.7	149.1	44.6	16.4	213.9	169.3
Standard Deviation	3.9	37.4	17.1	2.6	39.8	36.9

The breakdown point is where G' is equal to G'' and phase angle (δ) is 45° . In order to do multiple breakdowns of the mucus, the shear strain were increased from 10^{-1} to around 10^3 for the first breakdown. For the repeated breakdown of the mucus, the shear strain were restarted from 10^{-1} and increased to around 10^3 .

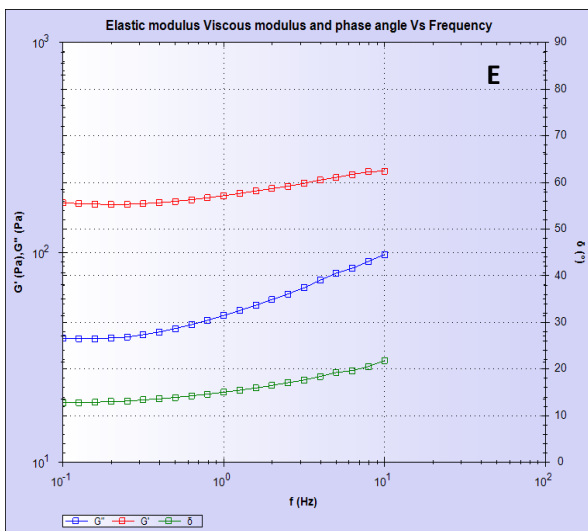
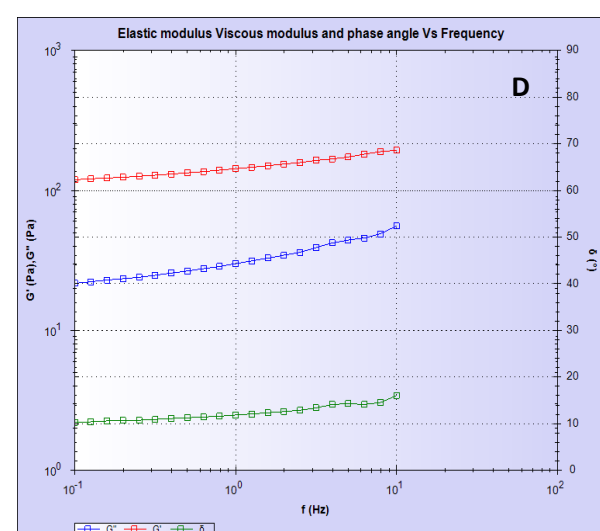
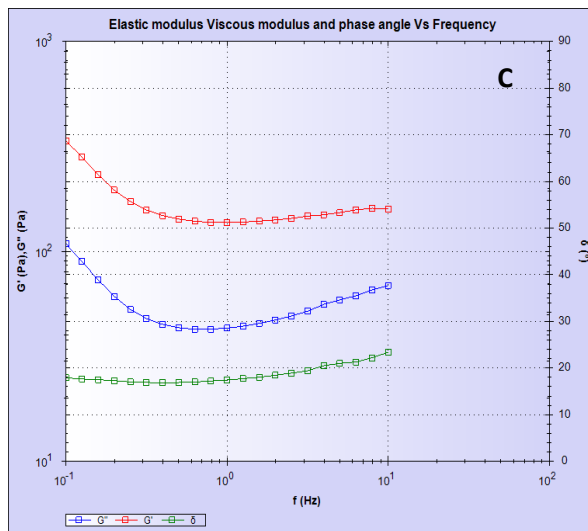
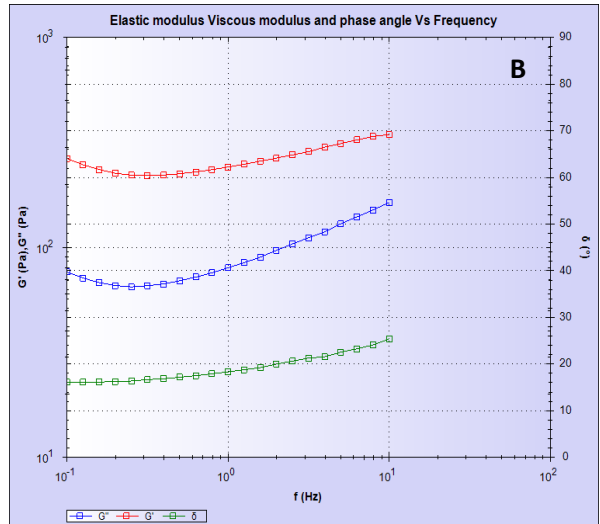
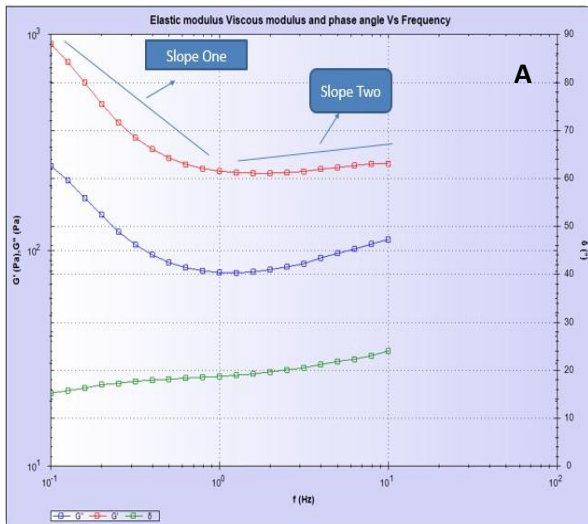


Figure 20. Gradient slopes of G' and G'' . A) Slope one was negative and slope two was positive. B) Slope one was negative and slope two was positive. C) Slope one was negative and slope two was positive. D) Both slopes were positive. E) Slope one was negative and slope two was positive.

Table 29. Gradient Slopes of G' and G''

Experiments	G'		G''	
	Slope 1	Slope 2	Slope 1	Slope 2
1	-208.6	12.9	-76.3	10.1
2	-222.2	2.4	-124.9	2.8
3	-357.5	2.9	-144.5	3.8
4	N/A	7.6	N/A	3.4
5	-30.2	7.7	-2.4	6

N/A= not applicable. The value of slopes were taken as shown in figure 10 (a). It should be noted that I used an amplitude sweep to determine LVER and the frequency sweep was carried out at a shear strain in the LVER.

Chapter Five: General Discussion, Conclusion, and Future Works

5.1.Introduction:

The current burden of lung disease in the world means that there is a clear need for research into new drug treatments and new ways of delivering drugs. Nanotechnology may have an important role in this.

Chronic obstructive pulmonary disease (COPD) is a leading chronic respiratory disease in the world and is characterized by persistent airflow restriction which is normally progressive. This is linked to a higher inflammatory response in the airways and the lung due to noxious particles or gases [144, 145]. The World Health Organization (WHO) estimates that about 63 million people suffer from COPD and 3 million people died of COPD in 2010 which matches around 5% of all deaths globally [145, 146]. More than 90% of COPD deaths happen in low and middle-income countries. WHO expects that COPD will become the third leading cause of death globally by 2030 [146]. COPD is more common in men than in women; however, the increase in tobacco smoking among women and the higher risk of exposure to indoor air pollution might result in matching occurrence in the sexes in the future [147]. The annual cost of COPD is expected to be close to 55 billion US dollars yearly as indicated by the European Respiratory Society. Most of these costs are linked to losses in productivity because of work disability and severe restrictions in functionality. However, costs are commonly undervalued because the cost of home care and home health visits are understated and hard to monetize [145].

Asthma is a chronic inflammatory disease of the conducting airways where several cells of the innate and adaptive immune systems act together with epithelial cells, resulting in bronchial hyper-reactivity (BHR) (the tendency of smooth muscle cells in people with asthma to respond to general stimuli, for example, cold air and exercise), mucus overproduction, airway wall remodelling and airway reduction. This may cause frequent attacks of shortness of breath,

wheezing and chest tightness [148]. Although, asthma affects people from all age groups, the highest occurrence is in childhood. Asthma affects females more than males. It has been estimated that 1-18% of population in the world suffer from lifetime asthma [149]. Accordingly, it is predictable that more than 300 million people have asthma global and at least 10% of all Europeans [149, 150]. By 2025, it is estimated that more than 100 million could have asthma [149]. Nearly 250,000 people die prematurely from asthma yearly [151]. Over 80% of asthma death happens in low and lower-middle income countries [152]. It has been estimated that the mean cost per patient per year in Europe is \$USD 1,900 which is lower than USA with an estimated mean of \$USD 3,100. The overall cost of asthma in the UK has been predicted as around \$5 billion. Almost 20 million working-days are missed as a result of asthma yearly [149].

Cystic fibrosis (CF) is a common autosomal recessive genetic disorder and is caused by the mutation of a gene that encodes a chloride-conducting transmembrane channel called the cystic fibrosis transmembrane conductance regulator (CFTR). CFTR regulates anion transport and mucociliary clearance in the airways. CFTR dysfunction leads to mucus retention and chronic infection and, subsequently, local airway inflammation which is damaging to the lungs. CF is common in Europe, North America, and Australia. In Europe, the number of CF patients is expected to increase by about 70% by 2025 [153]. Cystic fibrosis happens in about 1 in 2500 live births in the UK with around 200–300 new diagnoses yearly. CF patients consequently need intensive support from family and health care services. Most patients die prematurely from their disease via respiratory failure [154]. Given the above background, there is a clear need for further research relevant to COPD, asthma, and CF treatment.

Animal studies are most costly in term of money and time in addition to ethical issues and may not be optimum for studying human diseases. Therefore, tissue and cell studies are very useful for the toxicity screening of new compounds. This may offer endpoint result which are

directly related to specific organs [155]. Cultured cells are an important and crucial tool to investigate biological processes [156]. Cell lines are regularly used instead of primary cells to study biological processes. However, as cell lines are genetically manipulated, this might change their phenotype, native functions and their reaction to stimuli. Serial passage of cell lines may further lead to genotypic and phenotypic difference over a long time and genetic drift may also result in heterogeneity in cultures at a single point of time. Therefore, care needs to be taken when interpreting the results because cell lines do not always precisely mirror primary cells. Hence, important control experiments using primary cells should continually be done to strengthen the results [157]. In COPD, exacerbation may lead to an increase in disease severity, while repeated exacerbations can lead to constant injuries to the airway epithelium and if common, could shorten the time available for epithelial repair. This results in further damage to the integrity of the epithelium because of continuing inflammation. More investigation of the function and structure of airway epithelial in COPD can result in a better understanding of the mechanisms of disease and to improved therapies. Although airway epithelial cells were considered a simple barrier that stops entry of inhaled matter into the lung, the epithelial cells are at present known to have a significant role in the inflammatory response of the respiratory system to inhaled exposures; irregularities in these responses are assumed to be central to asthma pathogenesis [158]. Asthma represents part of an important unmet medical requirement with few new drugs making it to the clinic in the past 50 years. Considerable asthma research is now carried out in non-human models. Nevertheless, it is hard to translate findings from these models to effective therapies since asthma is an exclusively human condition. It has been suggested that the use of human tissue studies are needed to offer more appropriate models that better translate to the clinic and which decrease the dependence of the asthma community on less predictive animal models [159]. Brodlie et al. (2010) have successfully cultured primary epithelial cells from 14 of 22 patients with cystic fibrosis in our lab. They demonstrated that the cells show typical epithelial morphology, cytokine profile and remained viable after storage in

liquid nitrogen, indicating that these cells are likely to retain the behaviour of bronchial epithelial cells *in vivo* [28]. Brodlie et al. (2011) investigated the role of IL-17 in the lower airway in cystic fibrosis using our primary epithelial cells. They found that IL-17 levels are increased in the lower airway of people with CF and localised to both neutrophils and mononuclear cells, suggesting the potential for a positive feedback element in airway inflammation [160]. The main benefit of primary cell models is that they are closer to lung cell physiology [161]. However, there are some limitations to using primary cells: 1) Preparation of primary cell cultures remains difficult and since most primary cultures ultimately stop dividing, a continuous supply of fresh cells is needed; 2) Almost all cells undergo major phenotypic changes once removed from their physiological environment and put into a culture flask [156]; 3) Inter-individual variability; 4) The limited resource; and 5) The limited life span does not permit long term genetic manipulation [161].

COPD is characterised by chronic inflammation and mucus production affecting the lung parenchyma and peripheral airways causing largely permanent and progressive airflow restriction. The inflammation is categorised by enlarged amounts of alveolar macrophages, neutrophils, T lymphocytes and innate lymphoid cells recruited from the circulation [162]. Emphysema and small airway inflammation and injury causes the increase of alveolar air spaces, airway wall fibrosis, smooth muscle hypertrophy, loss of elastic recoil, goblet cell hyperplasia and mucus plugging. Furthermore, remodeling leads to thickening of the small airway walls, resulting in airflow obstruction and hyperinflation, causing the cardinal symptom of breathlessness. In the advanced stages of COPD, this causes progressive ventilator failure and death [163]. Asthma is considered as a chronic inflammatory disorder that is linked to hyper-responsiveness and tissue remodelling of the airway structure [164]. It is characterized by the penetration of airway T cells, CD4+ (T helper) cells, basophils, mast cells, macrophages and eosinophils [165]. These inflammatory cells release mediators which then initiate

bronchoconstriction, mucus secretion and remodeling. These mediators include chemokines, growth factors, lipid mediators, immunoglobulins and histamine [166]. Cystic fibrosis is categorised by an excessively exuberant neutrophilic inflammatory response to pathogens and other stimuli which begins very early in the disease [167]. In addition, the inflammation in CF is also characterised by a large release of soluble pro-inflammatory mediators such as interleukin (IL)-6, IL-1 β and IL-8 cytokines. However, release of the anti-inflammatory mediator IL-10 is decreased, accordingly reproducing a pro-/anti-inflammatory imbalance [168].

I have shown that different PDLG NPs do not effecting the productions of IL-8 and were not toxic to primary epithelial cells. Therefore, these NPs could potentially be used for the delivery of anti-inflammatory therapies for these lung diseases.

5.2.The Oxidative Stress Model Approach:

Nanoparticles may lead to the formation of pro-oxidants, causing the disruption of the balance between the biological system's capability to produce and detoxify reactive oxygen species (ROS) [1]. Nel et al. (2006) have considered oxidative stress models as an approach to assessing an extensive collection of cellular injury responses caused by NPs (**Figure 22**) [48]. A predictive toxicological method can be defined as creating and using mechanisms and pathways of injury at cellular and molecular levels to develop screening for adverse biological effects and health consequences *in vivo*. As it is associated with NPs, a predictive method has to take into account the physicochemical properties of NPs which causes molecular or cellular injury and also has to be useful in terms of disease progression in whole organisms [169]. At tier 1 (lowest level of oxidative stress) the induction of protective cellular responses occurs. At tier 2 (a higher level of oxidative stress), there is activation of pro-inflammatory signalling pathways that control the activation of pro-inflammatory responses, potentially leading to the release of cytokines and chemokines that are characteristic for specific cellular phenotypes. At tier 3,

which is the highest level of oxidative stress, damage of mitochondria may trigger cellular apoptosis and cytotoxicity [48, 170-172]. Examples of toxicity paradigms are given in **table 30**. For example, it is possible to test Tier 2 oxidative stress responses either by assessing cytokines release into the cell culture supernatant or by monitoring the activation of signaling cascades linked to transcriptional activation of cytokine promoters. The most common method to measure the production of cytokines or chemokines is by classical ELISAs and TR-FRET technology [172].

There are several sequences of pathological events that happen due to NP-mediated ROS generation (**Figure 22**). These include inflammation, fibrosis, genotoxicity and carcinogenesis. These pathological events are controlled by physicochemical features of NPs (e.g. size, charge, surface area, and chemical structure) and NPs internalization. Nanotoxicity may cause expression of pro-inflammatory and fibrotic cytokines, as well as activation of inflammatory cells (e.g. macrophages and neutrophils) which are able to produce further generation of ROS. Mitochondria are considered a key organelle involved in NP-mediated cellular ROS in which NPs interfere with the electron transport chain via activation of NADPH-related enzymes. NP-induced production of free radicals causes a decrease of GSH into its oxidized form – glutathione disulphide, which is associated with oxidative stress. When exposed to low NP concentrations, it has been shown that potent antioxidant defence was able to overcome oxidative stress and improve the redox balance. On exposure to high NP concentrations, the antioxidant systems becomes overwhelmed which may lead to cytotoxicity and inflammation [173].

Large scale investigation of the effect of oxidative stress was out of the scope of my thesis. However, the results showing no significant difference in IL-8 production when I stimulated the cells with different concentrations of polystyrene and PDLG NPs, and the low levels of cytotoxicity would suggest a lack of tier 2 or 3 oxidative damage. In future studies, oxidative stress could be studied using a plasmid assay, DCFH, luminol-enhanced chemiluminescence,

$O_2\cdot^-$ detection by the cytochrome C reduction assay or by lucigenin-enhanced chemiluminescence, H_2O_2 detection using horseradish peroxidase and so on. My cytotoxicity data showed interference with the CTB and MTT assays. However, other assays could be used for future study to assess the cytotoxicity. These assay could include a variation of the MTT assay (MTS, XTT, WEST-1, etc), the LDH assay, trypan blue exclusion, the fluorescent dye propidium iodide (PI) and many others. In future studies, different cytokines and chemokines could be investigated using ELISA techniques and mRNA expression using PCR techniques [39].

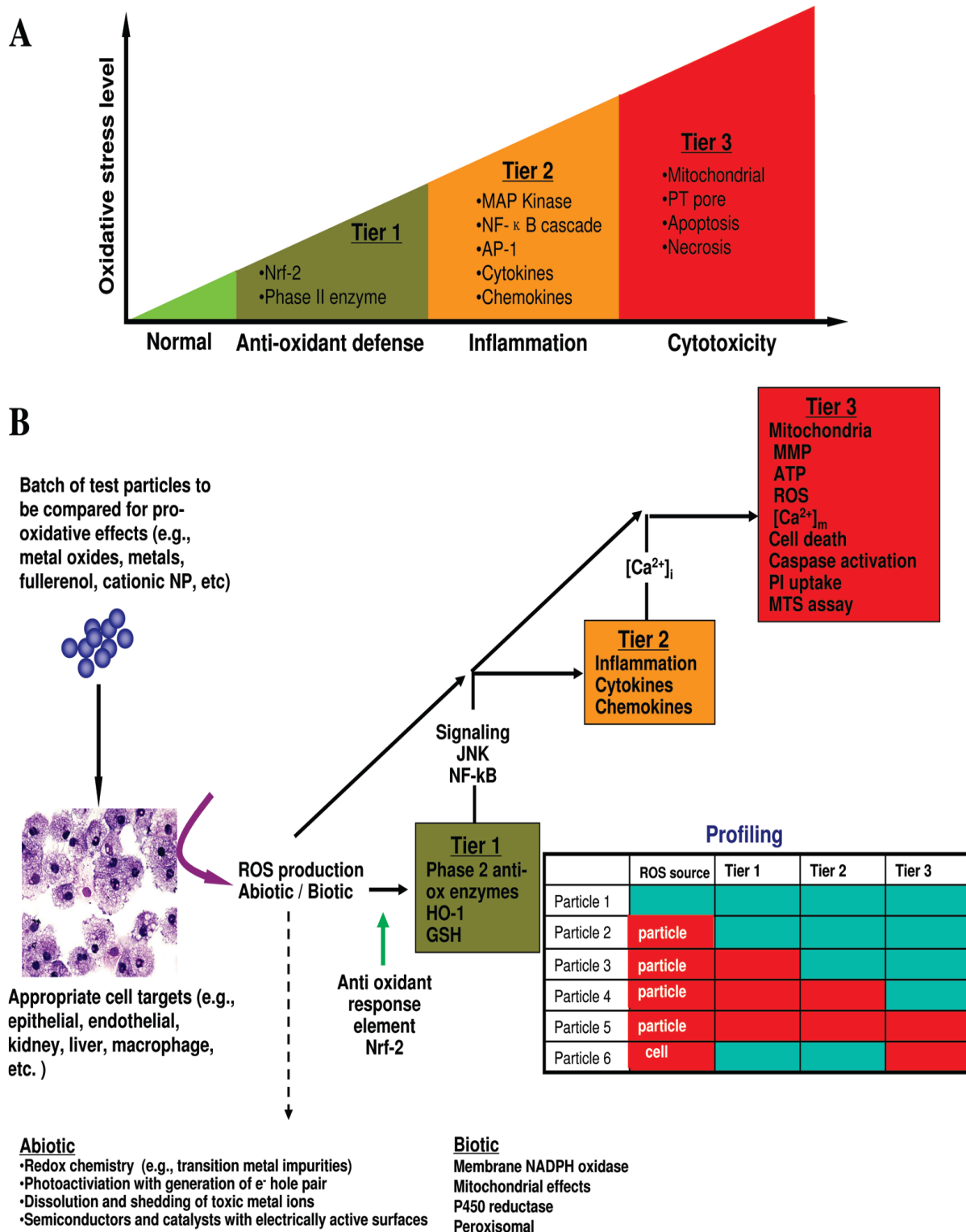


Figure 21: The use of oxidative stress models as methods for predictions of nanoparticles hazard. (A) nanoparticle-induced oxidative stress include a series of cellular responses. These responses can be classified as antioxidant defence, pro-inflammatory effects, and cytotoxicity. Each of these response tiers are originated by particular biological sensors and activation mechanisms. (B) Application of the oxidative stress model to monitor groups of engineered nanomaterials that are able to produce reactive oxygen species production under experimental conditions. Adapted from [169].

Table 30: Examples of toxicity paradigms. Possible analysis, readout modes and potential problems when using various readouts for NPs toxicity screening.

Toxicity type or paradigm	Analysis	Probes	Readout mode	Utility	Potential problem
Cytotoxicity	Cell number/proliferation	Hoechst 33342/DAPI	Fluorimetry/High content assay	Cell quantification, nuclear content	Background signal from NPs with blue fluorescence
	Membrane leakage	Propidium iodide/Syto 9	Fluorimetry/High content assay	compromised cell membrane integrity	Background signal from NPs with red fluorescence (e.g. QDs)
	Membrane integrity	LDH assay	Absorbance at 490 nm	Cell viability	NPs may inhibit enzyme and/or absorb at 490nm (CNTs, Ag)
	ATP	ATPlite™	luminescence	Mitochondrial activity and viability status of cells	Not appropriate for NPs that may inhibit enzyme and/or absorb light e.g. CNTs
	Mitochondrial membrane potential	JC1/TMRM/chlorromethyl-X-rodhamine	Fluorimetry/high content assay	Loss of MMP	Background signal from NPs with red or green fluorescence
	Metabolic activity	MTT, WST-1, XTT	Absorbance	Mitochondrial activity and viability status of cells	NPs may inhibit enzyme and/or absorb light or substrates
	Intracellular calcium flux	Fluo-4/Fura 2-AM/Rho 2-AM	Fluorometry/high content assay	Increased intra-cellular calcium level	Background signal from NPs with green fluorescence
	Apoptosis	Calcein-AM	Fluorometry/high content assay	Mitochondrial membrane permeability transition (MPT)	Background signal from NPs with green fluorescence

Genotoxicity	DNA cleavage	Micro-nuclei assay (HCS), BrDU incorporation	High Content Screening	Chromosome damage	Background signal from NPs with blue fluorescence
inflammation	IL-1, IL-8, TNF- α	Antibody based ELISA or TR-FRET	Luminescence / TR-FRET	Expression level of inflammatory markers	Not appropriate for NPs that interfere with TR-FRET (e.g. absorb protein) or luminescence reactions
	NF-kB and AP-1 activation	Reporter genes	luminescence	Activation of inflammatory pathways	Not appropriate for NPs that may inhibit enzyme and/or absorb light
Oxidative stress	GSH, ROS	Absorbance/HCS using 161 fluorescence probes	Fluorometry/ High content assay	Free radical generation, Glutathione depletion	Not appropriate for NPs that may interfere with fluorescence output

Adapted from [172].

5.3. Interference with Viability Assays:

Recently, nanotechnology have been in increasing development with the generation of a wide range of consumer products including nanoparticles which are at least one dimension <100nm. Nanoparticles have unique properties because of their small size, resulting in greater surface area per unit mass ratio and, hence, the potential for greater biological reactivity and perhaps novel hazards. Although the human health effects are uncertain now, it is essential that researchers develop a clear understanding of any risks related to exposure of NPs. Cytotoxicity assays offer a common method for measuring the safety of new chemicals and drugs, and are mostly plate-reader based with readouts. These can include luminescence, absorbance, fluorescence, time-resolved fluorescence or fluorescence polarization [174]. Nanoparticles have a high potential to influence classical cytotoxicity assays because of high adsorption capacity and optical activity. As a consequence of their large surface area and high surface energy, nanoparticles may adsorb assay reagents or reporting dyes, thus, changing the assay outcome [129]. Additionally, the physicochemical properties of nanoparticles may be accountable for unforeseen interactions with components of classical toxicity assays. Prior to assessing particle toxicity using in vitro toxicity tests, interference testing should be done to avoid false readings [125].

A detailed physicochemical characterization of the nanoparticles may allow us to predict interferences as specific nanoparticle properties could be problematic for specific techniques and assays (**figure 23**). Interference with spectrophotometric and fluorimetric analyses depends on the optical properties of the nanoparticles. The chemical composition, particularly the surface chemistry, defines these properties and, consequently, coatings might affect light absorption. For example, the light scattering properties of TiO₂ nanoparticles can alter OD measurements and fluorimetric analyses. The agglomeration of nanoparticles appears to have a minor part in interference with spectrophotometric and fluorimetric

analyses. Furthermore, the surface reactivity of the nanoparticles controls their adsorption capacities and responses with assay reagents or biomolecules [174]. It has been proposed that results achieved may not be consistent due to nanoparticle interference with assay components, hence, cell death indexes may be either underestimated or overestimated. Possible interference may include nanoparticle interference with light absorption, chemical reactions between nanoparticles and reactants, and dye adsorption on the nanoparticle surface [175].

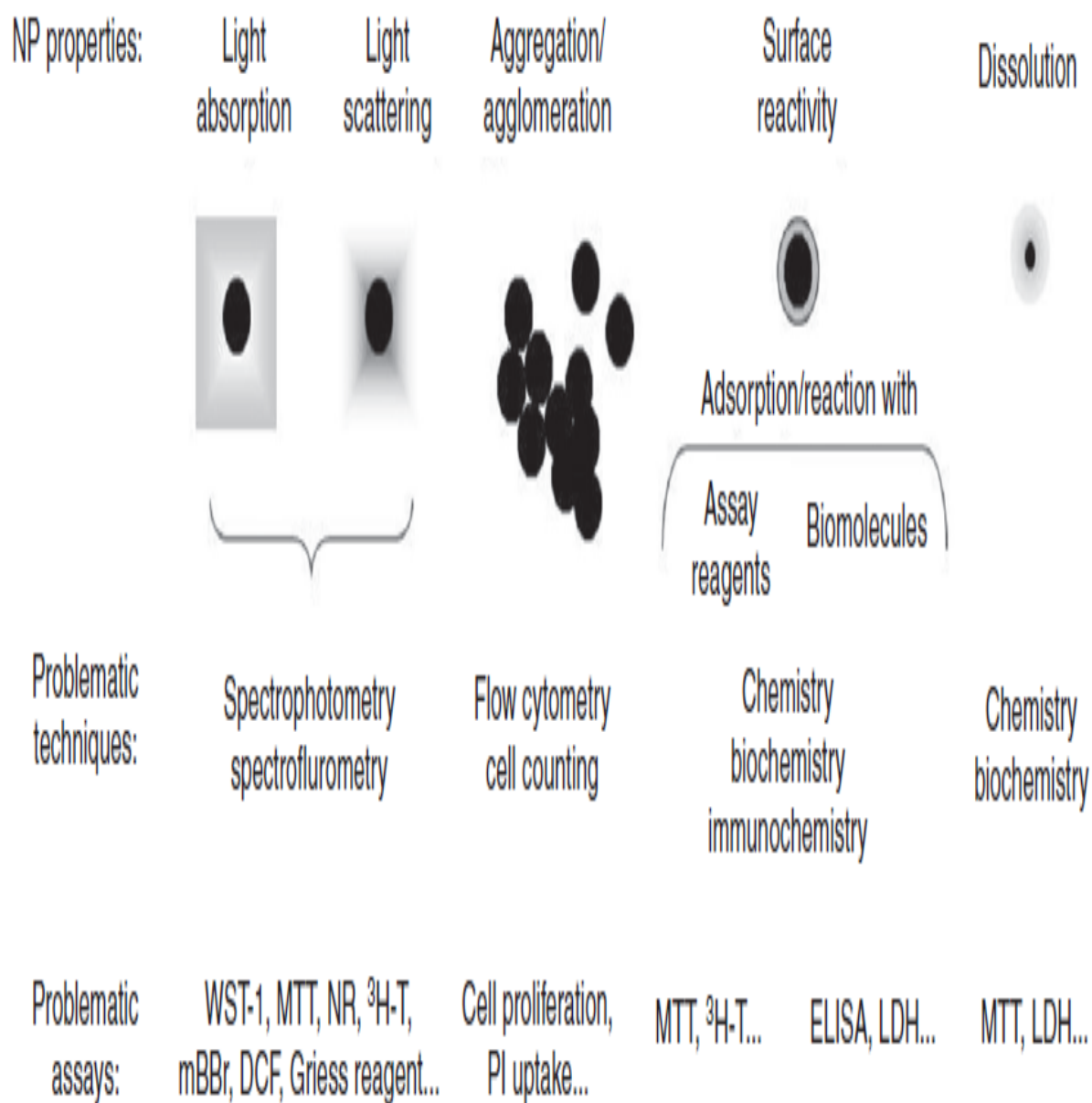


Figure 22. Nanoparticles Characterization and Interference with Assays. Adapted from [92].

5.3.1. *The Mechanism of NPs Interference with CTB Assay:*

Oostingh et al. (2011) found that the CTB assay was not suitable for testing viability for metal oxide NPs. They showed that the fluorescence measurement displayed an artificial increase in cell viability, probably as a result of the physical presence of NPs rather than to real NPs-induced effects [131]. Hoskins et al. (2012) studied the effect of magnetic NPs (MNPs) cytotoxicity in human neuroblastoma (SH-SY5Y) and mouse macrophage (RAW 264.7) cells. They showed that the Celltiter blue assay seems to overestimate the cell viability, suggesting that interactions were happening between the assay systems and NPs, causing incorrect cell viability measurements. They demonstrated that polymer coated MNPs resulted in a significant rise in the fluorescent measurement, indicating that the existence of the NPs in cellular environments increases the fluorescent intensity exhibited by the resorufin dye. They also studied the effect of NPs with assay reagents in the absence of cells. They suggested that the false increase in the CTB assay could result from the physical interference by the NPs and/or from changes in cellular activities, involved in redox reactions, in response to MNPs [128]. Breznan et al. (2015) investigated the viability of different carbon nanotubes (CNT) with A549 and murine macrophage (J774A.1) cell lines. They found that there was no indication of reduction of resazurin by CNTs. They also assessed the stability of resorufin (the fluorescent product of resazurin reduction) and found that polar CNTs may reduce the fluorescent signal of resorufin. This could be a result of chemical interference in the assay, possibly by re-oxidation of resorufin or hyper-reduction of resorufin to non-fluorescent hydroresorufin [176].

5.3.2. *The Mechanism of NPs Interference with MTT Assay:*

Belyanskaya et al. (2007) studied the effect of single walled carbon nanotubes (SWCNTs) on A549 cells using the MTT assay. SWCNTs were capable of changing MTT into its MTT-formazan insoluble form in the absence of cells. They suggested that the interference of carbon nanotubes with the MTT assay can be influenced by the MTT protocol used, the surfactant used

to suspend carbon nanotubes and the types of CNT products [116]. Kroll et al. (2012) investigated 24 NPs with the MTT assay and found that interference occurred. They found a concentration-dependent increase in MTT-formazan light absorption for each NP, indicating NPs may adsorb to MTT-formazan. Light scattering effects could also be the reason for this interference [129]. Vinković Vrčeketal. (2015) suggested that the optical properties of NPs could be the main reason for interference during optical readouts of the MTT assay. Therefore, they investigated the absorbance of NPs alone at the wavelengths used for MTT assay. They showed a significant absorbance increase compared to tetrazolium salt (TS) controls, leading to an underestimation of NP toxicity. In my experiments, a subtraction of background absorbance on the plate reader was done to avoid this problem. They also investigated other modes of interference such as reaction with or binding of assay components. While it is questionable that formazan would be formed from MTT in the absence of cells, they showed an increase in absorbance with an increase in NP concentration even after the subtraction of the NPs background absorbance. They also compared the adsorption of MTT or their formazan products on the NPs by adding a centrifugation step after the formazan solubilisation step (i.e. addition of DMSO). Centrifugation could be helpful in solving interference problems if the NPs do not adsorb assay dyes, accordingly inhibiting their measurement. They found that centrifugation was effective in decreasing optical signals as both types of formazan products bound to the NP surface, suggesting that the addition of DMSO could weaken their binding with MTT-formazan [139].

5.3.3. Summary of Cytotoxicity Results:

I demonstrated that there was no statistical difference between cells with polystyrene NPs (52nm) and cells without NPs (control cells) in terms of cell viability. I also showed that three different PDLG NPs seem to have little or no effect on the viability of human primary epithelial cells. Despite this, I found that many of my viability results were higher in OD values than 100% alive cells (untreated cells), suggesting that these difference may be because of

different cell density and/or interference with the CTB assay. I proved that seeding densities on Calu-3 seems to have a major effect on the CTB assay. When I used a different viability assay (MTT), I found that SNEDDS-a was only cytotoxic at the highest concentration. I also revealed that SNEDDS-b and -c were not cytotoxic. However, these results also indicate interference with the MTT assay even after washing the cells with PBS twice before applying the viability assays, suggesting that these SNEDDS had attached to or were taken up by the cells. This can be explained by the fact that SNEDDS are lipid and are, therefore, compatible with cell membranes. Finally, it appears that fluorescence labelling did not affect cytotoxicity results.

Hoskins et al. (2012) demonstrated that magnetic nanoparticles appears to have steadily overestimated the viability when using CTB and MTS. They suggested that interactions occurred between the nanoparticles and the assay systems, resulting in incorrect cell viability investigations [128]. Monterio-Riviere et al. (2009) showed that CTB and MTT assays produce incorrect results with some nanoparticles as a result of nanoparticle adsorption of the dye/dye products and/or nanoparticles/dye interaction. They suggested that more than one assay needs to be used to assess the nanoparticles cytotoxicity besides imaging techniques to confirm chemical marker-based viability assays [130]. Furthermore, Oostingh et al. (2011) found that the CTB assay was unacceptable for measuring cell viability as the fluorescence measurement indicated a false increase in the cell viability, perhaps as a consequence of the physical presence of the particles rather than to real particle induced effects [131]. Belyanskaya et al. (2007) suggested that an interference with MTT assays could be related to the types of nanoparticles products, surfactant used to suspend nanoparticles and the MTT protocol used [116]. Kroll et al. (2012) showed that 24 nanoparticles interfere with classic cytotoxicity assays in a particle and assay specific manner, and was highly concentration dependent. They suggested that interference would be avoided by lowering particle concentrations and altering assay protocols [129]. Guadagnini et al. (2015) also found that many nanoparticles characteristics such as

coatings, size, composition and agglomeration, interfere with variety of in vitro cytotoxicity assays (WST-1, MTT, LDH, neutral red, popidium iodide, H³-thymidine incorporation, and cell counting) [174]. Vinković Vrček et al. (2015) demonstrated that the cell viability assays leads to false interpretation due to interference, indicating that interference was dependent on the type and surface coating of nanoparticles as well as their stability in biological media [139].

5.3.4. Approaches to Avoid Cytotoxicity Interferences:

Possible reasons for interference could be nanoparticle interference with light absorption, chemical reactions between nanoparticles and reactants, and dye adsorption on the nanoparticle surface. Several approaches have been used to avoid interference between nanoparticles and assay reading. These include the use of cells treated with the same concentration of nanoparticles but without assay reagents as blanks, plate centrifugation before absorbance measurements, use of cell-free systems (wells without cells but with all assay reagents) as blanks, or cell washing after the incubation period to remove the remaining nanoparticles [175]. In the final step of the MTT assay, solubilization of the cells and the formazan product using a solvent is necessary. It has been suggested that centrifugation of the plates at this stage, followed by transfer of the supernatant to a new plate, could eliminate this interference. Extra control experiments should be done before assessing NP cytotoxicity. Therefore, a subtraction of the background absorbance of the cells in the presence of the particles without the assay is needed to control this interference. The large surface area or other surface properties may cause a high adsorptive capability which allows the NPs to remove some of the coloured product from the cell extract, resulting in an underestimation of cell viability. An alternative assay is recommended when this adsorption happens. NPs may also display oxidative surface properties, resulting in colour production. Therefore, it is important to assess whether the NPs without the cells could trigger an increase in absorbance. Finally, it is essential to include positive and negative control NPs to benchmark against the NPs under investigation [39].

5.4.Nanoparticles and the Mucus Barrier:

Mucus gels can be a major a problem in relation to drug delivery. It is hard to obtain human mucus as post mortem samples are usually degraded and only restricted amounts can be obtained from resection specimens and these may well have abnormal mucus. If the mucus is isolated immediately after death, then animal sources can be used. Pig is the animal of choice for the digestive tract, due to its close match to the human digestive tract. The mucus layer varies in thickness depending on the anatomical site, therefore, to develop active penetration, the following nanoparticle properties should be defined: size, surface functional groups and charge density. Two mechanisms can stop nanoparticles penetrating a mucus gel: 1) size filtering based on the pore size of the mucus; and 2) interaction filtering based on the ability of the nanoparticle to avoid interaction with the gel (**figure 24**) [15].

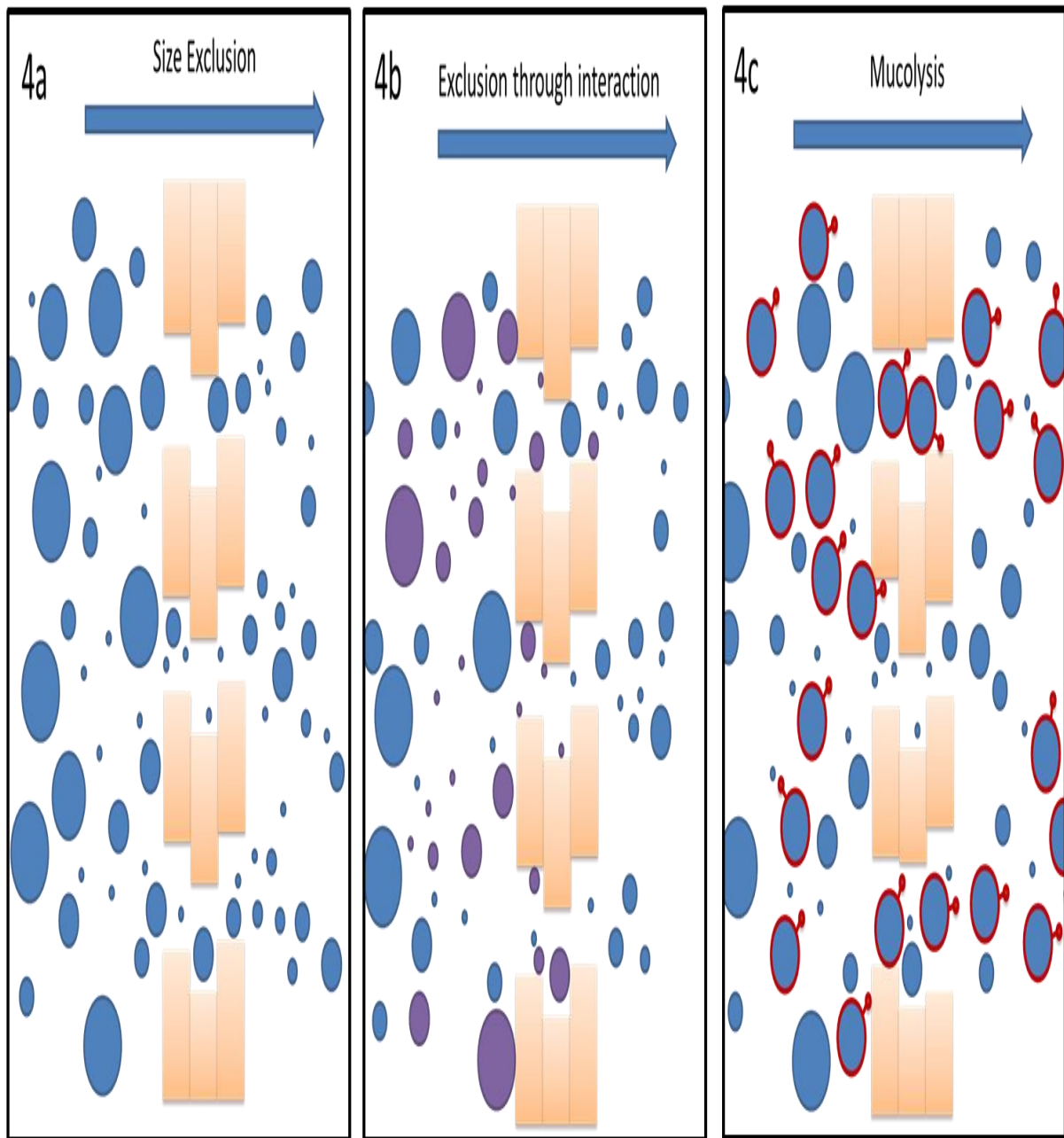


Figure 23. Characterization of permeation through the pores in the mucus gel. 4a) shows small particles can permeate while large particles are delayed. 4b) shows that if the particles interact, size becomes redundant. Interacting particles are symbolised in purple, non-interacting particles are in blue. The blue particles pass through when they are small, whereas, even small purple particles are delayed because of their interaction with the mucus. 4c) Particles with surface mucolytic agents can increase the pores of mucus and, thus, permeate the mucus barrier. Particles with red surface and nobs are mucolytic particles. Adapted from [14].

I demonstrated that there was no difference in permeation of mucus. These results suggested that there is no size dependency of mucus permeation. On the other hand, I showed that SNEDDS composition could play a major role in determining the permeation of mucus. In the rheological characterization of small intestine mucus, I found that G' is dominant over G'' , suggesting that the mucus was in gel state. I also showed that the phase angle was between 12.3 to 19.4°. Moreover, I found that the initial breakdown stress were dominant over the repeated breakdown stress, demonstrating that whatever the initial interactions, when broken, they cannot reform. I also showed that G' , G'' , and δ were shear strain independent within the linear viscoelastic region; however, it revealed that they are dependent as the shear strain was increased. At low frequency, G' and G'' were generally decreased, indicating that the gel is going to flow. At a higher frequency, G' and G'' were generally increase, demonstrating that the mucus became more gel-like. This variation at high frequency is confirmed by an increase in the phase angle demonstrating a weaker gel. This biphasic behaviour might be described by the gel forming interactions taking time to break and make at low frequency but at high frequency, they do not have time to reform.

5.5 Future Works to Overcome the Mucus Barrier:

It has been suggested that strategies should be directed to nanocarrier systems able to permeate the mucus without any or with only very limited damage to it. In general, there are two types of mucus permeating particle: active and passive systems. Active systems interact with the mucus, making it permeable for the particles. These systems are basically established from disulphide bridge breaking agents and proteolytic enzymes (see **figure 24**). In addition to this, strategies to escape back diffusion of particles out of the mucus gel layer are based on thiomers and zeta potential changing systems. In contrast to active systems, passive systems try to escape as many of the interaction of the particle with mucus as possible. Particles demonstrating a slippery surface and SNEDDS are the most favourable systems [137].

There are several strategies to overcome the mucus gel barrier which are potential future works. These include slippery surface strategies, SNEDDS strategies, disulphide breaking strategies, the proteolytic enzyme strategies, and the thiomers and zeta potential changing systems [137]. In slippery surface strategies, it has been shown that unmodified polystyrene nanoparticles (59nm) were able to penetrate deeply into human cervical mucus while carboxyl-modified polystyrene nanoparticles of the same size were totally immobilized in the mucus gel layer [136, 137, 177]. In other words, Olmsted et al. (2001) showed that polystyrene NPs (both unmodified and carboxyl-modified) mixed into mucus stuck strongly to mucins and collapsed the mucus gel into thick collections of aggregated mucin strands. Both of these NPs were capable of diffusion in mucus as quickly as they diffuse in water, suggesting that the size of the mesh-spacings in the mucus did not significantly delay or block the diffusion [177]. These results indicate that surface chemistry of the nanoparticle plays a vital role on the mucus permeating behaviour of nanoparticles. Moreover, it has been argued that a great and equal density of positive and negative surface charges can help particles be transported through a mucus layer by decreasing the electrostatic interactions with mucus. In SNEDDS strategies, their interactions with the mucus layer would be small because of the hydrophobic surface of the shaped nanodroplets. Furthermore, SNEDDS deformation capability can permit their diffusion through mucus gel layers of small mesh size as a result of their small size and changing shape of the nanodroplets. In disulphide breaking strategies, it has been shown that the effectiveness of mucolytic agents like N-acetylcysteine (NAC), in penetrating the mucus gel barrier. NAC is able to minimize the cross-linking of mucin fibres by cutting the disulphide bonds causing a decrease of the bulk mucus viscosity. The proteolytic enzyme strategy is centred on the immobilization of the mucolytic enzymes – trypsin, papain and bromelain – on the surface of polymer nanoparticles. These enzymes, which are capable of cleaving the mucus glycoprotein cross-linked networks, could act as mucolytic agents, thus, allowing local interference of the mucus layer. Enzyme immobilization on the surface of nanoparticles can be

gained by covalent bonding with and without spacers or ionic interactions [137].

In addition to the strategies to overcome the mucus gel barrier, there are some strategies to avoid back-diffusion. After nanoparticles have come into contact with the epithelium, they should remain there and discharge their load in a concentration dependent manner. Particles on the surface of the mucus are quickly removed because the surface of the mucus layer is continuously being shed into the lumen and, hence, the concentration gradient of particles goes in the reverse direction causing a back-diffusion of them out of the mucus. In other words, the more quickly particles can move in the mucus layer, the more quickly they are moving back out of it. There are two strategies so far to avoid back diffusion: the thiomers and zeta potential changing systems. Thiomers are able to form disulfide bonds with cysteine-rich subdomains of mucus glycoproteins by thiol-disulphide exchange reaction as a result of the immobilization of thiol groups on well-established polymers. Thiol groups immobilized on polymers show a pH dependent reactivity. The concentration of thiolate anions can be increased at greater pH values as the negative thiolate anion S⁻ is the reactive form of thiomers which can form disulphide bonds with mucus glycoproteins. Thiomers-based nanoparticles would be capable of overcoming the more luminal mucus gel layer without reacting by disulfide bond formation because the mucus gel layer of various mucosal membranes like the duodenal mucosa or vaginal mucosa, displays a pH gradient from acidic in the lumen to almost neutral at the mucosal surface. Nevertheless, once they are near to the absorption membrane with a greater pH value, their thiol groups become more reactive and form disulphide bonds with the mucus glycoproteins causing greater mucoadhesion to the applied particles. The approaches acceptable to avoid back-diffusion are centred on thiolated polymers reacting to a greater extent with the cysteine subunits of the mucus at pH 7 in deeper mucus regions than at pH 5 which is dominant in the luminal mucus regions of the duodenal and vaginal mucosa. In zeta potential changing systems, nanoparticles are able to change their zeta potential once they have overcome the mucus gel layer and reached the

epithelium. This is an encouraging method to overcome the mucus gel barrier. The mucus barrier exhibits a negative net charge due to sialic acid and ester sulphate; therefore, negatively charged particles can transfer without difficulty within the mucus as long as the three-dimensional network of mucus glycoproteins is sufficiently open. In contrast, nanoparticles demonstrating a positive zeta potential are immobilized within the mucus caused by charge: charge interactions. Despite this, nanoparticles need to have positive zeta potential to initiate their endocytosis into epithelial cells. Only very few nanoparticles will reach epithelial cells during administration to mucosal membranes as a result of the ionic immobilization of positively charged nanoparticles. Hence, nanoparticles which are able to change their zeta potential in a controlled manner could be a favourable approach to escape back-diffusion and to enhance the interaction of particles with epithelial cells [137].

- **References:**

1. Arora, S., J.M. Rajwade, and K.M. Paknikar, *Nanotoxicology and in vitro studies: The need of the hour*. Toxicology and Applied Pharmacology, 2012. **258**(2): p. 151-165.
2. Krug, H.F. and P. Wick, *Nanotoxicology: An Interdisciplinary Challenge*. Angewandte Chemie International Edition, 2011. **50**(6): p. 1260-1278.
3. Oberdorster, G., E. Oberdorster, and J. Oberdorster, *Nanotoxicology: an emerging discipline evolving from studies of ultrafine particles*. Environ Health Perspect, 2005. **113**(7): p. 823-39.
4. Borm, P., et al., *The potential risks of nanomaterials: a review carried out for ECETOC*. Particle and Fibre Toxicology, 2006. **3**(1): p. 11.
5. Oberdörster, G., *Safety assessment for nanotechnology and nanomedicine: Concepts of nanotoxicology*. Journal of Internal Medicine, 2010. **267**(1): p. 89-105.
6. Kreuter, J., *Nanoparticles—a historical perspective*. International Journal of Pharmaceutics, 2007. **331**(1): p. 1-10.
7. Elsaesser, A. and C.V. Howard, *Toxicology of nanoparticles*. Advanced Drug Delivery Reviews, 2012. **64**(2): p. 129-137.
8. Donaldson, K., et al., *Nanotoxicology*. Occupational and Environmental Medicine, 2004. **61**(9): p. 727-728.
9. Oberdörster, G., V. Stone, and K. Donaldson, *Toxicology of nanoparticles: A historical perspective*. Nanotoxicology, 2007. **1**(1): p. 2-25.
10. Powers, K.W., et al., *Characterization of the size, shape, and state of dispersion of nanoparticles for toxicological studies*. Nanotoxicology, 2007. **1**(1): p. 42-51.
11. Jiang, J., G. Oberdörster, and P. Biswas, *Characterization of size, surface charge, and agglomeration state of nanoparticle dispersions for toxicological studies*. Journal of Nanoparticle Research, 2009. **11**(1): p. 77-89.
12. Sayes, C.M. and D.B. Warheit, *Characterization of nanomaterials for toxicity assessment*. Wiley Interdisciplinary Reviews: Nanomedicine and Nanobiotechnology, 2009. **1**(6): p. 660- 670.
13. BéruBé, K., et al., *Human primary bronchial lung cell constructs: The new respiratory models*. Toxicology, 2010. **278**(3): p. 311-318.
14. Nahar, K., et al., *In vitro, in vivo and ex vivo models for studying particle deposition and drug absorption of inhaled pharmaceuticals*. Eur J Pharm Sci, 2013. **49**(5): p. 805-18.
15. Pearson, J.P., P.I. Chater, and M.D. Wilcox, *The properties of the mucus barrier, a unique gel - how can nanoparticles cross it?* Ther Deliv, 2016. **7**(4): p. 229-44.
16. Nordgård, C.T., et al., *Alterations in mucus barrier function and matrix structure induced by guluronate oligomers*. Biomacromolecules, 2014. **15**(6): p. 2294-2300.
17. Round, A.N., et al., *Lamellar Structures of MUC2-Rich Mucin: A Potential Role in Governing the Barrier and Lubricating Functions of Intestinal Mucus*. Biomacromolecules, 2012. **13**(10): p. 3253-3261.
18. Macierzanka, A., et al., *Transport of particles in intestinal mucus under simulated*

- infant and adult physiological conditions: Impact of mucus structure and extracellular DNA.* PLoS ONE, 2014. **9**(4).
19. Groo, A.C., et al., *Fate of paclitaxel lipid nanocapsules in intestinal mucus in view of their oral delivery.* International Journal of Nanomedicine, 2013. **8**: p. 4291-4302.
 20. Stone, V., H. Johnston, and R.P.F. Schins, *Development of in vitro systems for nanotoxicology: methodological considerations.* Critical Reviews in Toxicology, 2009. **39**(7): p. 613-626.
 21. Paur, H.-R., et al., *In-vitro cell exposure studies for the assessment of nanoparticle toxicity in the lung—A dialog between aerosol science and biology.* Journal of Aerosol Science, 2011. **42**(10): p. 668-692.
 22. Soto, K., K.M. Garza, and L.E. Murr, *Cytotoxic effects of aggregated nanomaterials.* Acta Biomaterialia, 2007. **3**(3): p. 351-358.
 23. Soenen, S.J., et al., *Cellular toxicity of inorganic nanoparticles: Common aspects and guidelines for improved nanotoxicity evaluation.* Nano Today, 2011. **6**(5): p. 446-465.
 24. Drexler, H.G., et al., *False leukemia-lymphoma cell lines: An update on over 500 cell lines.* Leukemia, 2003. **17**(2): p. 416-426.
 25. Wilkinson, K.E., et al., *Solution-Engineered Palladium Nanoparticles: Model for Health Effect Studies of Automotive Particulate Pollution.* ACS Nano, 2011. **5**(7): p. 5312-5324.
 26. Jones, C.F. and D.W. Grainger, *In vitro assessments of nanomaterial toxicity.* Advanced Drug Delivery Reviews, 2009. **61**(6): p. 438-456.
 27. Forrest, I.A., et al., *Primary airway epithelial cell culture from lung transplant recipients.* Eur Respir J, 2005. **26**(6): p. 1080-5.
 28. Brodlie, M., et al., *Primary bronchial epithelial cell culture from explanted cystic fibrosis lungs.* Exp Lung Res, 2010. **36**(2): p. 101-10.
 29. Bur, M. and C.M. Lehr, *Pulmonary cell culture models to study the safety and efficacy of innovative aerosol medicines.* Expert Opinion on Drug Delivery, 2008. **5**(6): p. 641-652.
 30. Gosalia, N., S.H. Leir, and A. Harris, *Coordinate regulation of the gel-forming mucin genes at chromosome 11p15.5.* Journal of Biological Chemistry, 2013. **288**(9): p. 6717-6725.
 31. Bivas-Benita, M., et al., *PLGA-PEI nanoparticles for gene delivery to pulmonary epithelium.* European Journal of Pharmaceutics and Biopharmaceutics, 2004. **58**(1): p. 1-6.
 32. Amidi, M., et al., *Preparation and characterization of protein-loaded N-trimethyl chitosan nanoparticles as nasal delivery system.* Journal of Controlled Release, 2006. **111**(1-2): p. 107- 116.
 33. Grenha, A., et al., *Chitosan nanoparticles are compatible with respiratory epithelial cells in vitro.* European Journal of Pharmaceutical Sciences, 2007. **31**(2): p. 73-84.
 34. Burgess, B.L., et al., *A phospholipid-apolipoprotein A-I nanoparticle containing amphotericin B as a drug delivery platform with cell membrane protective properties.* International Journal of Pharmaceutics, 2010. **399**(1-2): p. 148-155.
 35. Mura, S., et al., *Biodegradable nanoparticles meet the bronchial airway barrier: How surface properties affect their interaction with mucus and epithelial cells.* Biomacromolecules, 2011. **12**(11): p. 4136-4143.
 36. Lee, J., et al., *Self-assembled glycol chitosan nanogels containing palmityl-acylated exendin-4*

- peptide as a long-acting anti-diabetic inhalation system. Journal of Controlled Release*, 2012. **161**(3): p. 728-734.
37. Ong, H.X., et al., *Liposomal nanoparticles control the uptake of ciprofloxacin across respiratory epithelia. Pharmaceutical Research*, 2012. **29**(12): p. 3335-3346.
 38. Lewinski, N., V. Colvin, and R. Drezek, *Cytotoxicity of Nanoparticles. Small*, 2008. **4**(1): p. 26- 49.
 39. Stone, V., H. Johnston, and R.P.F. Schins, *Development of in vitro systems for nanotoxicology: Methodological considerations in vitro methods for nanotoxicology Vicki Stone et al. Critical Reviews in Toxicology*, 2009. **39**(7): p. 613-626.
 40. Hillegass, J.M., et al., *Assessing nanotoxicity in cells in vitro. Wiley Interdisciplinary Reviews: Nanomedicine and Nanobiotechnology*, 2010. **2**(3): p. 219-231.
 41. Kong, B., et al., *Experimental considerations on the cytotoxicity of nanoparticles. Nanomedicine*, 2011. **6**(5): p. 929-941.
 42. Dobrovolskaia, M.A., D.R. Germolec, and J.L. Weaver, *Evaluation of nanoparticle immunotoxicity. Nature Nanotechnology*, 2009. **4**(7): p. 411-414.
 43. Pirooznia, N., et al., *Encapsulation of Alpha-1 antitrypsin in PLGA nanoparticles: In Vitro characterization as an effective aerosol formulation in pulmonary diseases. Journal of Nanobiotechnology*, 2012. **10**.
 44. Chittasupho, C., et al., *Targeted delivery of doxorubicin to A549 lung cancer cells by CXCR4 antagonist conjugated PLGA nanoparticles. European Journal of Pharmaceutics and Biopharmaceutics*, 2014. **88**(2): p. 529-538.
 45. Grabowski, N., et al., *Toxicity of surface-modified PLGA nanoparticles toward lung alveolar epithelial cells. International Journal of Pharmaceutics*, 2013. **454**(2): p. 686-694.
 46. Geys, J., B. Nemery, and P.H. Hoet, *Assay conditions can influence the outcome of cytotoxicity tests of nanomaterials: better assay characterization is needed to compare studies. Toxicol In Vitro*, 2010. **24**(2): p. 620-9.
 47. Xia, T., N. Li, and A.E. Nel, *Potential Health Impact of Nanoparticles. Annual Review of Public Health*, 2009. **30**(1): p. 137-150.
 48. Nel, A., et al., *Toxic Potential of Materials at the Nanolevel. Science*, 2006. **311**(5761): p. 622- 627.
 49. Bose, T., et al., *Overview of nano-drugs characteristics for clinical application: the journey from the entry to the exit point. Journal of Nanoparticle Research*, 2014. **16**(8): p. 1-25.
 50. Hammer, A.M., et al., *The First Line of Defense: The Effects of Alcohol on Post-Burn Intestinal Barrier, Immune Cells, and Microbiome. Alcohol Research : Current Reviews*, 2015. **37**(2): p. 209-222.
 51. Singh, R. and J.W. Lillard, Jr., *Nanoparticle-based targeted drug delivery. Exp Mol Pathol*, 2009. **86**(3): p. 215-23.
 52. Desai, M.P., et al., *Gastrointestinal Uptake of Biodegradable Microparticles: Effect of Particle Size. Pharmaceutical Research*, 1996. **13**(12): p. 1838-1845.
 53. Redhead, H.M., S.S. Davis, and L. Illum, *Drug delivery in poly(lactide-co-glycolide) nanoparticles surface modified with poloxamer 407 and poloxamine 908: in vitro characterisation and in vivo evaluation. Journal of Controlled Release*, 2001. **70**(3): p. 353- 363.
 54. Dunn, S.E., et al., *In vitro cell interaction and in vivo biodistribution of poly(lactide-*

- co- glycolide) nanospheres surface modified by poloxamer and poloxamine copolymers. Journal of Controlled Release, 1997. 44(1): p. 65-76.*
55. Gaur, U., et al., *Biodistribution of fluoresceinated dextran using novel nanoparticles evading reticuloendothelial system. International Journal of Pharmaceutics, 2000. 202(1): p. 1-10.*
 56. Liu, L., et al., *Biodistribution of TAT-LHRH conjugated chitosan/DNA nanoparticles in the mice bearing hepatoma xenografts. Journal of Biomedical Materials Research Part A, 2016. 104(10): p. 2394-2400.*
 57. Kumar, R., et al., *In Vivo Biodistribution and Clearance Studies Using Multimodal Organically Modified Silica Nanoparticles. ACS Nano, 2010. 4(2): p. 699-708.*
 58. Huang, X., et al., *The Shape Effect of Mesoporous Silica Nanoparticles on Biodistribution, Clearance, and Biocompatibility in Vivo. ACS Nano, 2011. 5(7): p. 5390-5399.*
 59. Kumar, B., et al., *Recent advances in nanoparticle-mediated drug delivery. Journal of Drug Delivery Science and Technology, 2017. 41: p. 260-268.*
 60. Sadat, S.M.A., S.T. Jahan, and A. Haddadi, *Effects of Size and Surface Charge of Polymeric Nanoparticles on <i>in Vitro</i> and <i>in Vivo</i> Applications. Journal of Biomaterials and Nanobiotechnology, 2016. Vol.07No.02: p. 18.*
 61. Bhattacharjee, S., et al., *Cytotoxicity and cellular uptake of tri-block copolymer nanoparticles with different size and surface characteristics. Particle and Fibre Toxicology, 2012. 9(1): p. 11.*
 62. Liu, Y., et al., *The shape of things to come: importance of design in nanotechnology for drug delivery. Therapeutic delivery, 2012. 3(2): p. 181-194.*
 63. Datta, N.R., et al., *Magnetic nanoparticle-induced hyperthermia with appropriate payloads: Paul Ehrlich's "magic (nano)bullet" for cancer theranostics? Cancer Treat Rev, 2016. 50: p. 217-227.*
 64. Yokoyama, M., *Drug targeting with nano-sized carrier systems. J Artif Organs, 2005. 8(2): p. 77-84.*
 65. Yu, X., et al., *Design of Nanoparticle-Based Carriers for Targeted Drug Delivery. Journal of Nanomaterials, 2016. 2016: p. 15.*
 66. Bertrand, N., et al., *Cancer nanotechnology: the impact of passive and active targeting in the era of modern cancer biology. Adv Drug Deliv Rev, 2014. 66: p. 2-25.*
 67. von Roemeling, C., et al., *Breaking Down the Barriers to Precision Cancer Nanomedicine. Trends in Biotechnology, 2017. 35(2): p. 159-171.*
 68. Suk, J.S., et al., *PEGylation as a strategy for improving nanoparticle-based drug and gene delivery. Advanced Drug Delivery Reviews, 2016. 99: p. 28-51.*
 69. Xu, X., et al., *Cancer nanomedicine: from targeted delivery to combination therapy. Trends in Molecular Medicine, 2015. 21(4): p. 223-232.*
 70. Semete, B., et al., *Effects of protein binding on the biodistribution of PEGylated PLGA nanoparticles post oral administration. International Journal of Pharmaceutics, 2012. 424(1): p. 115-120.*
 71. Nissinen, T., et al., *Tailored Dual PEGylation of Inorganic Porous Nanocarriers for Extremely Long Blood Circulation in Vivo. ACS Applied Materials & Interfaces, 2016. 8(48): p. 32723- 32731.*
 72. Saneja, A., et al., *Development and evaluation of long-circulating nanoparticles*

- loaded with betulinic acid for improved anti-tumor efficacy.* International Journal of Pharmaceutics, 2017. **531**(1): p. 153-166.
73. Oh, N. and J.-H. Park, *Surface Chemistry of Gold Nanoparticles Mediates Their Exocytosis in Macrophages.* ACS Nano, 2014. **8**(6): p. 6232-6241.
 74. Hare, J.I., et al., *Challenges and strategies in anti-cancer nanomedicine development: An industry perspective.* Adv Drug Deliv Rev, 2017. **108**: p. 25-38.
 75. Pillai, G., *Nanomedicines for Cancer Therapy: An Update of FDA Approved and Those under Various Stages of Development.* SOJ Pharm Pharm Sci, 2014. **1**(2), 13.
 76. Anselmo, A.C. and S. Mitragotri, *Nanoparticles in the clinic.* Bioengineering & Translational Medicine, 2016. **1**(1): p. 10-29.
 77. Ventola, C.L., *Progress in Nanomedicine: Approved and Investigational Nanodrugs.* P t, 2017. **42**(12): p. 742-755.
 78. Zhang, H., et al., *Mucus as a barrier for biopharmaceuticals and drug delivery systems,* in *Mucosal Delivery of Biopharmaceuticals: Biology, Challenges and Strategies.* 2014. p. 59-97.
 79. Wu, L., et al., *Engineering nanomaterials to overcome the mucosal barrier by modulating surface properties.* Advanced Drug Delivery Reviews, 2018. **124**: p. 150-163.
 80. Cone, R.A., *Barrier properties of mucus.* Adv Drug Deliv Rev, 2009. **61**(2): p. 75-85.
 81. Chater, P.I., M.D. Wilcox, and J.P. Pearson, *Efficacy and safety concerns over the use of mucus modulating agents for drug delivery using nanoscale systems.* Advanced Drug Delivery Reviews, 2018. **124**: p. 184-192.
 82. Newby, J.M., et al., *Technological strategies to estimate and control diffusive passage times through the mucus barrier in mucosal drug delivery.* Adv Drug Deliv Rev, 2018. **124**: p. 64-81.
 83. Mahapatro, A. and D.K. Singh, *Biodegradable nanoparticles are excellent vehicle for site directed in-vivo delivery of drugs and vaccines.* J Nanobiotechnology, 2011. **9**: p. 55.
 84. Andersen, E.S., et al., *Self-assembly of a nanoscale DNA box with a controllable lid.* Nature, 2009. **459**(7243): p. 73-6.
 85. Dobson, J., *Magnetic nanoparticles for drug delivery.* Drug Development Research, 2006. **67**(1): p. 55-60.
 86. Riedinger, A., et al., *Subnanometer local temperature probing and remotely controlled drug release based on azo-functionalized iron oxide nanoparticles.* Nano Lett, 2013. **13**(6): p. 2399-406.
 87. Tomoda, K., et al., *Preparation and properties of inhalable nanocomposite particles for treatment of lung cancer.* Colloids and Surfaces B: Biointerfaces, 2009. **71**(2): p. 177-182.
 88. Baoum, A., et al., *Cationic surface modification of PLG nanoparticles offers sustained gene delivery to pulmonary epithelial cells.* Journal of Pharmaceutical Sciences, 2010. **99**(5): p. 2413-2422.
 89. Bains, B.K., et al., *In vitro reporter gene transfection via plasmid DNA delivered by metered dose inhaler.* Journal of Pharmaceutical Sciences, 2010. **99**(7): p. 3089-3099.
 90. Ungaro, F., et al., *Dry powders based on PLGA nanoparticles for pulmonary delivery of antibiotics: Modulation of encapsulation efficiency, release rate and lung deposition*

- pattern by hydrophilic polymers*. Journal of Controlled Release, 2012. **157**(1): p. 149-159.
91. Griset, A.P., et al., *Expansile Nanoparticles: Synthesis, Characterization, and in Vivo Efficacy of an Acid-Responsive Polymeric Drug Delivery System*. Journal of the American Chemical Society, 2009. **131**(7): p. 2469-2471.
 92. Boylan, N.J., et al., *Enhancement of airway gene transfer by DNA nanoparticles using a pH- responsive block copolymer of polyethylene glycol and poly-L-lysine*. Biomaterials, 2012. **33**(7): p. 2361-2371.
 93. Murata, M., et al., *Surface modification of liposomes using polymer-wheat germ agglutinin conjugates to improve the absorption of peptide drugs by pulmonary administration*. Journal of Pharmaceutical Sciences, 2013. **102**(4): p. 1281-1289.
 94. Jiang, L., et al., *Thiolated chitosan-modified PLA-PCL-TPGS nanoparticles for oral chemotherapy of lung cancer*. Nanoscale Research Letters, 2013. **8**(1): p. 1-6.
 95. Kim, H., et al., *Bioimaging and pulmonary applications of self-assembled Flt1 peptide- hyaluronic acid conjugate nanoparticles*. Biomaterials, 2013. **34**(33): p. 8478-8490.
 96. Arunraj, T.R., et al., *Doxorubicin-chitin-poly(caprolactone) composite nanogel for drug delivery*. International Journal of Biological Macromolecules, 2013. **62**: p. 35-43.
 97. Mohammadi, Z., et al., *Preparation and evaluation of chitosan-DNA-FAP-B nanoparticles as a novel non-viral vector for gene delivery to the lung epithelial cells*. International Journal of Pharmaceutics, 2011. **409**(1-2): p. 307-313.
 98. Feliu, N., et al., *Next-generation sequencing reveals low-dose effects of cationic dendrimers in primary human bronchial epithelial cells*. ACS Nano, 2015. **9**(1): p. 146-163.
 99. Lee, C., et al., *Long-acting inhalable chitosan-coated poly(lactic-co-glycolic acid) nanoparticles containing hydrophobically modified exendin-4 for treating type 2 diabetes*. International Journal of Nanomedicine, 2013. **8**: p. 2975-2983.
 100. ZHAO, T., et al., *DDAB-MODIFIED TPGS-b-(PCL-ran-PGA) NANOPARTICLES AS ORAL ANTICANCER DRUG CARRIER FOR LUNG CANCER CHEMOTHERAPY*. Nano, 2013. **08**(02): p. 1350014.
 101. Lamichhane, S.P., et al., *Glycosaminoglycan-Functionalized Poly-Lactide-Co-Glycolide nanoparticles: Synthesis, characterization, cytocompatibility, and cellular uptake*. International Journal of Nanomedicine, 2015. **10**: p. 775-789.
 102. Griebinger, J., et al., *Methods to determine the interactions of micro- and nanoparticles with mucus*. European Journal of Pharmaceutics and Biopharmaceutics, 2015. **96**: p. 464-476.
 103. Pearson, J.P., A. Allen, and D.A. Hutton, *Rheology of Mucin*, in *Glycoprotein Methods and Protocols: The Mucins*, A.P. Corfield, Editor. 2000, Humana Press: Totowa, NJ. p. 99-109.
 104. Cooke, M.J., et al., *Enhanced cell attachment using a novel cell culture surface presenting functional domains from extracellular matrix proteins*. Cytotechnology, 2008. **56**(2): p. 71-79.
 105. Topman, G., O. Sharabani-Yosef, and A. Gefen, *A method for quick, low-cost automated confluency measurements*. Microsc Microanal, 2011. **17**(6): p. 915-22.
 106. Jaccard, N., et al., *Automated method for the rapid and precise estimation of adherent cell culture characteristics from phase contrast microscopy images*.

- Biotechnol Bioeng, 2014. **111**(3): p. 504-17.
107. DeliveReD, G., *atcc animal cell culture guide*. ATCC 2014.
 108. Fogh, J., J.M. Fogh, and T. Orfeo, *One hundred and twenty seven cultured human tumor cell lines producing tumors in nude mice*. Journal of the National Cancer Institute, 1977. **59**(1): p. 221-226.
 109. Kreda, S.M., et al., *Coordinated release of nucleotides and mucin from human airway epithelial Calu-3 cells*. Journal of Physiology, 2007. **584**(1): p. 245-259.
 110. Shan, J., et al., *Anion secretion by a model epithelium: more lessons from Calu-3*. Acta Physiologica, 2011. **202**(3): p. 523-531.
 111. *Calu-3 (ATCC® HTB-55™)*. ATCC, 2016.
 112. Riss, T. and R. Moravec, *Simplifying Cytotoxicity Screening: Introducing the CellTiter-Blue™ Cell Viability Assay*. Promega Corporation, 2003.
 113. Moravec, R. and T. Riss, *THE CELLTITER-BLUE™ CELL VIABILITY ASSAY: MONITORING CELL VIABILITY USING A FLUORESCENT REDOX INDICATOR DYE*. PROMEGA CORPORATION, 2003.
 114. *CellTiter-Blue Cell Viability Assay*. Promega Corporation, 2016.
 115. Mosmann, T., *Rapid colorimetric assay for cellular growth and survival: application to proliferation and cytotoxicity assays*. J Immunol Methods, 1983. **65**(1-2): p. 55-63.
 116. Belyanskaya, L., et al., *The reliability and limits of the MTT reduction assay for carbon nanotubes-cell interaction*. Carbon, 2007. **45**(13): p. 2643-2648.
 117. Wilcox, M.D., et al., *The effect of nanoparticle permeation on the bulk rheological properties of mucus from the small intestine*. European Journal of Pharmaceutics and Biopharmaceutics, 2015. **96**: p. 484-487.
 118. Friedl, H., et al., *Development and Evaluation of a Novel Mucus Diffusion Test System Approved by Self-Nanoemulsifying Drug Delivery Systems*. Journal of Pharmaceutical Sciences, 2013. **102**(12): p. 4406-4413.
 119. Kim, T.K., *T test as a parametric statistic*. Korean J Anesthesiol, 2015. **68**(6): p. 540-6.
 120. Correll, M. and M. Gleicher, *Error bars considered harmful: Exploring alternate encodings for mean and error*. IEEE Transactions on Visualization and Computer Graphics, 2014. **20**(12): p. 2142-2151.
 121. Kelly, D., J. Jasperse, and I. Westbrooke, *Designing science graphs for data analysis and presentation*. Department of Conservation Technical Series, 2005.
 122. Shintani, A., *Primer of statistics in dental research: Part I*. Journal of Prosthodontic Research, 2014. **58**(1): p. 11-16.
 123. Medina, C., et al., *Nanoparticles: Pharmacological and toxicological significance*. British Journal of Pharmacology, 2007. **150**(5): p. 552-558.
 124. Gwinn, M.R. and V. Vallyathan, *Nanoparticles: Health effects - Pros and cons*. Environmental Health Perspectives, 2006. **114**(12): p. 1818-1825.
 125. Darolles, C., et al., *In vitro assessment of cobalt oxide particle toxicity: Identifying and circumventing interference*. Toxicology in Vitro, 2013. **27**(6): p. 1699-1710.
 126. Oberdörster, G., E. Oberdörster, and J. Oberdörster, *Nanotoxicology: An emerging discipline evolving from studies of ultrafine particles*. Environmental Health Perspectives, 2005. **113**(7): p. 823-839.
 127. Holder, A.L., et al., *Particle-induced artifacts in the MTT and LDH viability assays*. Chemical Research in Toxicology, 2012. **25**(9): p. 1885-1892.

128. Hoskins, C., et al., *Dilemmas in the reliable estimation of the in-vitro cell viability in magnetic nanoparticle engineering: Which tests and what protocols?* Nanoscale Research Letters, 2012. **7**: p. 1-22.
129. Kroll, A., et al., *Interference of engineered nanoparticles with in vitro toxicity assays.* Archives of Toxicology, 2012. **86**(7): p. 1123-1136.
130. Monteiro-Riviere, N.A., A.O. Inman, and L.W. Zhang, *Limitations and relative utility of screening assays to assess engineered nanoparticle toxicity in a human cell line.* Toxicology and Applied Pharmacology, 2009. **234**(2): p. 222-235.
131. Oostingh, G.J., et al., *Problems and challenges in the development and validation of human cell-based assays to determine nanoparticle-induced immunomodulatory effects.* Particle and Fibre Toxicology, 2011. **8**.
132. AshaRani, P.V., et al., *Cytotoxicity and genotoxicity of silver nanoparticles in human cells.* ACS Nano, 2009. **3**(2): p. 279-290.
133. Schlinkert, P., et al., *The oxidative potential of differently charged silver and gold nanoparticles on three human lung epithelial cell types.* Journal of Nanobiotechnology, 2015. **13**(1).
134. Ruenraroengsak, P., et al., *Respiratory epithelial cytotoxicity and membrane damage (holes) caused by amine-modified nanoparticles.* Nanotoxicology, 2012. **6**(1): p. 94-108.
135. Thach, C.T. and J.N. Finkelstein, *Cationic nanoparticles disrupt cellular signaling in a cholesterol dependent manner.* Toxicology in Vitro, 2013. **27**(4): p. 1277-1286.
136. Lai, S.K., Y.-Y. Wang, and J. Hanes, *Mucus-penetrating nanoparticles for drug and gene delivery to mucosal tissues.* Advanced Drug Delivery Reviews, 2009. **61**(2): p. 158-171.
137. Dünnhaupt, S., et al., *Nano-carrier systems: Strategies to overcome the mucus gel barrier.* European Journal of Pharmaceutics and Biopharmaceutics, 2015. **96**: p. 447-453.
138. Chatterjee, B., et al., *Controversies with self-emulsifying drug delivery system from pharmacokinetic point of view.* Drug Deliv, 2016. **23**(9): p. 3639-3652.
139. Vinković Vrček, I., et al., *Does surface coating of metallic nanoparticles modulate their interference with in vitro assays?* RSC Advances, 2015. **5**(87): p. 70787-70807.
140. Karamanidou, T., et al., *Effective incorporation of insulin in mucus permeating self-nanoemulsifying drug delivery systems.* European Journal of Pharmaceutics and Biopharmaceutics, 2015. **97**: p. 223-229.
141. Taylor, C., *The structure of the mucus gel barrier and the interaction with alginates.* PhD thesis, 2002.
142. Taylor, C., et al., *Two rheologically different gastric mucus secretions with different putative functions.* Biochimica et Biophysica Acta (BBA) - General Subjects, 2004. **1674**(2): p. 131-138.
143. Taylor, C., et al., *Mucous systems show a novel mechanical response to applied deformation.* Biomacromolecules, 2005. **6**(3): p. 1524-30.
144. Hatipoglu, U., *Chronic obstructive pulmonary disease: More than meets the eye.* Ann Thorac Med, 2018. **13**(1): p. 1-6.
145. Mehta, G.R., et al., *Chronic obstructive pulmonary disease: A guide for the primary care physician.* Dis Mon, 2016. **62**(6): p. 164-87.
146. *Chronic obstructive pulmonary disease (COPD).* world health organization, 2018.
147. Rabe, K.F. and H. Watz, *Chronic obstructive pulmonary disease.* The Lancet, 2017. **389**(10082): p. 1931-1940.

148. Lambrecht, B.N. and H. Hammad, *The immunology of asthma*. Nat Immunol, 2015. **16**(1): p. 45-56.
149. Nunes, C., A.M. Pereira, and M. Morais-Almeida, *Asthma costs and social impact*. Asthma Research and Practice, 2017. **3**(1): p. 1.
150. Papadopoulos, N.G., et al., *Asthma research in Europe: a transformative agenda for innovation and competitiveness*. European Respiratory Journal, 2017. **49**(5).
151. D'Amato, G., et al., *Asthma-related deaths*. Multidisciplinary Respiratory Medicine, 2016. **11**: p. 37.
152. World Health Organisation, *Chronic Respiratory Diseases: Asthma*. 2018 <<http://who.int/respiratory/asthma/scope/en>>
153. Elborn, J.S., *Cystic fibrosis*. The Lancet, 2016. **388**(10059): p. 2519-2531.
154. Taylor-Robinson, D., et al., *Data Resource Profile: The UK Cystic Fibrosis Registry*. Int J Epidemiol, 2018. **47**(1): p. 9-10e.
155. Kura, A.U., et al., *Nanotechnology in drug delivery: the need for more cell culture based studies in screening*. Chemistry Central Journal, 2014. **8**: p. 46-46.
156. Kabgani, N. and M.J. Moeller, *The terminator mouse: salvation for primary cell culture*. Kidney Int, 2013. **84**(5): p. 866-8.
157. Kaur, G. and J.M. Dufour, *Cell lines: Valuable tools or useless artifacts*. Spermatogenesis, 2012. **2**(1): p. 1-5.
158. McLellan, K., et al., *Primary airway epithelial cell culture and asthma in children-lessons learnt and yet to come*. Pediatr Pulmonol, 2015. **50**(12): p. 1393-405.
159. Edwards, J., et al., *Human tissue models for a human disease: what are the barriers?* Thorax, 2015. **70**(7): p. 695-7.
160. Brodlie, M., et al., *Raised interleukin-17 is immunolocalised to neutrophils in cystic fibrosis lung disease*. Eur Respir J, 2011. **37**(6): p. 1378-85.
161. Gazdar, A.F., B. Gao, and J.D. Minna, *Lung cancer cell lines: Useless artifacts or invaluable tools for medical science?* Lung Cancer, 2010. **68**(3): p. 309-18.
162. Barnes, P.J., *Inflammatory mechanisms in patients with chronic obstructive pulmonary disease*. J Allergy Clin Immunol, 2016. **138**(1): p. 16-27.
163. Gabriel Heaney, L., J. Thomas Lindsay, and L. Patrick Augustine McGarvey, *Inflammation in Chronic Obstructive Pulmonary Disease: Implications for New Treatment Strategies*. Current Medicinal Chemistry, 2007. **14**(7): p. 787-796.
164. Murdoch, J.R. and C.M. Lloyd, *Chronic inflammation and asthma*. Mutation Research, 2010. **690**(1-2): p. 24-39.
165. Hamid, Q., et al., *Inflammatory cells in asthma: mechanisms and implications for therapy*. J Allergy Clin Immunol, 2003. **111**(1 Suppl): p. S5-S12; discussion S12-7.
166. Hamid, Q. and M. Tulic, *Immunobiology of asthma*. Annu Rev Physiol, 2009. **71**: p. 489-507.
167. Giddings, O. and C.R. Esther, Jr., *Mapping targetable inflammation and outcomes with cystic fibrosis biomarkers*. Pediatr Pulmonol, 2017. **52**(S48): p. S21-s28.
168. Dhooghe, B., et al., *Lung inflammation in cystic fibrosis: pathogenesis and novel therapies*. Clin Biochem, 2014. **47**(7-8): p. 539-46.
169. Meng, H., et al., *A predictive toxicological paradigm for the safety assessment of nanomaterials*. ACS Nano, 2009. **3**(7): p. 1620-7.
170. Xia, T., N. Li, and A.E. Nel, *Potential health impact of nanoparticles*, in Annual

- Review of Public Health*. 2009. p. 137-150.
171. Nel, A.E., *Implementation of alternative test strategies for the safety assessment of engineered nanomaterials*. *J Intern Med*, 2013. **274**(6): p. 561-77.
 172. Damoiseaux, R., et al., *No time to lose--high throughput screening to assess nanomaterial safety*. *Nanoscale*, 2011. **3**(4): p. 1345-60.
 173. Abdal Dayem, A., et al., *The Role of Reactive Oxygen Species (ROS) in the Biological Activities of Metallic Nanoparticles*. *International Journal of Molecular Sciences*, 2017. **18**(1): p. 120.
 174. Guadagnini, R., et al., *Toxicity screenings of nanomaterials: Challenges due to interference with assay processes and components of classic in vitro tests*. *Nanotoxicology*, 2015. **9**(S1): p. 13-24.
 175. Costa, C., et al., *In vitro cytotoxicity of superparamagnetic iron oxide nanoparticles on neuronal and glial cells. Evaluation of nanoparticle interference with viability tests*. *Journal of Applied Toxicology*, 2016. **36**(3): p. 361-372.
 176. Breznan, D., et al., *Non-specific interaction of carbon nanotubes with the resazurin assay reagent: Impact on in vitro assessment of nanoparticle cytotoxicity*. *Toxicology in Vitro*, 2015. **29**(1): p. 142-147.
 177. Olmsted, S.S., et al., *Diffusion of Macromolecules and Virus-Like Particles in Human Cervical Mucus*. *Biophysical Journal*, 2001. **81**(4): p. 1930-1937.

Appendix 1: Calculate Osmolarity as controls.

A) If I need 250 μ g/500 μ l. I must dilute the 500 μ g/ 500 μ l stock by 1(water):1(resting media; RM). Therefore, this means I had 250 μ l of H₂O and 250 μ l of RM.

B) If I need 50 μ g/500 μ l. I must dilute the 500 μ g/ 500 μ l stock by 1(water):9(resting media; RM). Therefore, I had 50 μ l of H₂O and 450 μ l of RM.